Helical3D Validation Manual

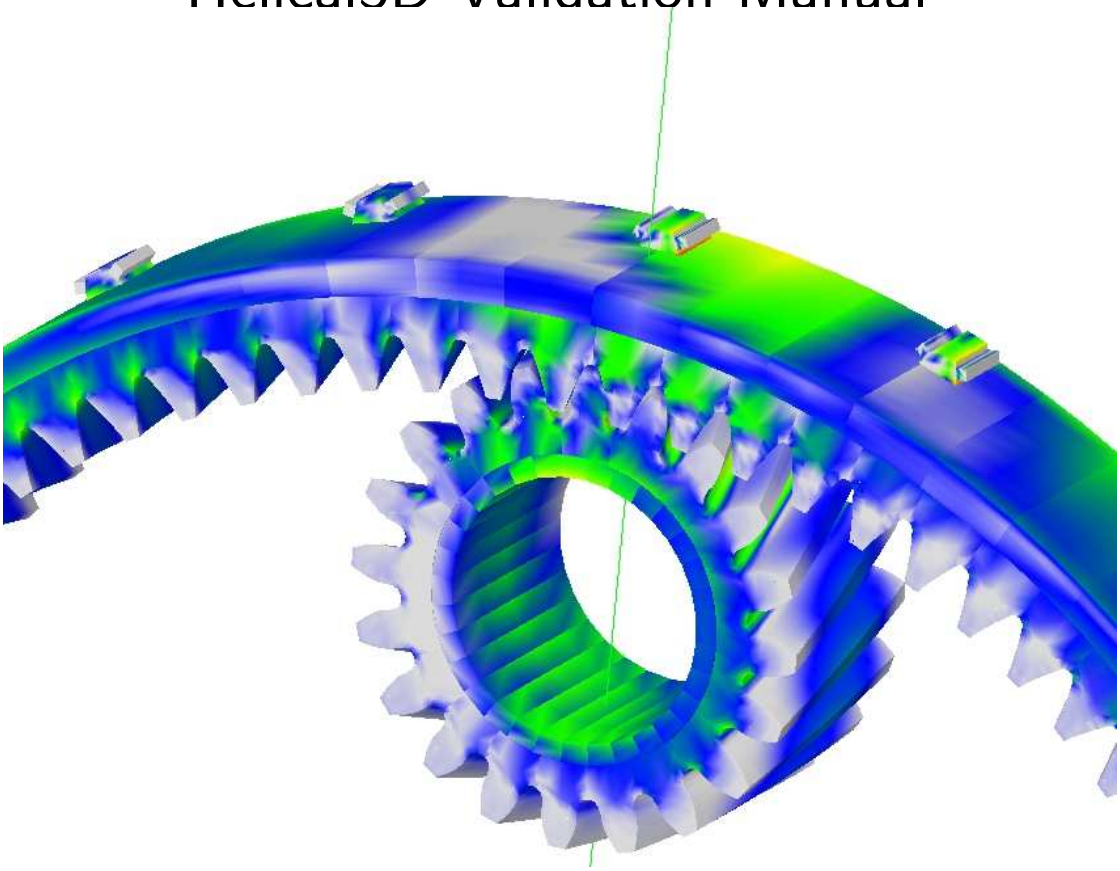

Advanced Numerical Solutions
Hilliard OH

February 24, 2005

Contents

Preface **xiii**

1 Introduction **1**

2 Calculation of contact pressure for a spur gear model using Calyx **3**
2.1 Contact pressure for spur gear model with no tooth tip modifications 3
2.1.1 The example file 3
2.1.2 Obtaining the contact pressure from the postprocessing menu 8
2.1.3 Contact pressure from theoretical calculations 11
2.2 Contact pressure for spur gear model with linear tooth tip modification 18
2.2.1 The example file 18
2.2.2 Obtaining the contact pressure from the postprocessing menu 19
2.2.3 Obtaining contact pressure from theoretical calculations 22
2.3 Contact pressure for spur gear model with quadratic tooth tip modification . . . 33
2.3.1 The example file 33
2.3.2 Obtaining the contact pressure from the postprocessing menu 33
2.3.3 Contact pressure from theoretical calculations 37
2.4 Contact pressure for spur gear model with lead crown tooth modification 45
2.4.1 The example file 45
2.4.2 Obtaining the contact pressure from the postprocessing menu 47
2.4.3 Contact pressure from theoretical calculations 50
2.5 Conclusion 55

3 Sub-surface stresses in a spur gear model using Calyx **57**
3.1 The spur gear model with no tooth modification 57
3.1.1 The example file 57
3.1.2 Obtaining the sub-surface stress from the postprocessing menu 57

4 Calculation of transmission error for a spur and helical gear model using Calyx **63**
4.1 Introduction 63
4.2 Measuring the transmission error using calyx 64
4.2.1 Comparison of transmission error values obtained from Calyx and LDP for Spur gears 64
4.2.2 Comparison of transmission error values obtained from Calyx and LDP for Helical gears 71
4.3 Conclusion 71

5 Internal helical gear pair example **75**
5.1 The example file 75
5.2 Results 81

6 Internal helical gear with webbed rim **83**
6.1 The example file . . . 83
6.2 Modeling the rim . . . 83
6.3 Results . . . 85

7 Modeling splines using the Helical 3D program **87**
7.1 Internal splines on external gear . . . 87
7.1.1 The example file . . . 87
7.1.2 Modeling the splines . . . 87
7.1.3 Results . . . 87
7.2 External splines on external gear . . . 91
7.2.1 The example file . . . 91
7.2.2 Modeling the splines . . . 91
7.2.3 Results . . . 93
7.3 External splines on internal gear . . . 95
7.3.1 The example file . . . 95
7.3.2 Modeling the splines . . . 95
7.3.3 Results . . . 97
7.4 Internal splines on internal gear . . . 99
7.4.1 The example file . . . 99
7.4.2 Modeling the splines . . . 99
7.4.3 Results . . . 101

8 Example of topographic modification **103**
8.1 The example file . . . 103
8.2 Applying topographic modifications on the pinion tooth . . . 103
8.3 Results . . . 107

9 Convergence study **113**
9.1 Effect of Tip radius on the max ppl normal stress . . . 113
9.1.1 The example file . . . 113
9.1.2 Results and discussion . . . 118
9.2 Effect of Tooth thickness on the max ppl normal stress . . . 121
9.3 Effect of number of elements in the face direction on the max ppl normal stress . . . 123
9.4 Effect of displacement order on the max ppl normal stress . . . 125
9.5 Conclusions . . . 125

10 Fatigue theory and life prediction using the Helical gear program **127**
10.1 Introduction . . . 127
10.2 Fatigue characteristics . . . 127
10.3 Low and High cycle fatigue . . . 128
10.4 Fatigue loading . . . 128
10.5 Example of a laboratory fatigue testing . . . 133
10.6 Gear fatigue failure . . . 134
10.7 Running the Helical3D program for fatigue failure . . . 135
10.7.1 The example file . . . 135
10.7.2 Locating the point of maximum stress . . . 135
10.7.3 Results . . . 141
10.8 Calculating the fatigue life . . . 142
10.8.1 Goodman's Linear relationship . . . 143
10.8.2 Gerber's parabolic relationship . . . 144
10.8.3 Soderberg's linear relationship . . . 144

10.8.4 Elliptic relationship 144
10.9 Effect of rigid internal diameter on fatigue life 146
10.9.1 Locating the point of maximum stress 146
10.9.2 Results 150
10.10Fatigue life for a thin flexible rim model 150
10.10.1 Locating the point of maximum stress 150
10.10.2 Results 154
10.11Cumulative damage 154
10.11.1 Linear damage theory 154
10.11.2 Gatts Cumulative damage theory 156
10.12Fatigue life based on **duty cycle** for a gear set 157
10.13Calculating life based on cumulative damage theory 163
10.14Conclusions 163

A Values of m and n for various values of θ **165**

List of Figures

2.1 Graph of contact pressure against time for pinion tooth no.1 9
2.2 Grid pressure histogram for pinion tooth no.1 at t=0 (Contact Pressure = 1.596110E+005 at Time = 0.000000E+000. Range of contact pressure is from 0.000000E+000 to 1.596110E+005 and each division corresponds to 2.000000E+004) 10
2.3 Drawing defining the radius of curvature(R) and the roll angle(θ) 12
2.4 Plot of tooth load against time for pinion tooth no.1 13
2.5 Toothload histogram at t=0.0 14
2.6 A graph comparing Calyx's and Hertz's contact pressure predictions 16
2.7 Linear tip relief applied to the pinion tooth 18
2.8 Linear tip relief applied to the gear tooth 19
2.9 Graph of contact pressure against time for pinion tooth no.1 20
2.10 Grid pressure histogram for pinion tooth no.1 at t=0.5s (Contact Pressure at Time = 5.000000E-001s. Range of contact pressure is from 0.000000E+000 to 1.183206E+005 and each division corresponds to 2.000000E+004 21
2.11 Toothload histogram at t=0.5s 28
2.12 A graph comparing Calyx's and Hertz's contact pressure predictions for linear modification at the teeth 30
2.13 A plot of contact pressure against time obtained from Calyx in the time range from 0.0s to 0.2s 31
2.14 Quadratic tip relief applied to the pinion tooth 33
2.15 Quadratic tip relief applied to the gear tooth 34
2.16 Plot of contact pressure against time for pinion tooth no.1 35
2.17 Grid pressure histogram for pinion tooth no.1 at t=0.5s (Contact Pressure at Time= 5.000000E-001 is 1.241488E+005s. Range of contact pressure is from 0.000000E+000 to 1.241488E+005 and each division corresponds to 2.000000E+004 36
2.18 Toothload histogram at t=0.5s 41
2.19 A graph comparing Calyx's and Hertz's contact pressure predictions for quadratic modification at the teeth 43
2.20 Crowning applied to the pinion tooth 45
2.21 Crowning applied to the gear tooth 46
2.22 Plot of contact pressure against time for pinion tooth no.1 48
2.23 Grid pressure histogram for crowned pinion tooth no.1 at t=0 (Contact Pressure at Time= 0.00 is 2.014838E+005. Range of contact pressure is from 0.000000E+000 to 2.014838E+005 and each division corresponds to 1.000000E+005 49
2.24 Figure showing the crowning curvature 50
2.25 Toothload histogram at the t=0 54

3.1 Graph of sub-surface Von Mises stress as a function of depth at pinion tooth no.1. The contact is at the pitch point. 59

3.2 Graph of sub-surface max. shear stress as a function of depth at pinion tooth no.1.The contact is at the pitch point. 60
3.3 Comparison of sub-surface σ_{xx} predicted by Calyx with that computed by the theory of elasticity (K. L. Johnson [20]). 61
3.4 Comparison of sub-surface σ_{yy} predicted by Calyx with that computed by the theory of elasticity (K. L. Johnson [20]). 61
3.5 Comparison of sub-surface σ_{zz} predicted by Calyx with that computed by the theory of elasticity (K. L. Johnson [20]). 62
3.6 Comparison of sub-surface $\tau_{max} = (\sigma_{xx} - \sigma_{zz})/2$ predicted by Calyx with that computed by the theory of elasticity (K. L. Johnson [20]). 62

4.1 Comparison of transmission error predicted by LDP and CAPP for a low contact ratio spur gear model under a load of $1000lbf - in$. Peak to Peak transmission error obtained from LDP is about $190\mu in$. CAPP predicts a peak to peak T.E of $150\mu in$. (From "Analysis of spur and helical gears using a combination of finite element and surface integral techniques", M.S. Thesis by Avinashchandra Singh at The Ohio State University). 65
4.2 Transmission error predicted by Calyx for a low contact ratio spur gear model under a load of $1000lbf - in$. Peak to Peak transmission error predicted by Calyx is $1.50132 \times 10^{-4} rads$. 66
4.3 Transmission error predicted by Calyx for a low contact ratio spur gear model under a load of $1000lbf - in$. Peak to Peak transmission error obtained from Calyx is about $180\mu in$. 67
4.4 Comparison of transmission error predicted by LDP and CAPP for a high contact ratio spur gear model under a load of $900lbf - in$. Peak to Peak transmission error obtained from LDP is about $50\mu in$. (From "Analysis of spur and helical gears using a combination of finite element and surface integral techniques", M.S. Thesis by Avinashchandra Singh at The Ohio State University). 69
4.5 Transmission error predicted by Calyx for a low contact ratio spur gear model under a load of $900lbf - in$. Peak to Peak transmission error obtained from Calyx is $37.411\mu in$. 70
4.6 Comparison of transmission error predicted by LDP and CAPP for a helical gear model under a load of $8040.0lbf - in$. Peak to Peak transmission error obtained from LDP is about $40\mu in$. (From "Analysis of spur and helical gears using a combination of finite element and surface integral techniques", M.S. Thesis by Avinashchandra Singh at The Ohio State University). 72
4.7 Transmission error predicted by CAPP for a helical gear model under a load of $8040lbf - in$. Peak to Peak transmission error obtained from CAPP is $23.40\mu in$. 73
4.8 Transmission error predicted by Calyx for a low contact ratio spur gear model under a load of $8040lbf - in$. Peak to Peak transmission error obtained from Calyx is $27.75\mu in$. 74

5.1 Finite element model of an internal helical gear set 76
5.2 Maximum principal normal stress contour for an internal helical gear set 81

6.1 Finite element model of an internal helical gear set with a webbed rim 84
6.2 Maximum principal normal stress contour for an internal helical gear set with a webbed rim 85

7.1 An internal helical gear set with internal splines on the external gear 88
7.2 Maximum principal normal stress contour for an internal helical gear set with internal splines on the pinion 88

7.3 Load distribution on the pinion and the splines 90
7.4 An internal helical gear set with external splines on the external gear 91
7.5 Maximum principal normal stress contour for an internal helical gear set with external splines on the pinion 93
7.6 Load distribution on the pinion and the splines 94
7.7 An internal helical gear set with external splines on the internal gear 95
7.8 Maximum principal normal stress contour for an internal helical gear set with external splines on the internal gear 97
7.9 Contact pressure distribution for an internal helical gear set with external splines on the internal gear 98
7.10 An internal helical gear set with internal splines on the internal gear 99
7.11 Maximum principal normal stress contour for an internal helical gear set with internal splines on the internal gear 101
7.12 Contact pressure distribution for an internal helical gear set with internal splines on the internal gear 102

8.1 An external helical gear set with topographical modifications applied on to the pinion tooth 104
8.2 Roll angle and zeta values for which modification is applied 105
8.3 Contact pattern for pinion tooth with topographical modifications 108
8.4 Contact pattern for pinion tooth without any modifications 109
8.5 Body deflection plot showing the transmission error for pinion tooth with topographical modifications 110
8.6 Body deflection plot showing the transmission error for pinion tooth without any modifications 111

9.1 Graph of Max ppl normal stresses against time for pinion tooth nos.20,1 and 2, for a tip radius 0.02in with a medium template 119
9.2 Graph of Max ppl normal stresses against tip radii (0.010 in-0.045 in) for medium, fineroot and finest templates 120
9.3 Graph of Max ppl normal stresses against tooth thickness (0.10in-0.16in) for medium, fineroot and finest templates 122
9.4 Graph of Max ppl normal stresses against No.of elements along the face width for medium and fineroot templates 124
9.5 Graph of Max ppl normal stresses against displacement order for medium and fineroot templates 126

10.1 Completely reversed cyclic stress plot 128
10.2 Nonzero mean stress-time pattern 129
10.3 Released tension, R=0, stress-time pattern 130
10.4 Changing amplitude stress-time pattern 130
10.5 Quasi-random stress-time pattern 131
10.6 Completely reversed ramp stress-time pattern 131
10.7 Stress-time pattern with distorted peaks 132
10.8 Schematic of the rotating-bending fatigue testing machine of the constant bending moment type 133
10.9 Stress-time pattern for point A at the surface of the critical section 133
10.10 Plot of maximum principal normal stress against time for pinion tooth no.1 using the SEARCHSTRESS menu 136
10.11 The MEDIUM.TPL template file. 137
10.12 Orientation of ξ, η and ζ on the tooth 138

10.13Plot of maximum and minimum principal normal stress for a point on the pinion tooth against time . . . 140
10.14An example of an S-N curve for predicting fatigue life . . . 142
10.15Various empirical relationships for estimating the influence of nonzero-mean stress on fatigue failure . . . 143
10.16Example of an S-N plot for wrought steel . . . 145
10.17Plot of maximum principal normal stress against time for pinion tooth no.1 using the SEARCHSTRESS menu . . . 147
10.18Plot of maximum and minimum principal stresses against time for pinion tooth for the case with rigid pinion inner diameter . . . 149
10.19Plot of maximum principal normal stress against time for pinion tooth no.1 using the SEARCHSTRESS menu . . . 151
10.20Plot of maximum and minimum principal stresses against time for pinion tooth for the case with thin flexible pinion inner diameter . . . 153
10.21S-N plot illustrating the linear damage theory . . . 155
10.22S-N curve approximation proposed by Gatt . . . 156
10.23Maximum principal normal stress plot against time for pinion tooth no.1 for a output torque of 1222.22 lbf.in . . . 158
10.24Maximum and minimum principal normal stress plot against time for pinion tooth for output torque of 1222.22 lbf.in . . . 159
10.25Maximum and minimum principal normal stress plot against time for pinion tooth for output torque of 1111.11 lbf.in . . . 160
10.26Maximum and minimum principal normal stress plot against time for pinion tooth for output torque of 500 lbf.in . . . 161
10.27Maximum and minimum principal normal stress plot against time for pinion tooth for output torque of 1000 lbf.in . . . 162

List of Tables

2.1 Units used for the test cases 4
2.2 System configuration parameters 4
2.3 Pinion input data 4
2.4 Pinion tooth input data 5
2.5 Pinion rim input data 5
2.6 Gear input data 5
2.7 Gear tooth input data 6
2.8 Gear rim input data 6
2.9 Setup input data 7
2.10 Contact menu inputs used to obtain the plot of pressure against time 8
2.11 GRIDPRHIST menu inputs used to obtain the grid pressure histogram for tooth no.1 at t=0.0 8
2.12 Toothload menu inputs used to obtain the plot of load against time 12
2.13 Toothldhist menu inputs used to obtain the tooth load histogram 12
2.14 Contact pressure values obtained from calyx and theoretical calculations for various pinion roll angles 17
2.15 Modification menu for the pinion tooth 18
2.16 Modification menu for the gear tooth 19
2.17 Toothload menu to obtain the contact load at t=0.5s 27
2.18 Toothldhist menu to obtain the tooth load histogram at t=0.5s 27
2.19 Contact pressure values for linear tip modified tooth obtained from calyx and theoretical calculations for various pinion roll angles 32
2.20 Modification menu for the pinion tooth 33
2.21 Modification menu for the gear tooth 34
2.22 Toothload menu to obtain the contact load at t=0.5s 40
2.23 Toothldhist menu to obtain the tooth load histogram at t=0.5s 40
2.24 Contact pressure values for quadratic tip modified tooth obtained from calyx and theoretical calculations for various pinion roll angles 44
2.25 Modification menu inputs used for the pinion tooth 45
2.26 Modification menu inputs used for the gear tooth 46
2.27 Toothload menu inputs used to obtain the contact load at t=0 53
2.28 Toothldhist menu inputs used to obtain the tooth load histogram at t=0 53

3.1 Setup menu inputs 58
3.2 Sub-surface menu inputs 58

4.1 Data for low contact ratio spur gear 64
4.2 Data for a high contact ratio spur gear 68
4.3 Data for a helical gear set 71

5.1 Units used for the internal helical gear set . . . 76
5.2 System configuration parameters . . . 77
5.3 Pinion data . . . 77
5.4 Pinion tooth data . . . 77
5.5 Pinion rim data . . . 78
5.6 Pinion bearing menu . . . 78
5.7 Gear data . . . 78
5.8 Gear tooth data . . . 79
5.9 Gear rim data . . . 79
5.10 Gear bearing menu . . . 79
5.11 Setup data . . . 80

6.1 Webbed rim data common to all segments . . . 84
6.2 Data for each segment of the webbed rim . . . 84

7.1 Pinion rim menu to model the internal splines . . . 89
7.2 Pinion rim menu to model the external splines . . . 92
7.3 Gear rim menu to model the external splines . . . 96
7.4 Gear rim menu to model the internal splines . . . 100

9.1 System configuration parameters . . . 114
9.2 Pinion data . . . 114
9.3 Pinion tooth data . . . 114
9.4 Modification menu for the pinion tooth . . . 115
9.5 Pinion rim data . . . 115
9.6 Gear data . . . 115
9.7 Gear tooth data . . . 116
9.8 Modification menu for the gear tooth . . . 116
9.9 Gear rim data . . . 116
9.10 Setup data . . . 117
9.11 Searchstress data . . . 118
9.12 Max ppl normal stress values for different radii . . . 120
9.13 Max ppl normal stress values for different tooth thicknesses . . . 121
9.14 Max ppl normal stress values for different number of elements along the face width 123
9.15 Max ppl normal stress values for different Displ. order . . . 125

10.1 Searchstress data . . . 139
10.2 FE probe data . . . 139
10.3 Bearing menu to specify rigid inner diameter for the pinion . . . 146
10.4 Searchstress data . . . 148
10.5 FE probe data . . . 148
10.6 Bearing menu to specify flexible inner diameter for the pinion . . . 150
10.7 Searchstress data . . . 152
10.8 FE probe data . . . 152
10.9 Fatigue life for a duty cycle . . . 157

A.1 Values of m and n for various values of θ . . . 165

Preface

The Helical3D computer program has been under development for many years, and is finally available for use by the gearing community. We have received active support and encouragement from many people. We would especially like to thank Timothy Krantz of the Army Research Laboratory at the NASA Glenn Research Center for his support and encouragement.

Sandeep Vijayakar
Samir Abad
Hilliard OH

Chapter 1

Introduction

The *Helical3D* program is used for the analysis of external and internal spur and helical gear pairs. The *Users manual* describes the various features of the *Helical3D* package. It provides detailed information to help you run the program. The *Validation manual* describes through examples some of the applications of the *Helical3D* program.

Various modeling aspects related to rim models and spline connections is discussed. Also, comparison of contact pressure and transmission error values obtained from *Calyx* with those obtained from analytical solutions is made. Test cases are documented so as to study the effect of various parameters such as tip radius, tooth thickness, number of face elements and displacement order on the stresses for helical gears and also the convergence of the stress values for different types of mesh templates. Finally the manual discusses the application of the *Helical3D* program related to fatigue theory and life prediction in helical gears.

Users should read the *Users manual* before trying out the examples in the *Validation manual*. All the files referred to in the *Validation manual* are in the Working directory created during the time of installation.

Chapter 2

Calculation of contact pressure for a spur gear model using Calyx

Following test cases are conducted to study the effects of tooth tip modifications and crowning on the contact pressure values for a spur gear pair and also to compare those values obtained from *Calyx* with theoretical results. A detailed procedure for calculating the contact pressure using the $Helical3D$ program in each case is given.

2.1 Contact pressure for spur gear model with no tooth tip modifications

This first example compares *Calyx's* predictions of contact pressure on unmodified spur gear teeth with those obtained from Hertz's equations. Simple involute calculations are used to obtain radii of curvature for Hertz's model.

2.1.1 The example file

After hitting the CONNECT button, choose the CONTACTPRESSURE directory under the SAMPLES directory. This in turn is located in the Working directory `WORKDIR` selected by the User at the installation time. Load the file `nomodification.ses` from the `CONTACTPRESSURE` directory.

As the session file name suggests no tooth tip modifications are applied at the gear or pinion tooth for this case. All the data describing the model is entered in the submenus of the EDIT menu. The data for the example problem is given in English units (force is in lbf, and length is in in). The outputs also appear in English units. Table 2.1 shows the English units for common physical quantities used to run the test cases.

Tables 2.2 through 2.9 show the data to be entered in the EDIT menu for running the analysis. No assembly errors are considered for the pinion and the gear. Also there are no bearings in the model.

Table 2.1: Units used for the test cases

Physical quantity	English
LENGTH	in
TIME	s
ANGLE	deg or rad
MASS	lbf.s^2/in
MOMENT OF INERTIA	lbf.s^2.in
STIFFNESS	lbf/in
SPEED	RPM or rad/s
TORQUE	lbf.in
YOUNGS MODULUS	lbf/in^2
DENSITY	lbf.s^2/in^4
LOAD	lbf
STRESSES	psi

Table 2.2: System configuration parameters

Item	Description
MESHTYPE	CALYX3D
CENTERDIST	3.00
OFFSET	0.00
ROTX	0.00
ROTY	0.00
INPUT	PINION
TORQUEINPUT	1000.00
RPMINPUT	-3.00
MU	0.00
MAGRUNOUTGEAR	0.00
ANGRUNOUTGEAR	0.00
MAGRUNOUTPINION	0.00
ANGRUNOUTPINION	0.00
BACKSIDECONTACT	FALSE

Table 2.3: Pinion input data

Item	Description
LUMPMASS	0.00
LUMPMOMINERTIA	0.00
LUMPALPHA	0.00

Table 2.4: Pinion tooth input data

Item	Description
NTEETH	20
NFACEELEMS	4
COORDORDER	10
DISPLORDER	3
PLANE	TRANSVERSE
XVERSEDIAMPITCH	10
XVERSEPRESSANGLE	20
XVERSETHICK	0.15708
FACEWIDTH	1
HAND	LEFT
HELIXANGLE	0.00
RACKTIPRAD	0.02
OUTERDIA	2.18
ROOTDIA	1.76
RIMDIA	1.40
YOUNGSMOD	$3x10^7$
POISSON	0.3
MSHFILE	pinion.msh
TPLFILE	medium.tpl

Table 2.5: Pinion rim input data

Item	Description
RIMTYPE	SIMPLE
RIMDIA	1.40
INNERDIA	1.20
WIDTH	1.00
OFFSET	0.00
AXIALORDER	2
CIRCORDER	8
ELEMTYPE	LINEAR
NDIVSRADIAL	2
NTHETA	32
NDIVSWIDTH	4

Table 2.6: Gear input data

Item	Description
TYPE	EXTERNAL
LUMPMASS	0.00
LUMPMOMINERTIA	0.00
LUMPALPHA	0.00

Table 2.7: Gear tooth input data

Item	Description
NTEETH	40
NFACEELEMS	4
COORDORDER	10
DISPLORDER	3
PLANE	TRANSVERSE
XVERSEDIAMPITCH	10
XVERSEPRESSANGLE	20
XVERSETHICK	0.15708
FACEWIDTH	1
HAND	RIGHT
HELIXANGLE	0.00
RACKTIPRAD	0.02
OUTERDIA	4.18
ROOTDIA	3.78
RIMDIA	3.40
YOUNGSMOD	$3x10^7$
POISSON	0.3
MSHFILE	gear.msh
TPLFILE	medium.tpl

Table 2.8: Gear rim input data

Item	Description
RIMTYPE	SIMPLE
RIMDIA	3.40
INNERDIA	2.40
WIDTH	1.00
OFFSET	0.00
AXIALORDER	2
CIRCORDER	16
ELEMTYPE	QUADRATIC
NDIVSRADIAL	4
NTHETA	64
NDIVSWIDTH	4

Table 2.9: Setup input data

Item	Description
SEPTOL	0.01
NPROFDIVS	8
NFACEDIVS	12
DSPROF	0.001
ZEROINITIAL	TRUE
INITIALTIME	-0.8
NRANGES	1
RANGE	1
SOLMETHOD	STATIC
NTIMESTEPS	15
DELTATIME	0.1
STARTSPEEDFACTOR	1.0
STARTTORQUEFACTOR	1.0
ENDTORQUEFACTOR	1.0
SAVEPERIODICALLY	FALSE
OUTPUTRESTART	FALSE
POSTPROCWRITE	TRUE
POSTFILENAME	postprocnotipmod.dat
NSTEPSWRITE	1

Table 2.10: Contact menu inputs used to obtain the plot of pressure against time

Item	Description
SURFACEPAIR	GEAR_SURFACE1_PINION_SURFACE1
MEMBER	PINION
TOOTHBEGIN	1
TOOTHEND	1
BEGINSTEP	1
ENDSTEP	15
SPROFBEGIN	0.0
SPROFEND	48.0
TFACEBEGIN	-1.0
TFACEEND	1.0
OUTPUTTOFILE	FALSE

Table 2.11: GRIDPRHIST menu inputs used to obtain the grid pressure histogram for tooth no.1 at t=0.0

Item	Description
SURFACEPAIR	GEAR_SURFACE1_PINION_SURFACE1
MEMBER	PINION
TOOTHBEGIN	1
TOOTHEND	1
TIMESTEP	8
OUTPUTTOFILE	FALSE

2.1.2 Obtaining the contact pressure from the postprocessing menu

During the analysis, a post processing data file is created in the working directory. The CONTACT command in the postprocessing menu is used to obtain the contact pressure at a particular instant. At $t = 0$, the pinion tooth no.1 is in contact with the gear tooth no.1 at the pitch point. Figure 2.1 shows the contact pressure plot against time. Table 2.10 shows the inputs in the contact menu used to obtain this plot. The exact value of the contact pressure at the pitch point can be obtained from the GRIDPRHIST plot at $t = 0$ as shown in Figure 2.2. The menu for such a plot is shown in Table 2.11.

The contact pressure obtained from *calyx* is $1.5961 \times 10^5 psi$.

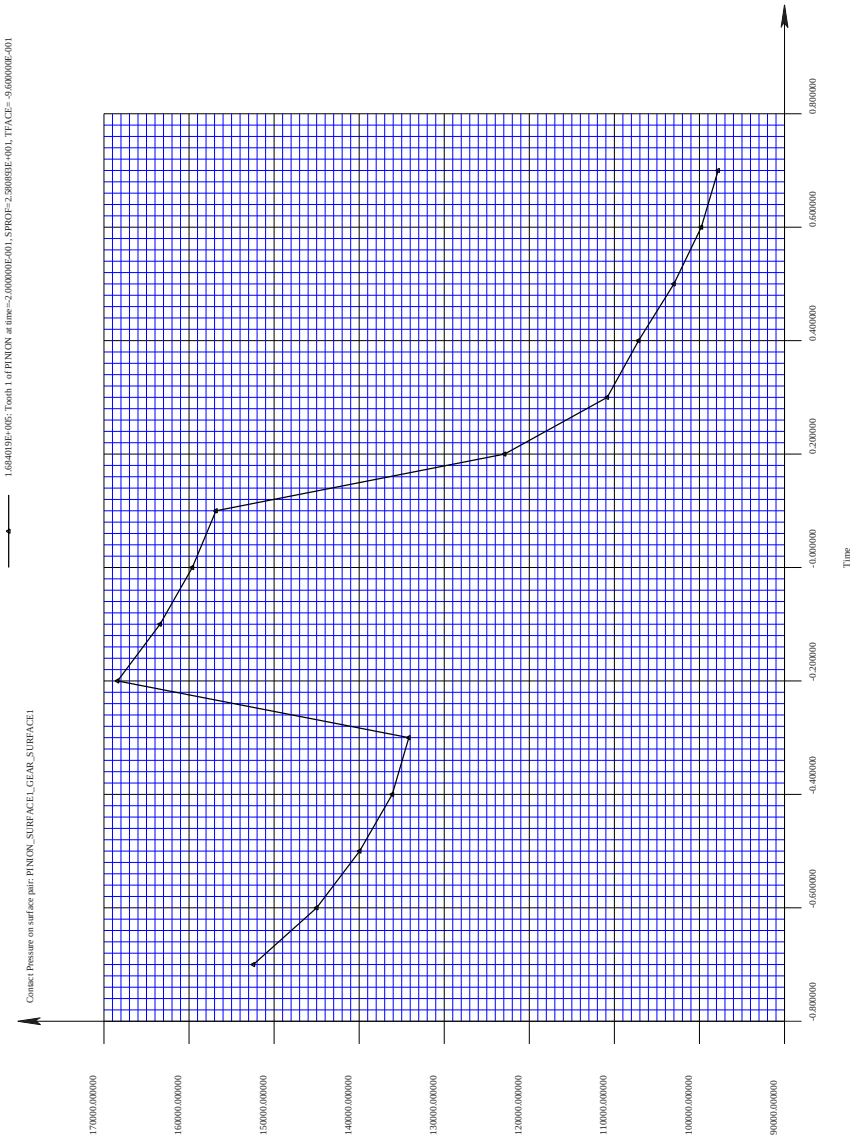

Figure 2.1: Graph of contact pressure against time for pinion tooth no.1

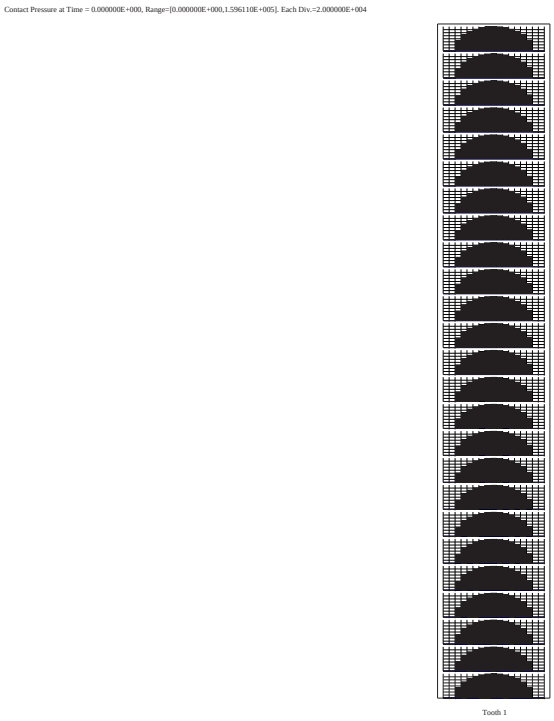

Figure 2.2: Grid pressure histogram for pinion tooth no.1 at t=0 (Contact Pressure = 1.596110E+005 at Time = 0.000000E+000. Range of contact pressure is from 0.000000E+000 to 1.596110E+005 and each division corresponds to 2.000000E+004)

2.1.3 Contact pressure from theoretical calculations

Relative Radius of curvature

As shown in Figure 2.3 an involute curve is evolved from origin point A on a base circle. The point P on a taut line containing point B describes the curve. The taut line is tangent to the base circle at point B, and normal to the involute curve at P. The length of this line segment BP is the *Radius of curvature(R)* of the involute curve at point P and is equal in length to the arc AB. The angle θ subtended by the arc AB is the roll angle of the involute to the point P.

For the Pinion,

$$\begin{aligned}
\text{Pitch diameter}, D_p &= 2.0in \\
\text{Pitch radius}, r_p &= 1.0in \\
\text{Pressure angle}, \phi &= 20.0^o \\
\text{Base radius}, r_b &= r_p cos\phi = 0.9396in \\
\text{Involute roll angle at pitch point}, \theta_p &= \sqrt{(\frac{r_p}{r_b})^2 - 1} = 0.3642rad \\
\text{Radius of curvature}, R_p &= r_b \times \theta_p = 0.342in
\end{aligned}$$

For the Gear,

$$\begin{aligned}
\text{Pitch diameter}, D_p &= 4.0in \\
\text{Pitch radius}, r_p &= 2.0in \\
\text{Pressure angle}, \phi &= 20.0^o \\
\text{Base radius}, r_b &= r_p cos\phi = 1.879in \\
\text{Involute roll angle at pitch point}, \theta_p &= \sqrt{(\frac{r_p}{r_b})^2 - 1} = 0.3642rad \\
\text{Radius of curvature}, R_g &= r_b \times \theta_p = 0.6839in
\end{aligned}$$

Hence,

$$\text{The Relative radius of curv}, \rho = \frac{R_p R_g}{R_p + R_g} = 0.216in \tag{2.1}$$

Calculating the Contact load

$$\begin{aligned}
\text{The total load on all teeth} &= Torque/r_b \\
\text{The total contact load per unit length}, P &= \frac{Torque/r_b}{Facewidth} = 1.064 \times 10^3 lbf/in
\end{aligned} \tag{2.2}$$

The user can find the contact load acting on individual teeth using the TOOTHLOAD or the TOOTHLDHIST command in the postprocessing menu. Figure 2.4 shows the plot of contact load against time for the pinion tooth no.1. Table 2.12 shows the TOOTHLOAD menu to obtain this plot. Figure 2.5 shows the tooth load histogram. Table 2.13 shows the data entered in to the TOOTHLDHIST menu in order to obtain this plot. The value of the contact load at the pitch point from the tooth load plot is $1.0641 \times 10^3 lbf$.

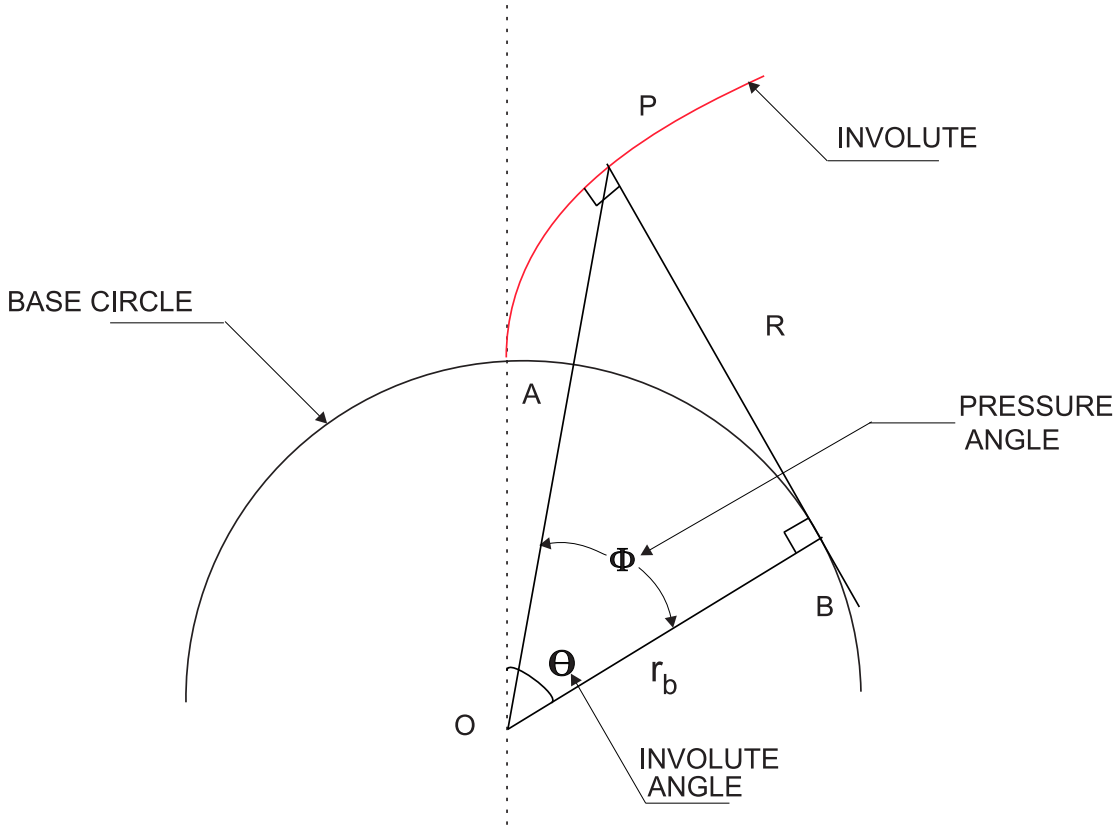

Figure 2.3: Drawing defining the radius of curvature(R) and the roll angle(θ)

Table 2.12: Toothload menu inputs used to obtain the plot of load against time

Item	Description
SURFACEPAIR	PINION_SURFACE1_GEAR_SURFACE1
MEMBER	PINION
TOOTHBEGIN	1
TOOTHEND	1
BEGINSTEP	1
ENDSTEP	15

Table 2.13: Toothldhist menu inputs used to obtain the tooth load histogram

Item	Description
SURFACEPAIR	PINION_SURFACE1_GEAR_SURFACE1
MEMBER	PINION
TIMESTEP	8
HISTCOLOR	BLACK
AUTOSCALE	TRUE
OUTPUTTOFILE	FALSE

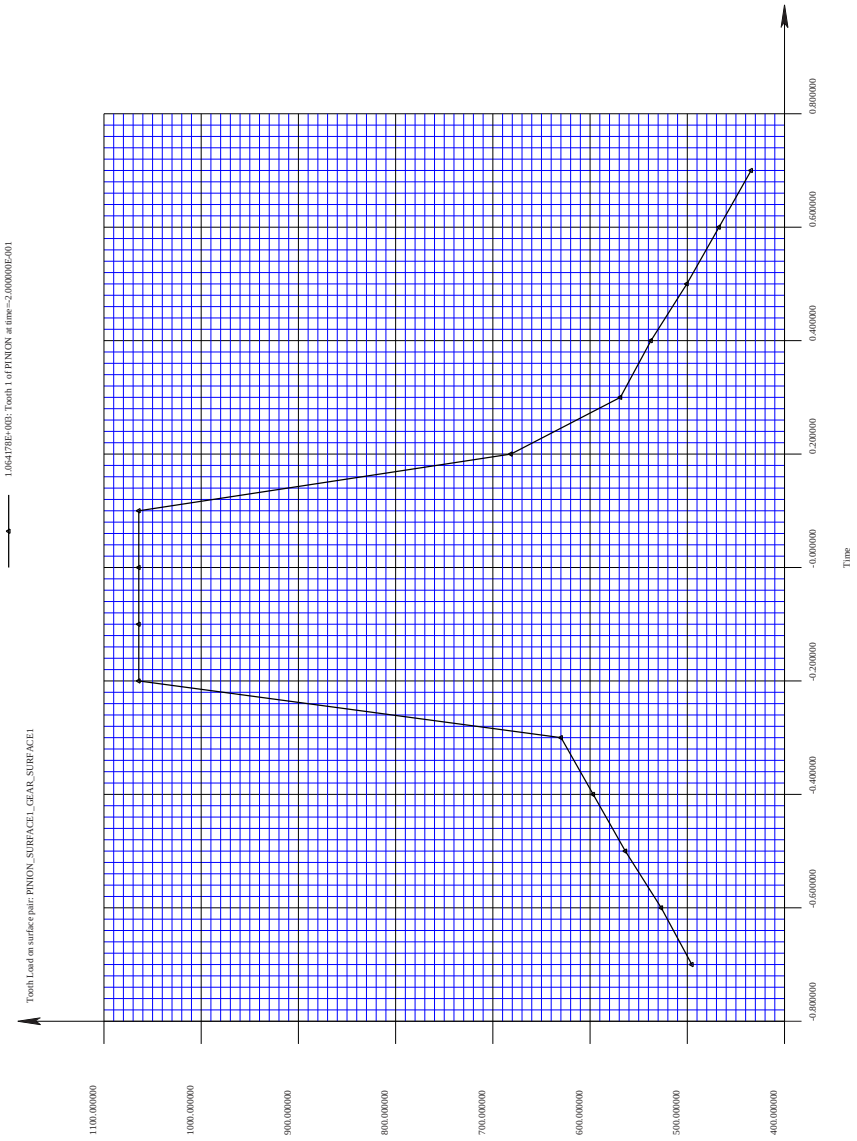

Figure 2.4: Plot of tooth load against time for pinion tooth no.1

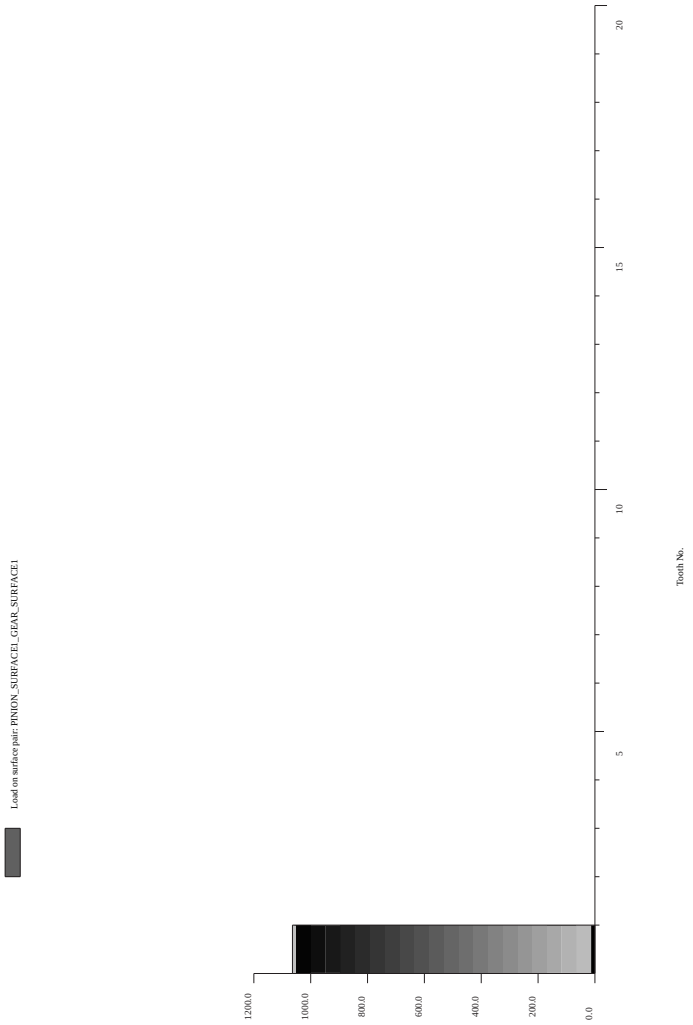

Figure 2.5: Toothload histogram at t=0.0

Calculating the Contact Pressure

For the present case, since we have not applied any tooth modifications, the contact between the pinion and gear tooth can be assumed to be a two dimensional contact of cylindrical bodies. Using the Hertz theory of elastic contact [20] for such cases the maximum pressure, p_o is given by,

$$p_o = \sqrt{\frac{PE_{eq}}{\pi\rho}} \tag{2.3}$$

where,

$$\begin{aligned}
p_o &= \text{ Maximum Contact pressure} \\
P &= \text{ Contact load } = \ 1.0641 \times 10^3 lbf/in \\
\rho &= \text{ Relative radius of curvature } = \ 0.216in \\
\nu_p &= \text{ Pinion Poissons ratio } = \ 0.3 \\
\nu_g &= \text{ Gear Poissons ratio } = \ 0.3 \\
E_p &= \text{ Pinion Young's modulus } = \ 3 \times 10^7 psi \\
E_g &= \text{ Gear Young's modulus } = \ 3 \times 10^7 psi \\
\frac{1}{E_{eq}} &= \ \frac{1-\nu_p^2}{E_p} + \frac{1-\nu_g^2}{E_g} = \ 1.6483516 \times 10^7 psi^{-1}
\end{aligned}$$

Substituting the values, the theoretical(Hertz) contact pressure is $1.5648 \times 10^5 psi$ compared to $1.5961 \times 10^5 psi$ obtained from *Calyx*. The contact pressure prediction at the mid-face (Range of TFACE is from -0.5 to 0.5) from Calyx is $1.5843 \times 10^5 psi$. The difference in the predicted contact pressure at mid-face as compared to the end of the face is $1.18 \times 10^3 psi$.

Table 2.14 shows the comparison of contact pressure values for pinion tooth no.1 obtained from *Calyx* and the theoretical calculations at various roll angles. The spreadsheet used to carry out the calculations shown in Table 2.14 is in file `nomodification.xls` in the `CONTACTPRESSURE` directory. A graph comparing *Calyx's* and Hertz's predictions is shown in Figure 2.6. This example shows that the predictions made by *Calyx* are very close to Hertz pedictions. *Calyx* predicts contact pressures about 3% higher than the Hertz formula.

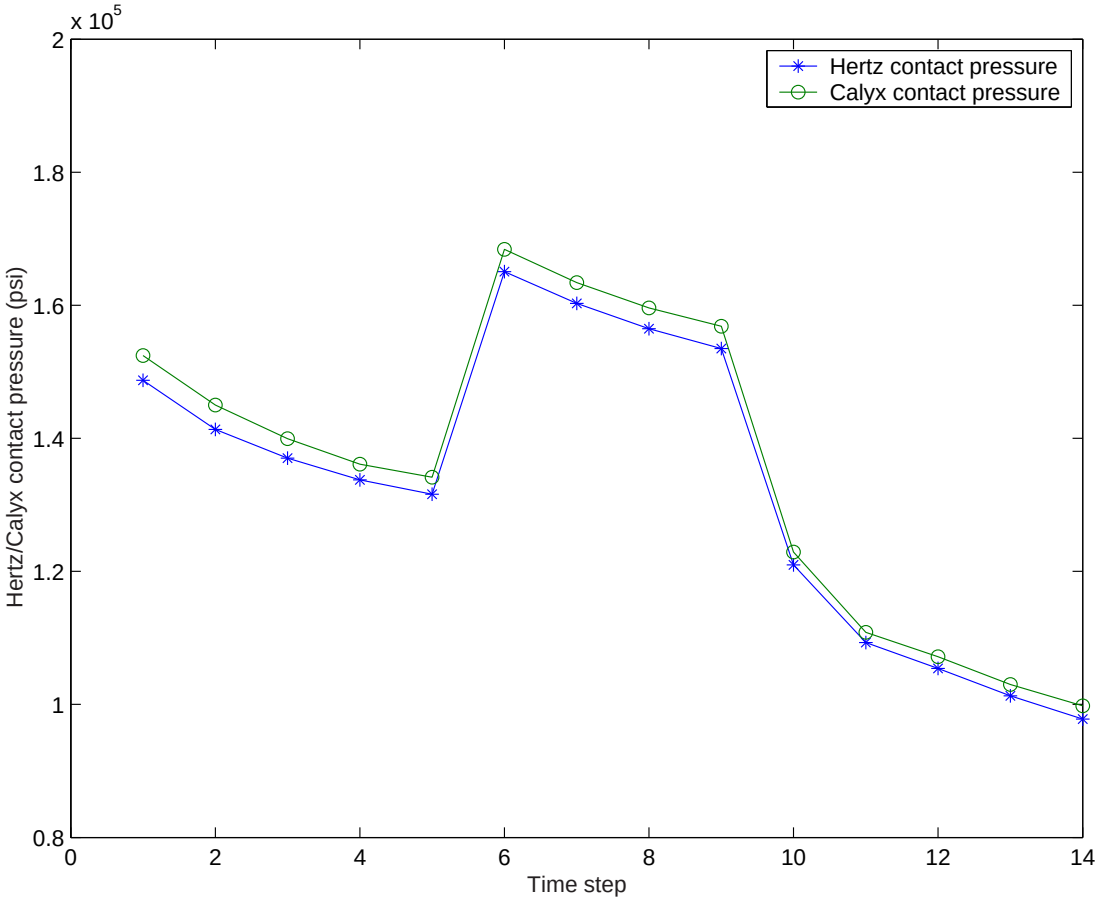

Figure 2.6: A graph comparing Calyx's and Hertz's contact pressure predictions

Table 2.14: Contact pressure values obtained from calyx and theoretical calculations for various pinion roll angles

Time (s)	Pinion involute roll angle (deg)	Gear involute roll angle (deg)	Pinion radius of curv (in)	Gear radius of curv (in)	Effective radius of curv (in)	Contact load (lbf/in)	Hertz contact pressure (psi)	Calyx contact pressure (psi)
-0.7	8.2539	27.1539	0.1353	0.8906	0.1175	495.34	1.4871×10^5	1.5243×10^5
-0.6	10.0539	26.2539	0.1648	0.8611	0.1383	526.80	1.4132×10^5	1.4499×10^5
-0.5	11.8539	25.3539	0.1944	0.8316	0.1575	563.73	1.3700×10^5	1.3994×10^5
-0.4	13.6539	24.4539	0.2239	0.8021	0.1750	596.79	1.3374×10^5	1.3611×10^5
-0.3	15.4539	23.5539	0.2534	0.7726	0.1908	629.82	1.3158×10^5	1.3416×10^5
-0.2	17.2539	22.6539	0.2829	0.7430	0.2049	1064.1	1.6506×10^5	1.6840×10^5
-0.1	19.0539	21.7539	0.3124	0.7135	0.2173	1064.1	1.6028×10^5	1.6340×10^5
0.0	20.8539	20.8539	0.3420	0.6840	0.2280	1064.1	1.5648×10^5	1.5961×10^5
0.1	22.6539	19.9539	0.3715	0.6545	0.2370	1064.1	1.5348×10^5	1.5683×10^5
0.2	24.4539	19.0539	0.4010	0.6249	0.2442	681.39	1.2097×10^5	1.2290×10^5
0.3	26.2539	18.1539	0.4305	0.5954	0.2498	568.83	1.0928×10^5	1.1084×10^5
0.4	28.0539	17.2539	0.4601	0.5659	0.2537	537.37	1.0540×10^5	1.0715×10^5
0.5	29.8539	16.3539	0.4896	0.5364	0.2559	500.44	1.0128×10^5	1.0300×10^5
0.6	31.6539	15.4539	0.5191	0.5069	0.2564	467.38	9.7782×10^4	9.9784×10^4
0.7	33.4539	14.5539	0.5486	0.4773	0.2552	434.35	9.4485×10^4	9.7802×10^4

2.2 Contact pressure for spur gear model with linear tooth tip modification

Applying a surface modification affects stresses in two ways. Firstly, it changes the load distribution between teeth. Secondly, it affects the curvature of the surfaces. This example illustrates this effect.

2.2.1 The example file

Load the file `lineartipmodification.ses` from the `CONTACTPRESSURE` directory.

To study the effect of linear tip relief on contact pressure, a linear tip modification is applied on pinion and gear tooth as shown in Figures 2.7 and 2.8. Tables 2.15 and 2.16 show the modification menus for pinion and gear teeth respectively. All the other menus including the setup menu are similar to the case with no tooth modifications.

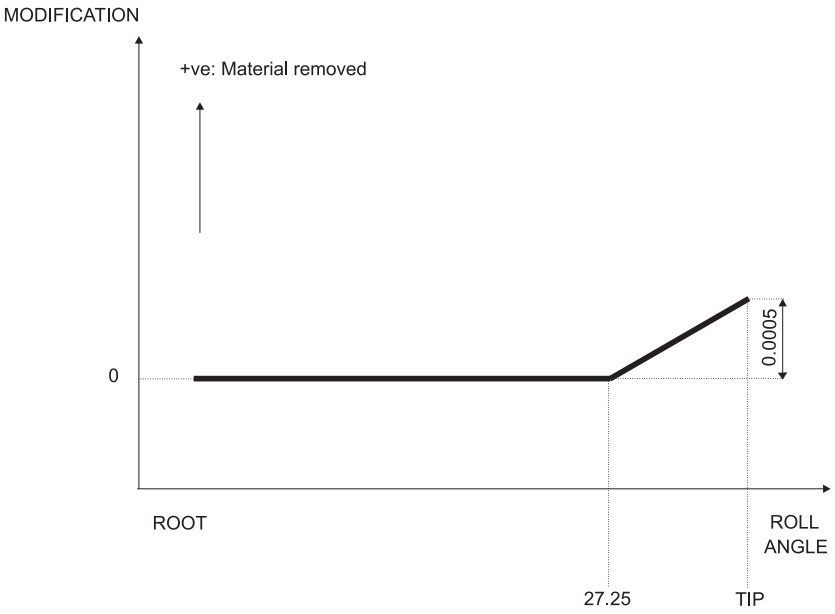

Figure 2.7: Linear tip relief applied to the pinion tooth

Table 2.15: Modification menu for the pinion tooth

Item	Description
LINEARTIPMOD	TRUE
ROLLLINEARTIPMOD	27.25
MAGLINEARTIPMOD	0.0005

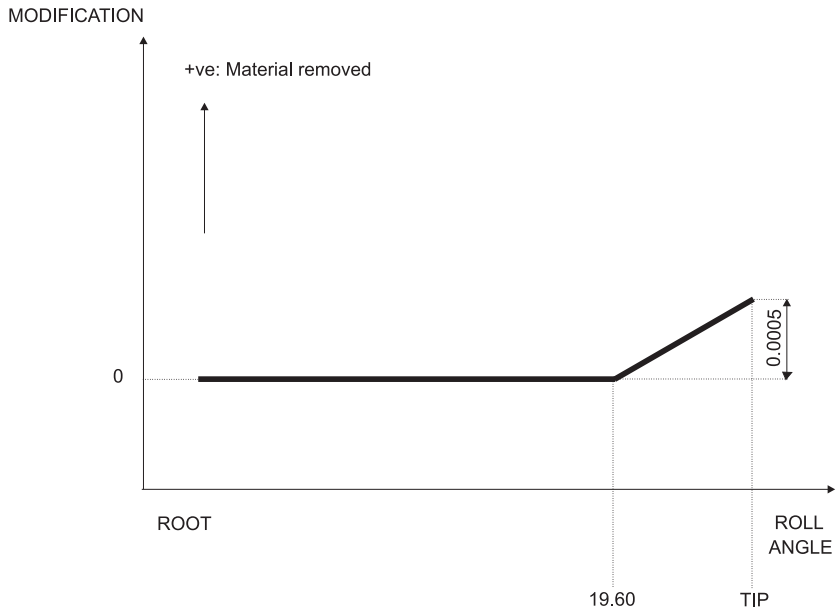

Figure 2.8: Linear tip relief applied to the gear tooth

Table 2.16: Modification menu for the gear tooth

Item	Description
LINEARTIPMOD	TRUE
ROLLLINEARTIPMOD	19.60
MAGLINEARTIPMOD	0.0005

2.2.2 Obtaining the contact pressure from the postprocessing menu

After the analysis is complete, a post processing data file is created in the working directory. CONTACT command in the postprocessing menu is used to obtain the contact pressure at a particular instant. Figure 2.9 shows the plot of contact pressure against time for pinion tooth no.1. The involute roll angle,θ at the start, θ_i, and at the tip, θ_o, of the linear tip relief for the pinion tooth is 27.25^o and 33.68^o respectively. At $t = 0$, the pinion tooth no.1 is in contact with the gear tooth no.1 at the pitch point. In order to look at the contact pressure value for the pinion in the tip relief region a value of θ somewhere between the start and the tip of the modified tooth is considered. The contact pressure value from the postprocessing menu at $t = 0.5s$ is $1.1832 \times 10^5 psi$. The exact value of the contact pressure at t=0.5s can be obtained by plotting the GRIDPRHIST plot as shown in Figure 2.10.

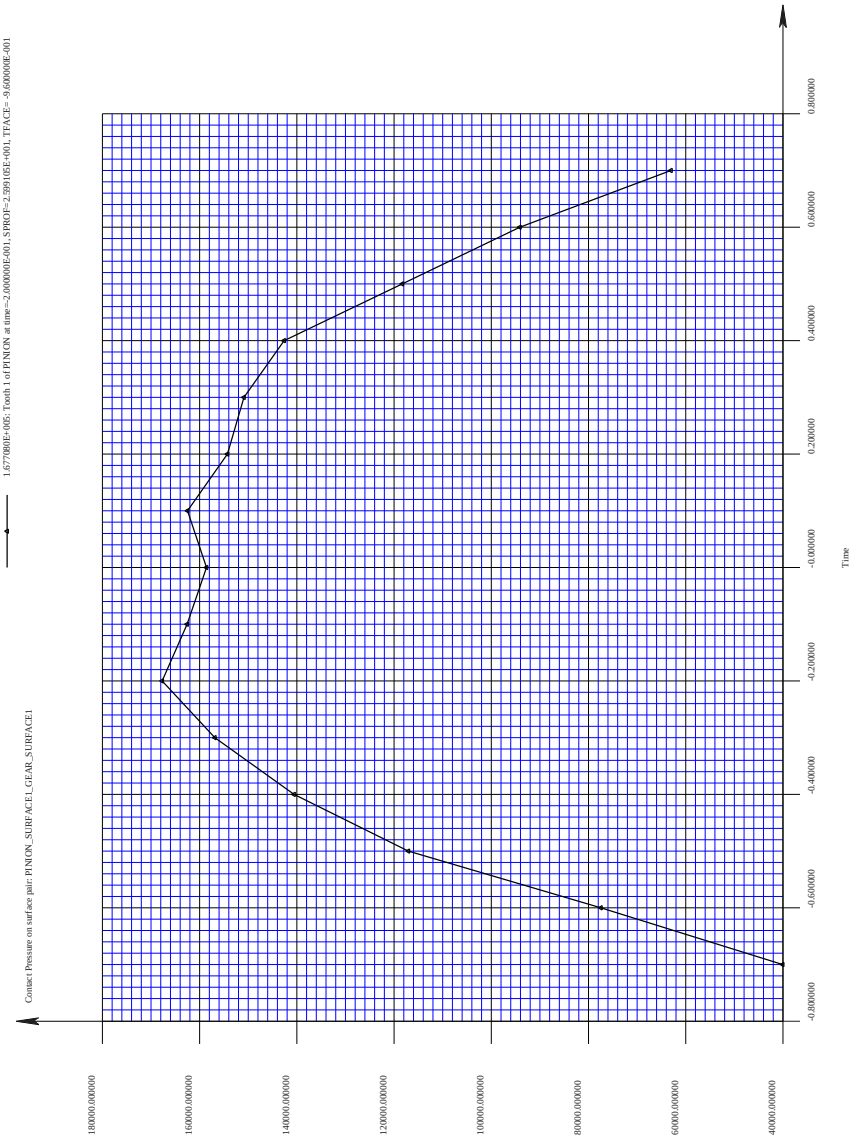

Figure 2.9: Graph of contact pressure against time for pinion tooth no.1

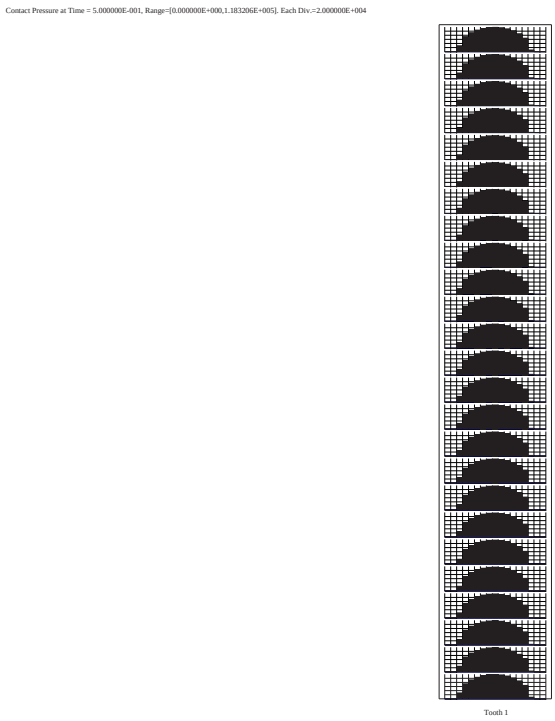

Figure 2.10: Grid pressure histogram for pinion tooth no.1 at t=0.5s (Contact Pressure at Time = 5.000000E-001s. Range of contact pressure is from 0.000000E+000 to 1.183206E+005 and each division corresponds to 2.000000E+004

2.2.3 Obtaining contact pressure from theoretical calculations

Relative Radius of curvature

S.Vijayakar [14] showed that applying tip relief changes the curvature of the surface significantly. The following derivation gives the formula for calculating the curvatures for an involute with linear tip modification.

If θ is the involute roll angle at a particular point on a involute curve, then the position vector and its derivatives for a point $r(\theta)$ on an unmodified involute curve are given by:

$$\begin{aligned}
r_x(\theta) &= r_b\sqrt{1+\theta^2}(\sin(\theta-\tan^{-1}\theta)) \\
r_y(\theta) &= r_b\sqrt{1+\theta^2}(\cos(\theta-\tan^{-1}\theta)) \\
\frac{dr_x}{d\theta} &= r_b\theta(\sin(\theta)) \\
\frac{dr_y}{d\theta} &= r_b\theta(\cos(\theta)) \\
\frac{d^2r_x}{d\theta^2} &= r_b(\sin(\theta)+\theta\cos(\theta)) \\
\frac{d^2r_y}{d\theta^2} &= r_b(\cos(\theta)-\theta\sin(\theta))
\end{aligned}$$

The unit normal vector to the involute and its derivatives are:

$$\begin{aligned}
n_x(\theta) &= -\cos(\theta) \\
n_y(\theta) &= +\sin(\theta) \\
\frac{dn_x}{d\theta} &= +\sin(\theta) \\
\frac{dn_y}{d\theta} &= +\cos(\theta) \\
\frac{d^2n_x}{d\theta^2} &= +\cos(\theta) \\
\frac{d^2n_y}{d\theta^2} &= -\sin(\theta)
\end{aligned}$$

If e(θ) is the modification for the involute at a particular roll angle θ, E is the magnitude of the linear modification at the tip, and θ_i and θ_o are the roll angles at the start of modification and at the tip, respectively, then the value of linear modification in the relieved part of the involute is:

$$\begin{aligned}
e(\theta) &= E\frac{\theta-\theta_i}{\theta_o-\theta_i} \\
\frac{de}{d\theta} &= \frac{E}{\theta_o-\theta_i} \\
\frac{d^2e}{d\theta^2} &= 0.0
\end{aligned}$$

The coordinate vector R and its derivatives for the *modified* involute is given by:

$$\begin{aligned}
R_x(\theta) &= r_x(\theta) - n_x(\theta)e(\theta) \\
R_y(\theta) &= r_y(\theta) - n_y(\theta)e(\theta) \\
\frac{dR_x}{d\theta} &= \frac{dr_x}{d\theta} - \frac{dn_x}{d\theta}e(\theta) - n_x(\theta)\frac{de}{d\theta} \\
\frac{dR_y}{d\theta} &= \frac{dr_y}{d\theta} - \frac{dn_y}{d\theta}e(\theta) - n_y(\theta)\frac{de}{d\theta} \\
\frac{d^2R_x}{d\theta^2} &= \frac{d^2r_x}{d\theta^2} - \frac{d^2n_x}{d\theta^2}e(\theta) - 2\frac{dn_x}{d\theta}\frac{de}{d\theta} - n_x\frac{d^2e}{d\theta^2} \\
\frac{d^2R_y}{d\theta^2} &= \frac{d^2r_y}{d\theta^2} - \frac{d^2n_y}{d\theta^2}e(\theta) - 2\frac{dn_y}{d\theta}\frac{de}{d\theta} - n_y\frac{d^2e}{d\theta^2}
\end{aligned}$$

The unit normal vector for the modified involute is:

$$\begin{aligned}
N_x(\theta) &= \frac{-\frac{dR_y}{d\theta}}{\sqrt{(\frac{dR_x}{d\theta})^2 + (\frac{dR_y}{d\theta})^2}} \\
N_y(\theta) &= \frac{\frac{dR_x}{d\theta}}{\sqrt{(\frac{dR_x}{d\theta})^2 + (\frac{dR_y}{d\theta})^2}}
\end{aligned}$$

The curvature of this modified involute is given by:

$$K(\theta) = \frac{N_x(\theta)\frac{d^2R_x}{d\theta^2} + N_y(\theta)\frac{d^2R_y}{d\theta^2}}{(\frac{dR_x}{d\theta})^2 + (\frac{dR_y}{d\theta})^2}$$

If the curvatures, K_{pinion} and K_{gear} of the pinion and gear are calculated in this manner, then the relative radius of curvature between the two is given by:

$$\rho = \frac{1}{K_{pinion} + K_{gear}} \tag{2.4}$$

Note that for our study case we will examine an instant of time where we need to apply the modified curvature only for the pinion tooth.

Calculating the value of θ at $0.5s$

Angular velocity of the pinion, $\omega_p = 3.0rpm = 0.31415rad/s$.

Therefore,
Rotation of the pinion in $0.5s = 0.5 \times 0.31415 = 0.1570rad$.
At $t = 0.0$(pitch point), the involute roll angle $= 0.36427rad$.

Thus,
At $t = 0.5s$, the pinion involute roll angle, $\theta = 0.36427 + 0.1570 = 0.5213rad$.
At $t = 0.5s$, the gear involute roll angle, $\theta = 0.36427 - (\frac{r_{bp}}{r_{bg}})0.1570 = 0.2854rad$.

For the pinion:

Base radius of the pinion is:

$$r_{bp} = 0.9396in$$

Involute roll angle at $0.5s$ is:

$$\theta = 29.85^o = 0.5213rad$$

Involute roll angle at the start of modification is:

$$\theta_i = 27.21^o = 0.475rad$$

Involute roll angle at the tip of modification is:

$$\theta_o = 33.68^o = 0.588rad$$

Modification at the tip is:

$$E = 0.0005in$$

If e(θ) is the modification for the involute at a roll angle $\theta = 29.85^o$, then,

$$\begin{aligned} e(\theta) &= 0.000204in \\ \frac{de}{d\theta} &= 0.004424in/rad \\ \frac{d^2e}{d\theta^2} &= 0.00 \end{aligned}$$

The position vector and its derivatives for a point r(θ) on an unmodified involute curve are given by:

$$\begin{aligned} r_x(\theta) &= 0.043118 \\ r_y(\theta) &= 1.058724 \\ \frac{dr_x}{d\theta} &= 0.243731 \\ \frac{dr_y}{d\theta} &= 0.424651 \\ \frac{d^2r_x}{d\theta^2} &= 0.892422 \\ \frac{d^2r_y}{d\theta^2} &= 0.571260 \end{aligned}$$

The unit normal vector to the involute and its derivatives are:

$$\begin{aligned} n_x(\theta) &= -0.867297 \\ n_y(\theta) &= 0.497791 \\ \frac{dn_x}{d\theta} &= 0.497791 \\ \frac{dn_y}{d\theta} &= 0.867297 \\ \frac{d^2n_x}{d\theta^2} &= 0.867297 \\ \frac{d^2n_y}{d\theta^2} &= -0.497791 \end{aligned}$$

The coordinate vector R and its derivatives for the *modified* involute is given by:

$$\begin{aligned} R_x(\theta) &= 0.043295 \\ R_y(\theta) &= 1.058622 \\ \frac{dR_x}{d\theta} &= 0.247467 \\ \frac{dR_y}{d\theta} &= 0.422272 \\ \frac{d^2R_x}{d\theta^2} &= 0.887840 \\ \frac{d^2R_y}{d\theta^2} &= 0.563687 \end{aligned}$$

The unit vector for the modified involute is:

$$\begin{aligned} N_x(\theta) &= -0.862761 \\ N_y(\theta) &= 0.505611 \end{aligned}$$

The curvature of this modified involute is:

$$K_p = 2.007843 in^{-1}$$

For the gear:

Base radius of the gear is:

$$r_{bg} = 1.8793in$$

Involute roll angle at 0.5s is:

$$\theta = 16.3539^o = 0.2854rad$$

The curvature of this unmodified involute is:

$$K_g = \frac{1}{r_{bg}\theta} = 1.864162in^{-1}$$

Thus, the relative radius of curvature is:

$$\rho = \frac{1}{(K_p + K_g)} = 0.258264in$$

Calculating the Contact load

The user can find the contact load on individual teeth using the TOOTHLOAD or the TOOTHLDHIST command in the postprocessing menu. Table 2.17 shows the TOOTHLOAD menu inputs used to obtain the contact load value at $t = 0.5s$. Figure 2.11 shows the tooth load histogram at $t = 0.5s$. Table 2.18 shows the TOOTHLDHIST menu inputs used to obtain this plot. The value of contact load at $t = 0.5s$ from the tooth load plot is $6.6757\times\ 10^2 lbf$.

$$\text{Contact load per unit length} \quad = \quad \frac{\text{Contact load}}{\text{Facewidth}} = 6.6757 \times 10^2 lbf/in \tag{2.5}$$

Table 2.17: Toothload menu to obtain the contact load at t=0.5s

Item	Description
SURFACEPAIR	PINION_SURFACE1_GEAR_SURFACE1
MEMBER	PINION
TOOTHBEGIN	1
TOOTHEND	1
BEGINSTEP	13
ENDSTEP	13

Table 2.18: Toothldhist menu to obtain the tooth load histogram at t=0.5s

Item	Description
SURFACEPAIR	PINION_SURFACE1_GEAR_SURFACE1
MEMBER	PINION
TIMESTEP	13
HISTCOLOR	BLACK
AUTOSCALE	TRUE
OUTPUTTOFILE	FALSE

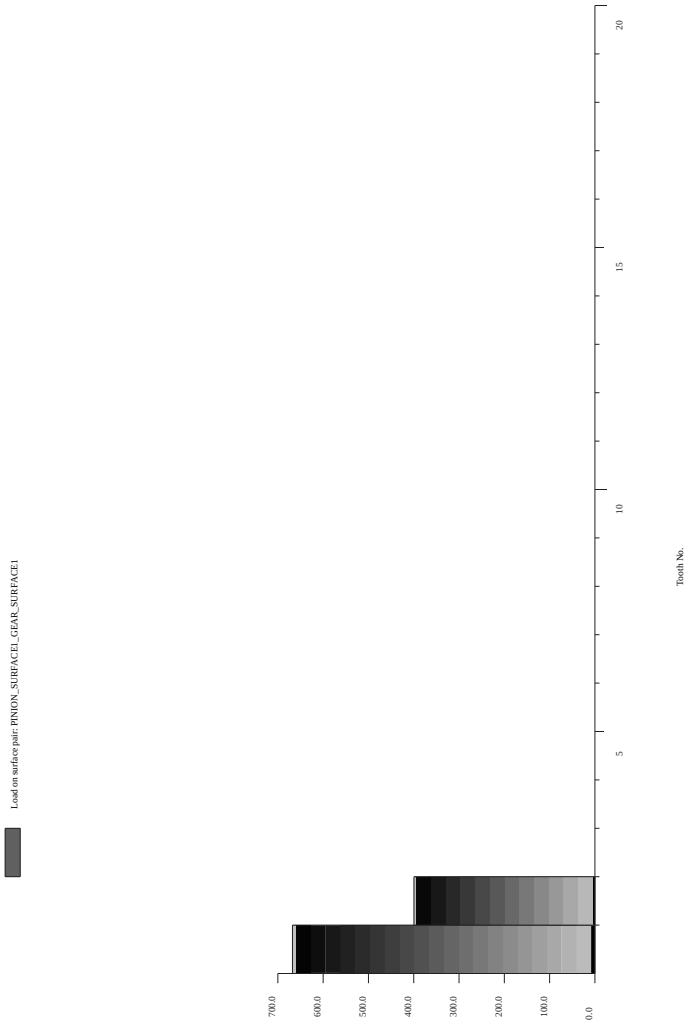

Figure 2.11: Toothload histogram at t=0.5s

Calculating the Contact Pressure

For the present case, since we have not applied any lead modifications the contact between the pinion and gear tooth can be assumed to be a two dimensional contact of cylindrical bodies. Using the Hertz theory of elastic contact for such cases the maximum pressure, p_o is given by,

$$p_o = \sqrt{\frac{PE_{eq}}{\pi\rho}} \tag{2.6}$$

where,

$$\begin{aligned}
p_o &= \text{Maximum Contact pressure} \\
P &= \text{Contact load per unit length} = 6.6757 \times 10^2 lbf/in \\
\rho &= \text{Relative radius of curvature} = 0.258264in \\
\nu_p &= \text{Pinion Poissons ratio} = 0.3 \\
\nu_g &= \text{Gear Poissons ratio} = 0.3 \\
E_p &= \text{Pinion Young's modulus} = 3 \times 10^7 psi \\
E_g &= \text{Gear Young's modulus} = 3 \times 10^7 psi \\
\frac{1}{E_{eq}} &= \frac{1-\nu_p^2}{E_p} + \frac{1-\nu_g^2}{E_g}
\end{aligned}$$

E_{eq} from above $= 1.648351 \times 10^7 psi$

Substituting the above values the theoretical contact pressure is $1.16457 \times 10^5 psi$, compared with $1.18321 \times 10^5 psi$ predicted by *Calyx*.

Table 2.19 shows the comparison of contact pressure values for pinion tooth no.1 obtained from *Calyx* and the Hertz calculations at various roll angles. The spreadsheet used to carry out the calculations shown in Table 2.19 is in file `lineartipmodification.xls` in the `CONTACTPRESSURE` directory. A graph comparing *Calyx's* and Hertz's predictions is shown in Figure 2.12. The peak at $t = 0.14s$ corresponding to Invoute angle for gear $= 19.60^o$ obtained in the contact pressure plot from *Calyx* is due to the start of the linear modification at the gear tooth. At this point the radius of curvature tends to 0.0 and hence we get a high value of contact pressure ($1.7650 \times 10^5 psi$). Hertz formula does not take in to consideration the change in curvature at the start of modification. Hence we do not see the peak in the contact pressure predictions from the Hertz theory. Figure 2.13 shows a plot of contact pressure against time obtained from *Calyx* in the time range from $0.0s$ to $0.2s$. The peak is clearly seen at $t = 0.14s$. This example shows that the predictions made by *Calyx* are very close to Hertz pedictions.

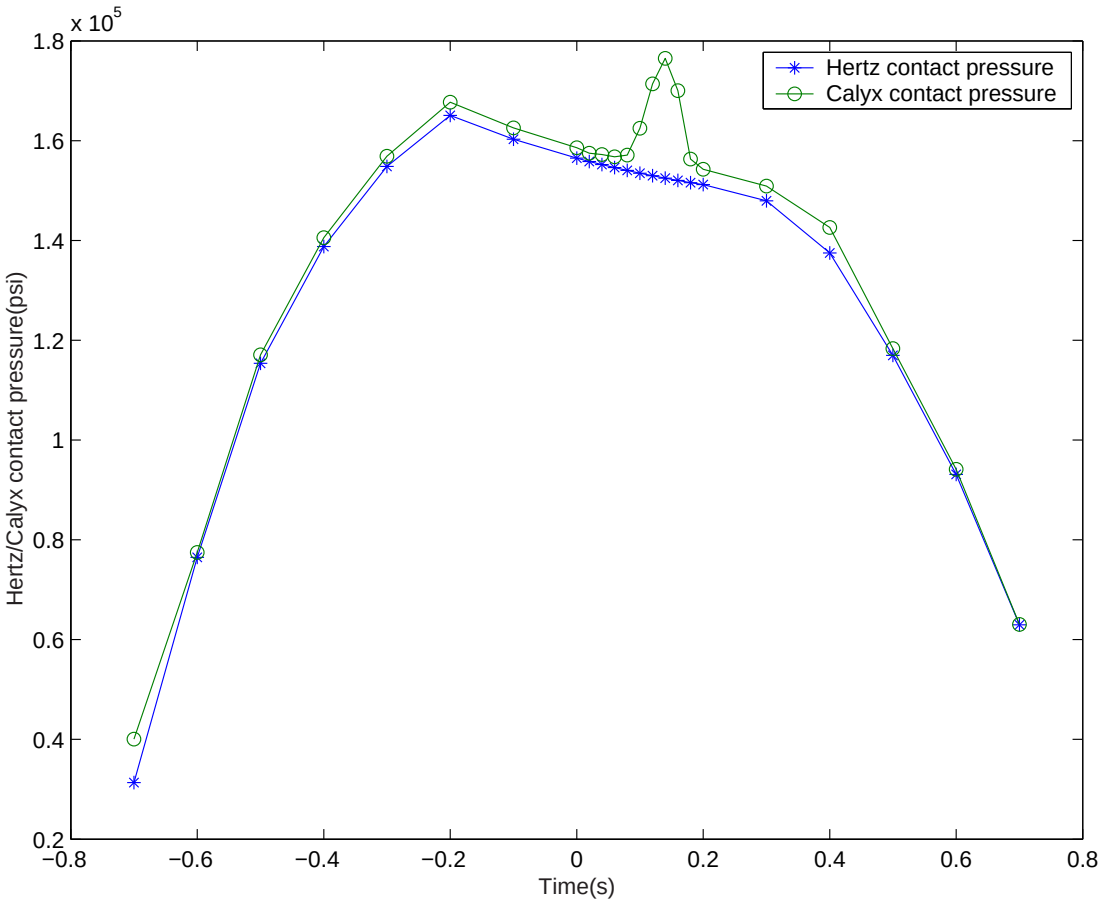

Figure 2.12: A graph comparing Calyx's and Hertz's contact pressure predictions for linear modification at the teeth

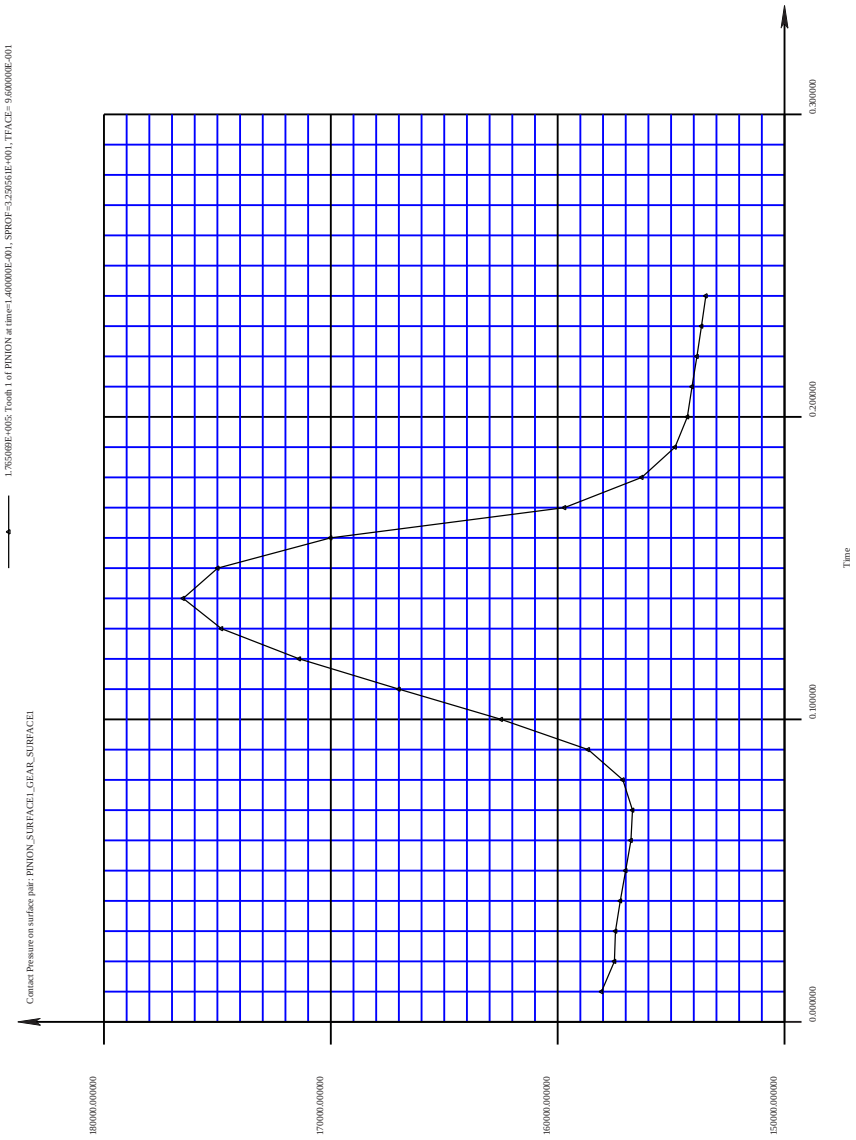

Figure 2.13: A plot of contact pressure against time obtained from Calyx in the time range from 0.0s to 0.2s

Table 2.19: Contact pressure values for linear tip modified tooth obtained from calyx and theoretical calculations for various pinion roll angles

Time(s)	Pinion involute roll angle (deg)	Gear involute roll angle (deg)	Pinion radius of curv (in)	Gear radius of curv (in)	Effective radius of curv (in)	Contact load (lbf/in)	Hertz contact pressure (psi)	Calyx contact pressure (psi)
-0.70	8.2539	27.1539	0.1353	0.8975	0.1176	22.015	3.1336×10^4	4.0065×10^4
-0.60	10.0539	26.2539	0.1648	0.8683	0.1385	154.255	7.6422×10^4	7.7455×10^4
-0.50	11.8539	25.3539	0.1944	0.8391	0.1578	399.800	1.1528×10^5	1.1706×10^5
-0.40	13.6539	24.4539	0.2239	0.8099	0.1754	642.476	1.3861×10^5	1.4057×10^5
-0.30	15.4539	23.5539	0.2534	0.7808	0.1913	872.134	1.5464×10^5	1.5687×10^5
-0.20	17.2539	22.6539	0.2829	0.7517	0.2055	1064.18	1.6480×10^5	1.6770×10^5
-0.10	19.0539	21.7539	0.3124	0.7226	0.2181	1064.18	1.5998×10^5	1.6257×10^5
0.00	20.8539	20.8539	0.3420	0.6935	0.2290	1064.18	1.5612×10^5	1.5858×10^5
0.02	21.2139	20.6739	0.3479	0.6781	0.2299	1064.18	1.5582×10^5	1.5749×10^5
0.04	21.5739	20.4939	0.3538	0.6722	0.2318	1064.18	1.5519×10^5	1.5724×10^5
0.06	21.9339	20.3139	0.3597	0.6663	0.2336	1064.18	1.5460×10^5	1.5677×10^5
0.08	22.2939	20.1339	0.3656	0.6604	0.2353	1064.18	1.5403×10^5	1.5712×10^5
0.10	22.6539	19.9539	0.3715	0.6545	0.2370	1064.18	1.5348×10^5	1.6248×10^5
0.12	23.0139	19.7739	0.3774	0.6486	0.2385	1064.18	1.5297×10^5	1.7139×10^5
0.14	23.3739	19.5939	0.3833	0.6427	0.2401	1064.18	1.5248×10^5	1.7650×10^5
0.16	23.7339	19.4139	0.3892	0.6368	0.2415	1064.18	1.5202×10^5	1.7001×10^5
0.18	24.0939	19.2339	0.3951	0.6309	0.2429	1064.18	1.5159×10^5	1.5629×10^5
0.20	24.4539	19.0539	0.4010	0.6249	0.2442	1064.18	1.5118×10^5	1.5428×10^5
0.30	26.2539	18.1539	0.4305	0.5954	0.2498	1042.16	1.4792×10^5	1.5088×10^5
0.40	28.0539	17.2539	0.4692	0.5659	0.2565	914.303	1.3674×10^5	1.4261×10^5
0.50	29.8539	16.3539	0.4980	0.5364	0.2582	667.574	1.1645×10^5	1.1832×10^5
0.60	31.6539	15.4539	0.5269	0.5069	0.2583	423.727	9.2763×10^4	9.4124×10^4
0.70	33.4539	14.5539	0.5558	0.4773	0.2568	192.965	6.2787×10^4	6.3045×10^4

2.3 Contact pressure for spur gear model with quadratic tooth tip modification

2.3.1 The example file

Load the file `quadtipmodification.ses` from the `CONTACTPRESSURE` directory.

To study the effect of quadratic tip relief on contact pressure, a quadratic tip modification is applied on pinion and gear tooth as shown in Figures 2.14 and 2.15. Tables 2.20 and 2.21 show the modification menus for pinion and gear teeth respectively. All the other menus including the setup menu are similar to the case with no tooth modifications.

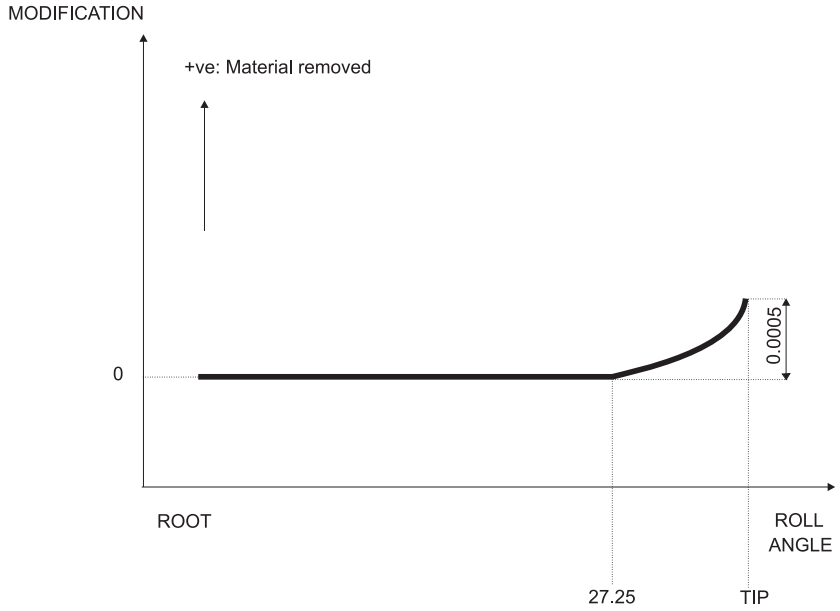

Figure 2.14: Quadratic tip relief applied to the pinion tooth

Table 2.20: Modification menu for the pinion tooth

Item	Description
QUADTIPMOD	TRUE
ROLLQUADTIPMOD	27.25
MAGQUADTIPMOD	0.0005

2.3.2 Obtaining the contact pressure from the postprocessing menu

After the analysis is complete, a post processing data file is created in the working directory. CONTACT command in the postprocessing menu is used to obtain the contact pressure at a particular instant. Figure 2.16 shows a plot of contact pressure against time for pinion tooth no.1. Involute roll angle, θ at the start, θ_i and at the tip, θ_o of the quadratic tip relief for the pinion tooth is 27.25^o and 33.68^o respectively. At $t = 0$, the pinion tooth no.1 is in contact with the gear tooth no.1 at the pitch point. So as to look at the contact pressure value for the pinion

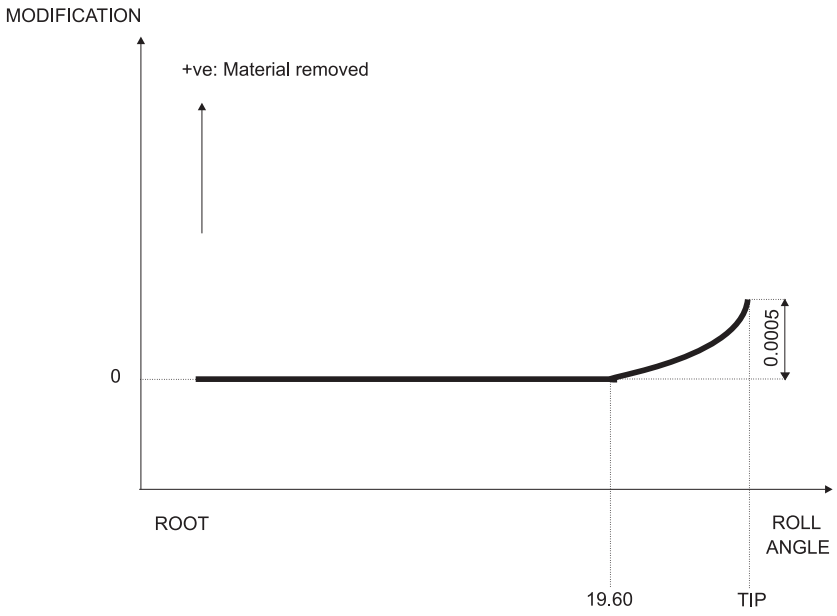

Figure 2.15: Quadratic tip relief applied to the gear tooth

Table 2.21: Modification menu for the gear tooth

Item	Description
QUADTIPMOD	TRUE
ROLLQUADTIPMOD	19.60
MAGQUADTIPMOD	0.0005

in the tip relief region a value of θ somewhere between the start and the tip of the modified tooth is considered. For our calculations we have taken the involute roll angle for the pinion, θ_p as 29.85^o (analysis time, $t = 0.5s$). At this point the involute roll angle for the gear, θ_g is 11.80^o. The contact pressure value from the postprocessing menu at $t = 0.5s$ is $1.241 \times 10^5 psi$. The exact value of the contact pressure at $t = 0.5s$ can be obtained by plotting the GRIDPRHIST plot as shown in Figure 2.17.

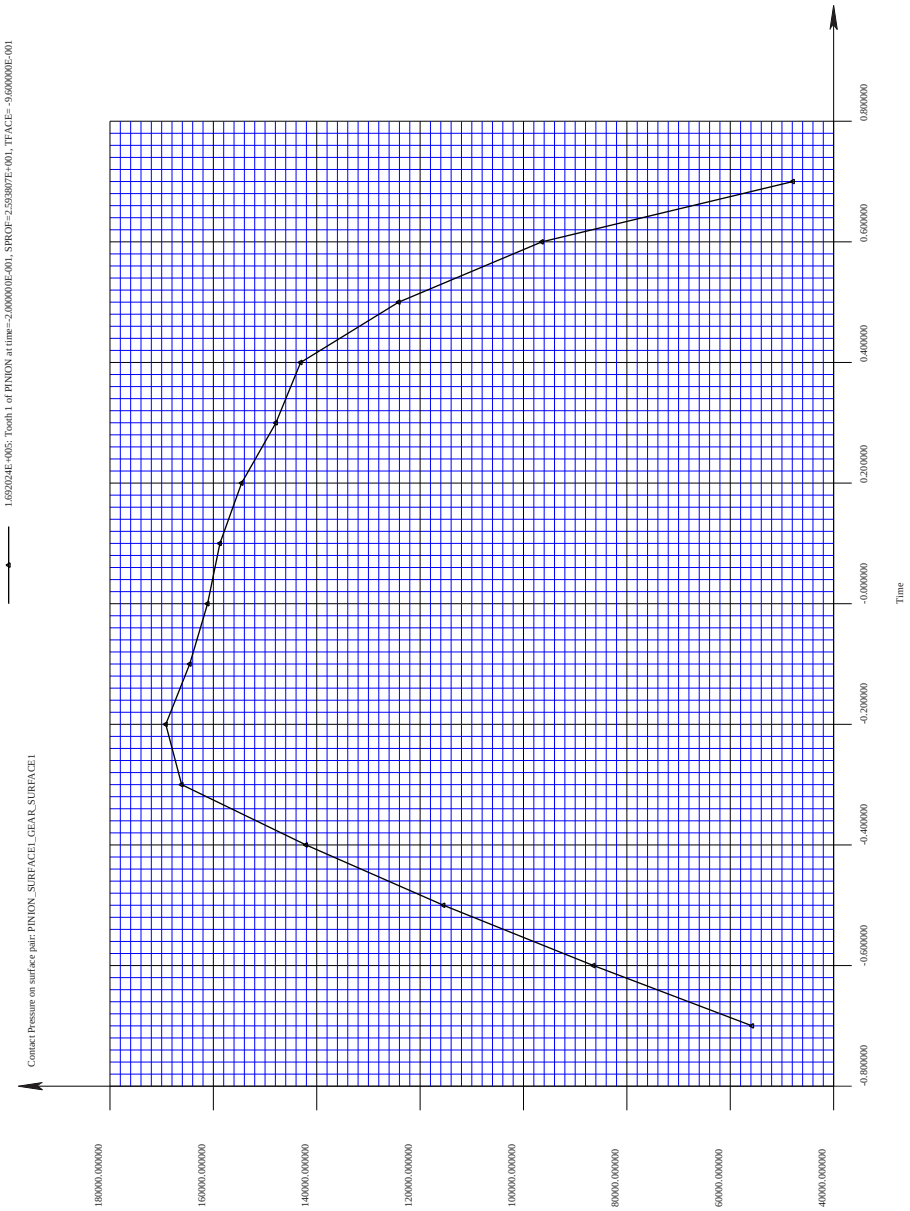

Figure 2.16: Plot of contact pressure against time for pinion tooth no.1

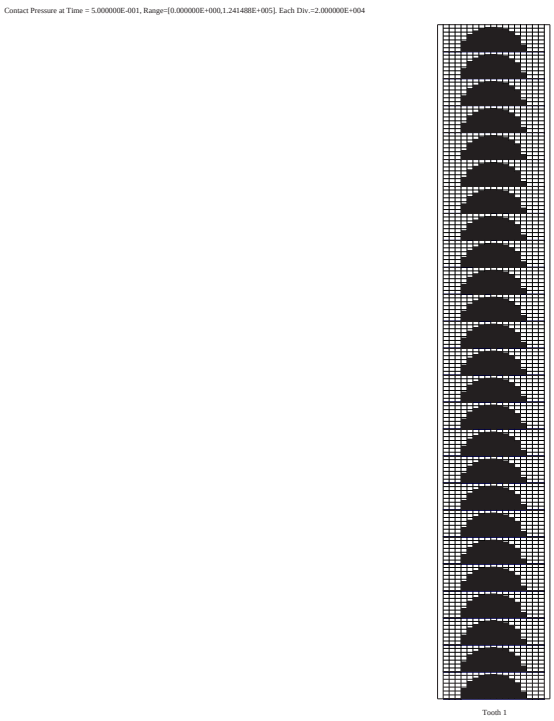

Figure 2.17: Grid pressure histogram for pinion tooth no.1 at t=0.5s (Contact Pressure at Time= 5.000000E-001 is 1.241488E+005s. Range of contact pressure is from 0.000000E+000 to 1.241488E+005 and each division corresponds to 2.000000E+004

2.3.3 Contact pressure from theoretical calculations

Relative Radius of curvature

If $e(\theta)$ is the quadratic modification for the involute at a particular roll angle θ, E is the magnitude of the modification at the tip, and θ_i and θ_o are the involute roll angles at the start of the modification and at the tip, respectively, then the value of the quadratic modification in the relieved part of the involute is given by:

$$\begin{aligned} e(\theta) &= E(\frac{\theta - \theta_i}{\theta_o - \theta_i})^2 \\ \frac{de}{d\theta} &= 2E\frac{(\theta - \theta_i)}{(\theta_o - \theta_i)^2} \\ \frac{d^2e}{d\theta^2} &= 2E\frac{1}{(\theta_o - \theta_i)^2} \end{aligned}$$

Note that for our study case we will need to apply the modified curvature only for the pinion tooth.

For the pinion:

Base radius of the pinion is:

$$r_{bp} = 0.9396in$$

Involute roll angle at 0.5s is:

$$\theta = 29.85^o = 0.5213rad$$

Involute roll angle at the start of modification is:

$$\theta_i = 27.21^o = 0.475rad$$

Involute roll angle at the tip of modification is:

$$\theta_o = 33.68^o = 0.588rad$$

Modification at the tip is:

$$E = 0.0005in$$

If e(θ) is the quadratic modification for the involute at a roll angle $\theta = 29.85^o$, then,

$$\begin{aligned} e(\theta) &= 8.3037 \times 10^{-5}in \\ \frac{de}{d\theta} &= 0.003606in/rad \\ \frac{d^2e}{d\theta^2} &= 0.078314in/(rad)^2 \end{aligned}$$

The position vector and its derivatives for a point r(θ) on an unmodified involute curve are given by:

$$\begin{aligned} r_x(\theta) &= 0.043118 \\ r_y(\theta) &= 1.058724 \\ \frac{dr_x}{d\theta} &= 0.243731 \\ \frac{dr_y}{d\theta} &= 0.424651 \\ \frac{d^2r_x}{d\theta^2} &= 0.892422 \\ \frac{d^2r_y}{d\theta^2} &= 0.571260 \end{aligned}$$

The unit normal vector to the involute and its derivatives are:

$$\begin{aligned} n_x(\theta) &= -0.867297 \\ n_y(\theta) &= 0.497791 \\ \frac{dn_x}{d\theta} &= 0.497791 \\ \frac{dn_y}{d\theta} &= 0.867297 \\ \frac{d^2n_x}{d\theta^2} &= 0.867297 \\ \frac{d^2n_y}{d\theta^2} &= -0.497791 \end{aligned}$$

The coordinate vector R and its derivatives for the *modified* involute is given by:

$$\begin{aligned} R_x(\theta) &= 0.0431907 \\ R_y(\theta) &= 1.058683 \\ \frac{dR_x}{d\theta} &= 0.246818 \\ \frac{dR_y}{d\theta} &= 0.422784 \\ \frac{d^2R_x}{d\theta^2} &= 0.956681 \\ \frac{d^2R_y}{d\theta^2} &= 0.526062 \end{aligned}$$

The unit vector for the modified involute is:

$$\begin{aligned} N_x(\theta) &= -0.863606 \\ N_y(\theta) &= 0.504166 \end{aligned}$$

The curvature of this modified involute is:

$$K_p = 2.340647 in^{-1}$$

For the gear:

Base radius of the gear is:

$$r_{bg} = 1.8793in$$

Involute roll angle at 0.5s is:

$$\theta = 16.3539^o = 0.2854rad$$

The curvature of this unmodified involute is:

$$K_g = \frac{1}{r_{bg}\theta} = 1.864162in^{-1}$$

Thus, the relative radius of curvature is:

$$\rho = \frac{1}{(K_p + K_g)} = 0.237823in$$

Calculating the Contact load

The user can find the contact load on individual teeth using the TOOTHLOAD or the TOOTHLDHIST command in the postprocessing menu. Table 2.22 shows the TOOTHLOAD menu inputs used to obtain the contact load value at $t = 0.5s$. Figure 2.18 shows the tooth load histogram at $t = 0.5s$. Table 2.23 shows the TOOTHLDHIST menu inputs used to obtain this plot. The value of contact load at the pitch point from the tooth load plot is $6.7563 \times 10^2 lbf$.

$$\text{Contact load per unit length} = \frac{\text{Contact load}}{\text{Facewidth}} = 6.7563 \times 10^2 lbf/in \tag{2.7}$$

Table 2.22: Toothload menu to obtain the contact load at t=0.5s

Item	Description
SURFACEPAIR	PINION_SURFACE1_GEAR_SURFACE1
MEMBER	PINION
TOOTHBEGIN	1
TOOTHEND	1
BEGINSTEP	13
ENDSTEP	13

Table 2.23: Toothldhist menu to obtain the tooth load histogram at t=0.5s

Item	Description
SURFACEPAIR	PINION_SURFACE1_GEAR_SURFACE1
MEMBER	PINION
TIMESTEP	13
HISTCOLOR	BLACK
AUTOSCALE	TRUE
OUTPUTTOFILE	FALSE

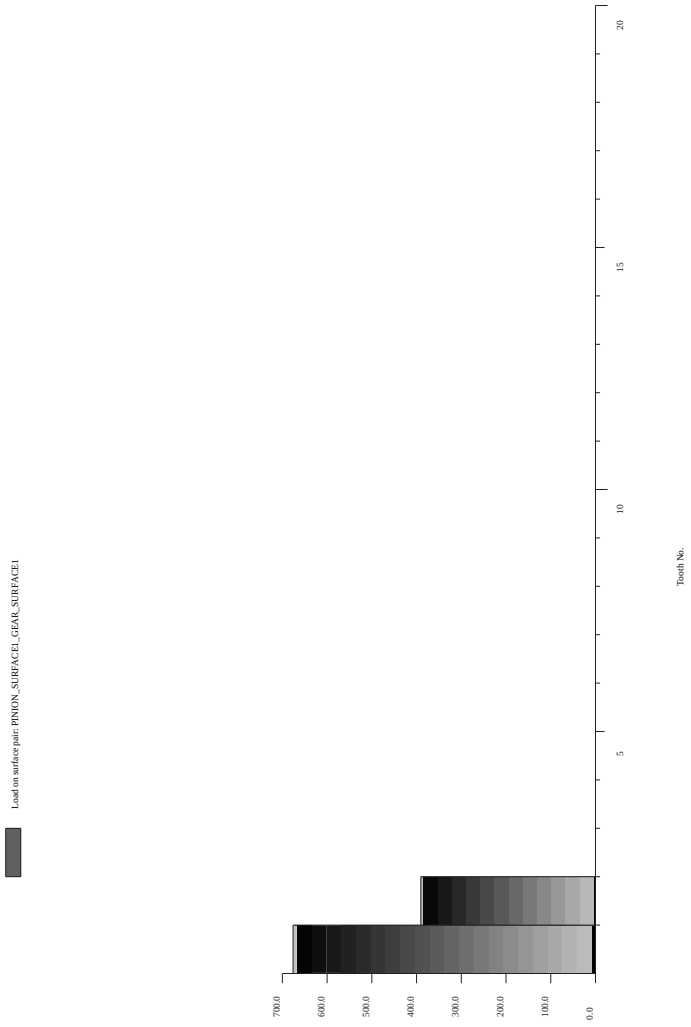

Figure 2.18: Toothload histogram at t=0.5s

Calculating the Contact Pressure

For the present case, since we have not applied any tooth modifications the contact between the pinion and gear tooth can be assumed to be a two dimensional contact of cylindrical bodies. Using the Hertz theory of elastic contact for such cases the maximum pressure, p_o is given by,

$$p_o = \frac{PE_{eq}}{\pi\rho} \tag{2.8}$$

where,

$$\begin{aligned}
p_o &= \text{Maximum Contact pressure} \\
P &= \text{Contact load per unit length} = 6.7563 \times 10^2 lbf/in \\
\rho &= \text{Relative radius of curvature} = 0.237823in \\
\nu_p &= \text{Pinion Poissons ratio} = 0.3 \\
\nu_g &= \text{Gear Poissons ratio} = 0.3 \\
E_p &= \text{Pinion Young's modulus} = 3 \times 10^7 psi \\
E_g &= \text{Gear Young's modulus} = 3 \times 10^7 psi \\
\frac{1}{E_{eq}} &= \frac{1-\nu_p^2}{E_p} + \frac{1-\nu_g^2}{E_g}
\end{aligned}$$

E_{eq} from above $= 1.648351 \times 10^7 psi$

Substituting the above values the theoretical contact pressure is $1.22089 \times 10^5 psi$, compared with $1.24148 \times 10^5 psi$ predicted by *Calyx*.

Table 2.24 shows the comparison of contact pressure values for pinion tooth no.1 obtained from *Calyx* and the theoretical calculations at various roll angles. The spreadsheet used to carry out the calculations shown in Table 2.24 is in file `quadtipmodification.xls` in the `CONTACTPRESSURE` directory. A graph comparing *Calyx's* and Hertz's predictions is shown in Figure 2.19. As can be seen from the plot there is no spike in the contact pressure value when the start of modified involute for the gear or pinion comes in contact. This is due to the gradual change in the curvature of the tooth when you apply quadratic tip modification. This example shows that the predictions made by *Calyx* are very close to Hertz pedictions.

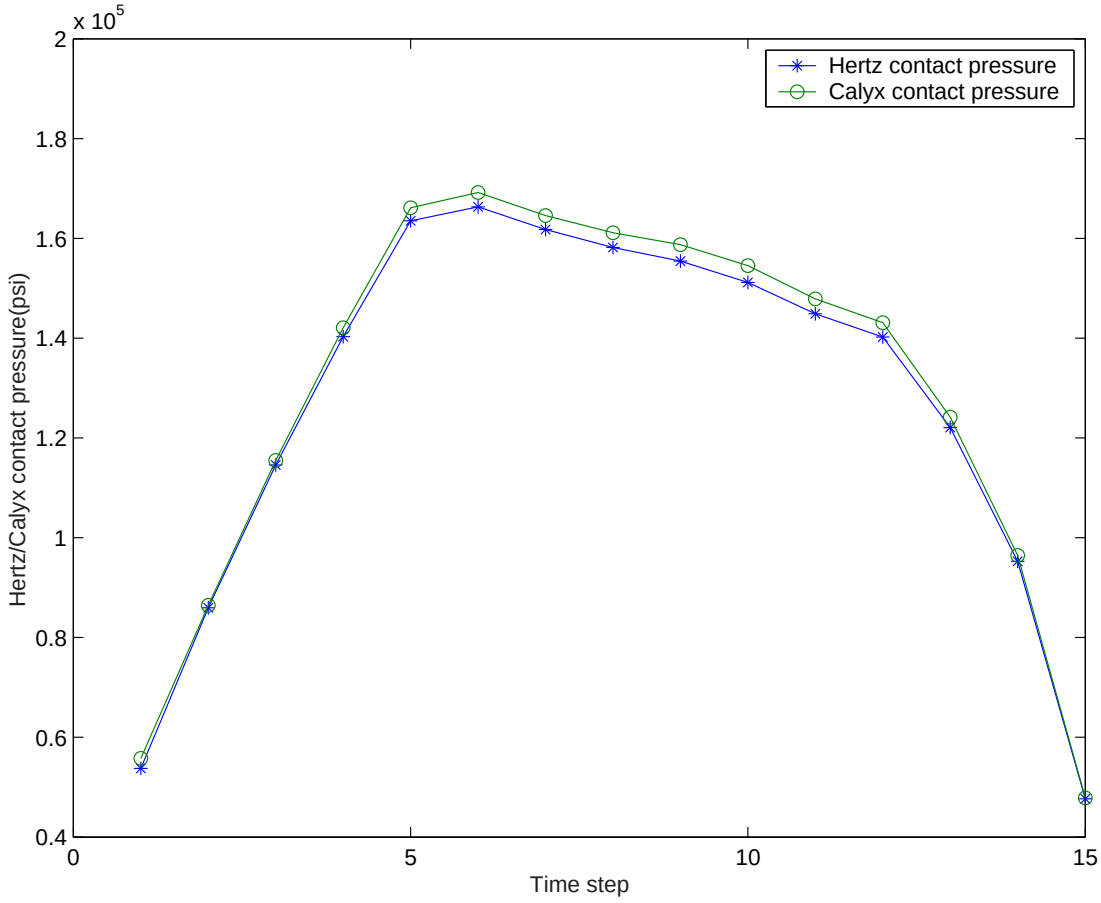

Figure 2.19: A graph comparing Calyx's and Hertz's contact pressure predictions for quadratic modification at the teeth

Table 2.24: Contact pressure values for quadratic tip modified tooth obtained from calyx and theoretical calculations for various pinion roll angles

Time(s)	Pinion involute roll angle (deg)	Gear involute roll angle (deg)	Pinion radius of curv (in)	Gear radius of curv (in)	Effective radius of curv (in)	Contact load (lbf/in)	Hertz contact pressure (psi)	Calyx contact pressure (psi)
-0.7	8.2539	27.1539	0.1353	0.8572	0.1169	64.4317	5.3774×10^4	5.5576×10^4
-0.6	10.0539	26.2539	0.1648	0.8266	0.1374	193.627	8.5966×10^4	8.6454×10^4
-0.5	11.8539	25.3539	0.1944	0.7960	0.1562	390.95	1.1457×10^5	1.1548×10^5
-0.4	13.6539	24.4539	0.2239	0.7654	0.1732	649.995	1.4030×10^5	1.4206×10^5
-0.3	15.4539	23.5539	0.2534	0.7347	0.1884	960.308	1.6351×10^5	1.6613×10^5
-0.2	17.2539	22.6539	0.2829	0.7039	0.2018	1064.18	1.6632×10^5	1.6920×10^5
-0.1	19.0539	21.7539	0.3124	0.6730	0.2134	1064.18	1.6175×10^5	1.6456×10^5
0.0	20.8539	20.8539	0.3420	0.6420	0.2231	1064.18	1.5818×10^5	1.6111×10^5
0.1	22.6539	19.9539	0.3715	0.6109	0.2310	1064.18	1.5546×10^5	1.5873×10^5
0.2	24.4539	19.0539	0.4010	0.6249	0.2442	1064.18	1.5118×10^5	1.5453×10^5
0.3	26.2539	18.1539	0.4305	0.5954	0.2498	999.747	1.4488×10^5	1.4789×10^5
0.4	28.0539	17.2539	0.3948	0.5659	0.2325	871.498	1.4021×10^5	1.4311×10^5
0.5	29.8539	16.3539	0.4272	0.5364	0.2378	675.636	1.2208×10^5	1.2414×10^5
0.6	31.6539	15.4539	0.4593	0.5069	0.2409	416.723	9.5256×10^4	9.6432×10^4
0.7	33.4539	14.5539	0.4911	0.4773	0.2420	104.778	4.7655×10^4	4.7873×10^4

2.4 Contact pressure for spur gear model with lead crown tooth modification

When the spur gear teeth are crowned, Hertz's equations for cylindrical contact can no longer be used. Hertz's relationships for elliptical contact need to be used.

2.4.1 The example file

Load the file `toothcrowning.ses` from the `CONTACTPRESSURE` directory.

To study the effect of crowning on Contact pressure, a lead crown is applied on pinion and gear tooth as shown in Figures 2.20 and 2.21. Tables 2.25 and 2.26 show the modification menus for pinion and gear teeth respectively. All the other menus including the setup menu are similar to the case with no tooth modifications.

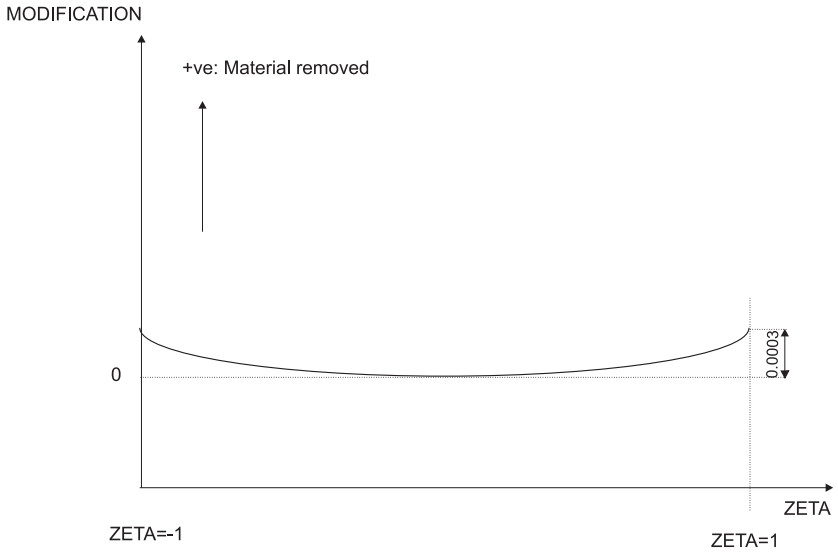

Figure 2.20: Crowning applied to the pinion tooth

Table 2.25: Modification menu inputs used for the pinion tooth

Item	Description
LEADCROWN	TRUE
MAGLEADCROWN	0.0003

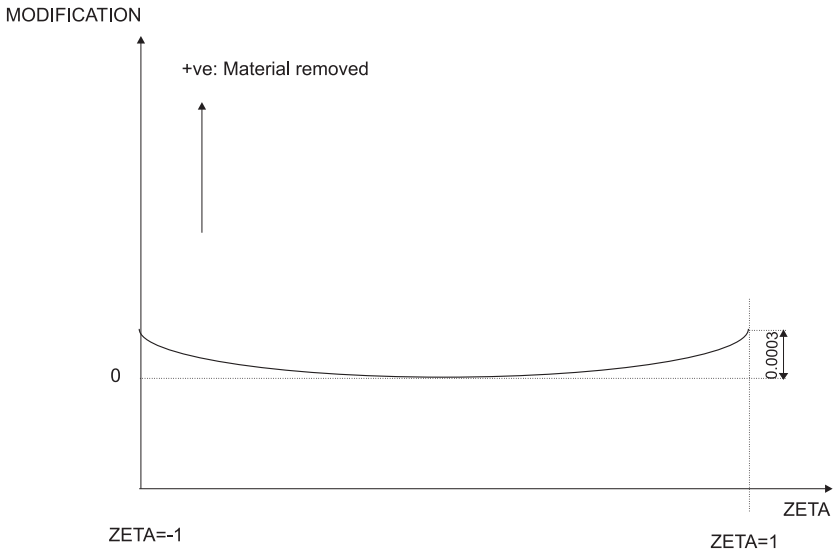

Figure 2.21: Crowning applied to the gear tooth

Table 2.26: Modification menu inputs used for the gear tooth

Item	Description
LEADCROWN	TRUE
MAGLEADCROWN	0.0003

2.4.2 Obtaining the contact pressure from the postprocessing menu

After the analysis is complete, a post processing data file is created in the working directory. CONTACT command in the postprocessing menu is used to obtain the contact pressure at a particular instant. Figure 2.22 shows the plot of contact pressure against time for pinion tooth no.1. At $t = 0$, the pinion tooth no.1 is in contact with the gear tooth no.1 at the pitch point. The contact pressure value from the postprocessing menu at $t = 0$ is $2.0148 \times 10^5 psi$. The exact value of the contact pressure at $t = 0$ can be obtained by plotting the GRIDPRHIST plot as shown in Figure 2.23.

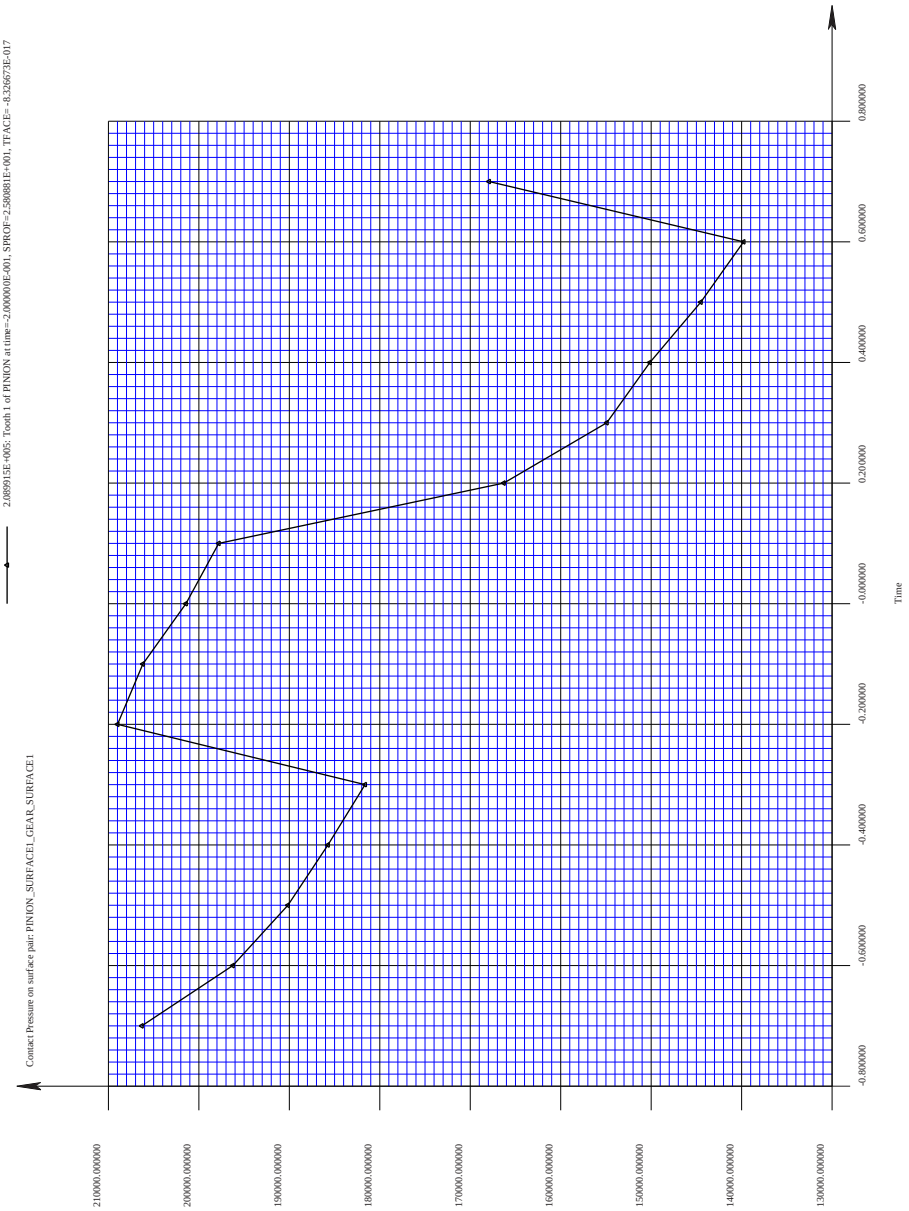

Figure 2.22: Plot of contact pressure against time for pinion tooth no.1

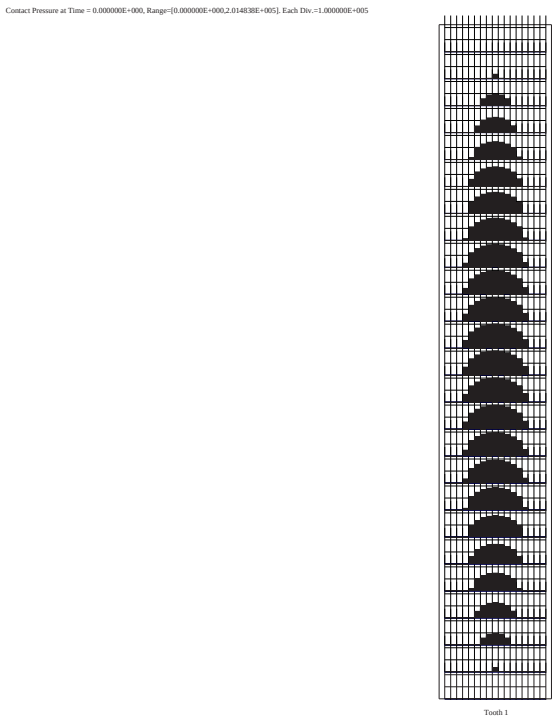

Figure 2.23: Grid pressure histogram for crowned pinion tooth no.1 at t=0 (Contact Pressure at Time= 0.00 is 2.014838E+005. Range of contact pressure is from 0.000000E+000 to 2.014838E+005 and each division corresponds to 1.000000E+005

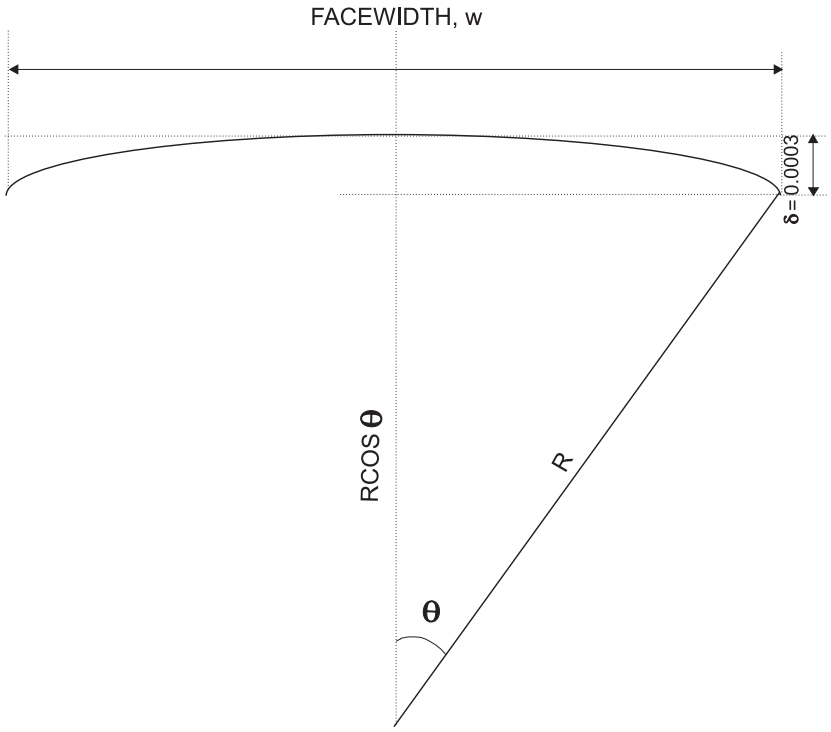

Figure 2.24: Figure showing the crowning curvature

2.4.3 Contact pressure from theoretical calculations

Relative Radius of curvature

From Figure 2.24 the crowning at an arbitrary location along the face width is given by:

$$\delta = R - R\cos\theta$$

where θ is the angle subtended at the center of curvature of the crown. Expanding θ in a Taylor series,

$$\cos\theta = 1 - \frac{\theta^2}{2} + \frac{\theta^4}{4} - \frac{\theta^6}{6}....$$

For small curvature (large R), θ is very small. Neglecting higher terms we get,

$$\delta = R - R(1 - \frac{\theta^2}{2}) = R\frac{\theta^2}{2}$$

From Figure 2.24, at the edge of the tooth,

$$\theta = \sin^{-1}(\frac{w}{2R})$$
$$\theta \approx \frac{w}{2R} \qquad \text{for large R}$$

Therefore,

$$\delta = \frac{w^2}{8R}$$

The Radius of curvature, is therefore,

$$R = \frac{w^2}{8\delta} \tag{2.9}$$

For contact at crowned teeth we assume that the shape of contact is elliptical having semi-axes a and b. To calculate the pressure for such bodies we use the Hertz theory of elastic contact [21] between two general bodies.

If R_1 & R_1' denote the principal radii of curvature at the point of contact of one of the bodies, and R_2 & R_2' those of the other, and ψ is the angle between the normal planes containing the curvatures $1/R_1$ and $1/R_2$, the constants A and B are determined from the equations:

$$A + B = \frac{1}{2}(\frac{1}{R_1} + \frac{1}{R_1'} + \frac{1}{R_2} + \frac{1}{R_2'}) \tag{2.10}$$

$$B - A = \frac{1}{2}[(\frac{1}{R_1} - \frac{1}{R_1'})^2 + (\frac{1}{R_2} - \frac{1}{R_2'})^2 + 2(\frac{1}{R_1} - \frac{1}{R_1'})(\frac{1}{R_2} - \frac{1}{R_2'})\cos\psi]^{1/2} \tag{2.11}$$

For our case we consider R as the radius of curvature in the profile direction and R' as the radius of curvature in the facewidth direction. For the case where in the contact is at the pitch point, the radius of curvature in the profile direction for the pinion, $R_1 = 0.3419in$ and that for the gear, $R_2 = 0.6839in$. Note that we have already calculated these values in the case where we do not have any tooth modifications. From equation 1.16, the radius of curvature in the facewidth direction for the pinion, $R_1' = 416.67in$ and that for the gear, $R_2' = 416.67in$. Also the angle, ψ between the normal planes containing the curvatures is 0.0.

Substituting the values of R_1, R_1', R_2, R_2' and ψ in equations for (A + B) and (B - A), we get $A + B = 2.1959$ and $B - A = 2.191$.

$$\cos\alpha = \frac{B - A}{A + B} = 0.9977$$

$$\alpha = 3.8283^o \tag{2.12}$$

Using the table given for m and n values in Appedix A, by linear interpolation, we get $m = 13.8577$ and $n = 0.2150$.

The magnitudes of the semi-axes for the ellipsoid can be calculated using the following:

$$a = m(\frac{3\pi}{4}\frac{P(k_p + k_g)}{(A+B)})^{1/3} \tag{2.13}$$

$$b = n(\frac{3\pi}{4}\frac{P(k_p + k_g)}{(A+B)})^{1/3} \tag{2.14}$$

where,

$$\begin{aligned}
a, b &= \text{semiaxes of the contact region} \\
m, n &= \text{constants} \\
P &= \text{Contact load per unit length} \\
\nu_p &= \text{Pinion Poissons ratio} = 0.3 \\
\nu_g &= \text{Gear Poissons ratio} = 0.3 \\
E_p &= \text{Pinion Young's modulus} = 3 \times 10^7 \\
E_g &= \text{Gear Young's modulus} = 3 \times 10^7 \\
k_p &= \frac{1 - \nu_p^2}{\pi E_p} \\
k_g &= \frac{1 - \nu_g^2}{\pi E_g}
\end{aligned}$$

Table 2.27: Toothload menu inputs used to obtain the contact load at t=0

Item	Description
SURFACEPAIR	PINION_SURFACE1_GEAR_SURFACE1
MEMBER	PINION
TOOTHBEGIN	1
TOOTHEND	1
BEGINSTEP	8
ENDSTEP	8

Table 2.28: Toothldhist menu inputs used to obtain the tooth load histogram at t=0

Item	Description
SURFACEPAIR	PINION_SURFACE1_GEAR_SURFACE1
MEMBER	PINION
TIMESTEP	8
HISTCOLOR	BLACK
AUTOSCALE	TRUE
OUTPUTTOFILE	FALSE

Calculating the Contact load

The user can find the contact load value using the TOOTHLOAD or the TOOTHLDHIST command in the postprocessing menu. Table 2.27 shows the TOOTHLOAD menu to obtain the contact load value at $t = 0$. Figure 2.25 shows the tooth load histogram at $t = 0$. Table 2.28 shows the TOOTHLDHIST menu to obtain this plot. The value of contact load at the pitch point from the tooth load plot is $1.0641 \times 10^3 lbf$.

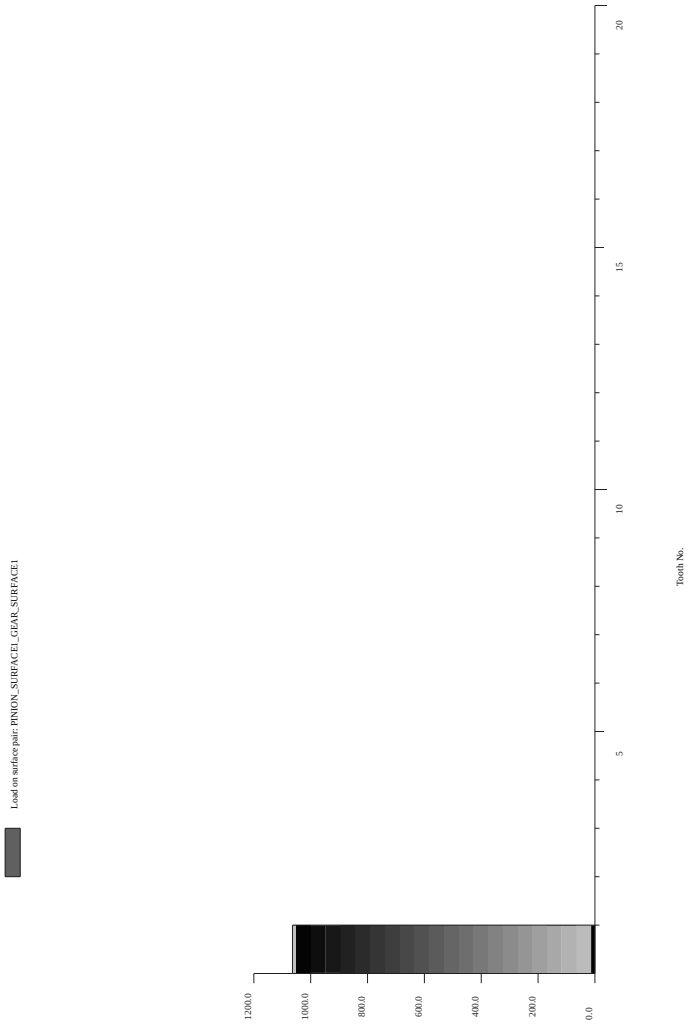

Figure 2.25: Toothload histogram at the t=0

Calculating the Contact Pressure

Using the Hertz theory of elastic contact for elliptical contact the maximum pressure, p_o is given by,

$$p_o = \frac{3}{2}\frac{P}{\pi ab} \tag{2.15}$$

Calculating a & b and Substituting the value of P from above the theoretical contact pressure is $2.161 \times 10^5 psi$, compared to $2.014 \times 10^5 psi$ from the program .

2.5 Conclusion

The difference between the theoretical contact pressure values and those obtained from *Calyx* is due to the assumption of a very large tooth thickness in the derivations for the Radius of curvatures given by the Hertz theory related to contacting bodies. In actual cases the gear bodies have finite thicknesses. Since *Calyx* takes in to consideration all the geometrical parameters we feel that it gives a more accurate representation of the contact pressure values. When you reduce the value of tooth thickness you can see the change in the value of the contact pressure. For tooth thickness=$0.15in$, the contact pressure value obtained from *calyx* is $2.003221 \times 10^5 psi$. Further reducing the thickness to $0.145in$ reduces the contact pressure value to $1.993894 \times 10^5 psi$. Furthermore, there is error in the analytical predictions because of the error in the values of m and n obtained from linear interpolation.

Chapter 3

Sub-surface stresses in a spur gear model using Calyx

A verification study comparing the sub-surface stresses predicted by Calyx with those predicted by the theory of elasticity is presented here.

3.1 The spur gear model with no tooth modification

This example uses an unmodified spur gear .

3.1.1 The example file

After hitting the `CONNECT` button, choose the `CONTACTPRESSURE` directory under the `SAMPLES` directory. This in turn is located in the Working directory(`WORKDIR`) selected by the User at the installation time. Load the file `subsurface.ses` from the `CONTACTPRESSURE` directory.

This session file contains a model identical to the spur gear set described in the previous chapter. The only difference is that only one time step will be analyzed. We have chosen to analyze the gear pair at the pitch point.

Tables 3.1 shows the analysis setup.

3.1.2 Obtaining the sub-surface stress from the postprocessing menu

During the analysis, a post processing data file is created in the working directory. The SUBSURFACE command in the postprocessing menu is used to obtain the sub-surface stress at a particular instant. At $t = 0$, the pinion tooth no.1 is in contact with the gear tooth no.1 at the pitch point. Figure 3.1 shows the sub-surface Von-Mises stress as a function of depth. Table 3.2 shows the inputs used to obtain this plot. The SUBSURFACE command selects the grid cell with the maximum contact pressure as the location for sub-surface stress computation. We restricted ourselves to the middle of the face width by setting TFACEBEGIN = -0.01 and TFACEEND = +0.01. The depth was varied from 0.00001 inch to 0.02 inch. A total of 101 points were sampled. The predicted maximum Von Mises stress is 41,529 psi at a depth of 0.003 inches, and the maximum shear stress is 47,551 psi at a depth of 0.0034 inches. The maximum shear stress predicted by the theory of elasticity is 47,928 psi at the same depth. Figure 3.2 shows the maximum shear as a function of depth.

Figures 3.3 through 3.6 show the comparison between Calyx and theory (K. L. Johnson [20]) of the normal stresses and maximum shear stress as a function of depth. An excel file `subsurface.xls` containing the theory of elasticity calculations can be found in the `CONTACTPRESSURE` directory.

Table 3.1: Setup menu inputs

Item	Description
SEPTOL	0.05
NPROFDIVS	8
NFACEDIVS	25
DSPROF	0.0005
ZEROINITIAL	TRUE
INITIALTIME	-0.1
NRANGES	1
RANGE	1
SOLMETHOD	STATIC
NTIMESTEPS	1
DELTATIME	0.1
STARTSPEEDFACTOR	1.0
STARTTORQUEFACTOR	1.0
ENDTORQUEFACTOR	1.0
SAVEPERIODICALLY	FALSE
OUTPUTRESTART	FALSE
POSTPROCWRITE	TRUE
POSTFILENAME	postproc.dat
NSTEPSWRITE	1

Table 3.2: Sub-surface menu inputs

Item	Description
SURFACEPAIR	PINION_SURFACE1_GEAR_SURFACE1
MEMBER	PINION
TOOTHBEGIN	1
TOOTHEND	1
TIMESTEP	1
SPROFBEGIN	0.0
SPROFEND	48.0
TFACEBEGIN	-0.01
TFACEEND	0.01
DEPTHBEGIN	0.00001
DEPTHEND	0.02
NUMDEPTH	101
COMPONENT	VONMISES
OUTPUTTOFILE	FALSE

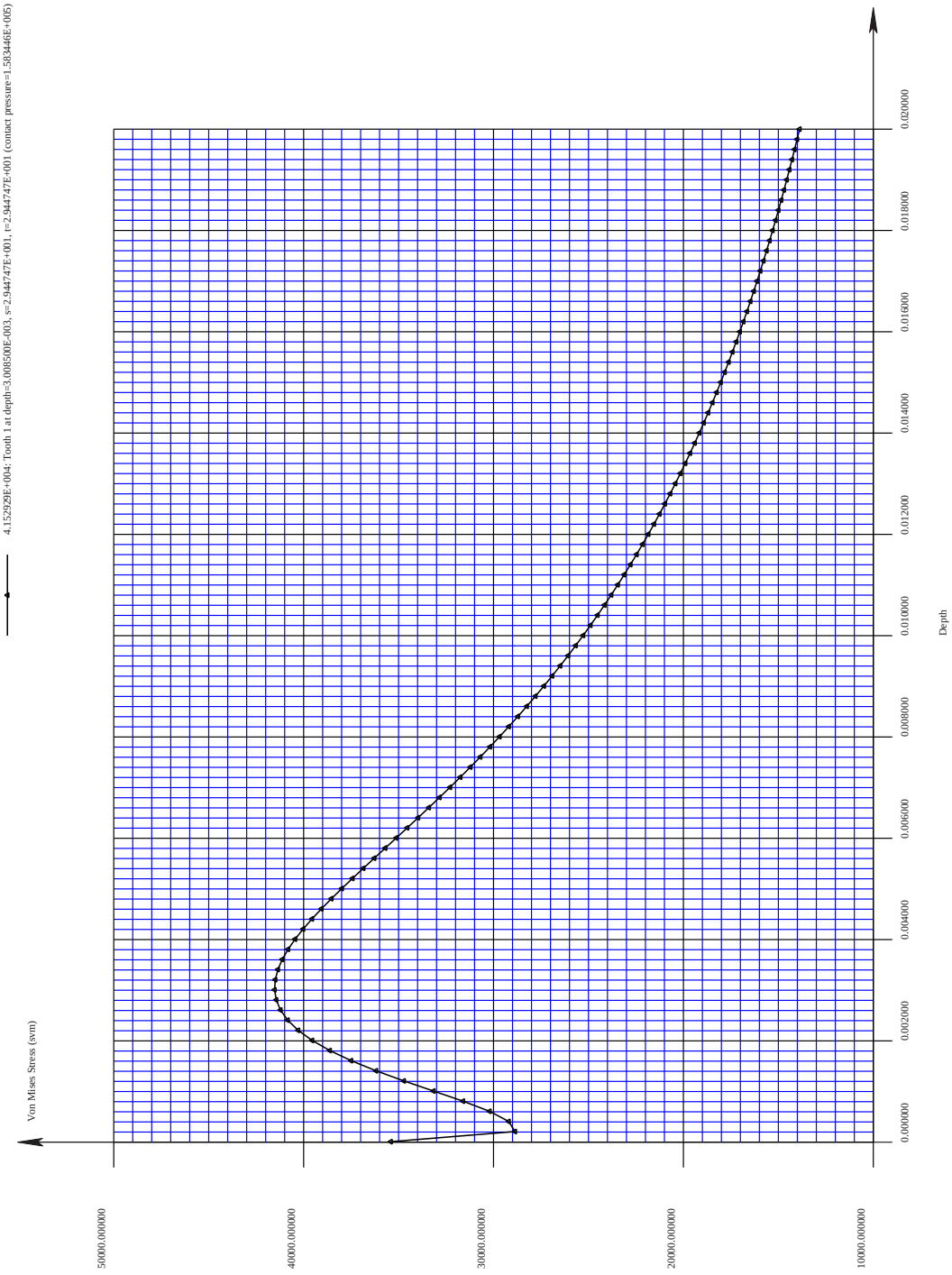

Figure 3.1: Graph of sub-surface Von Mises stress as a function of depth at pinion tooth no.1. The contact is at the pitch point.

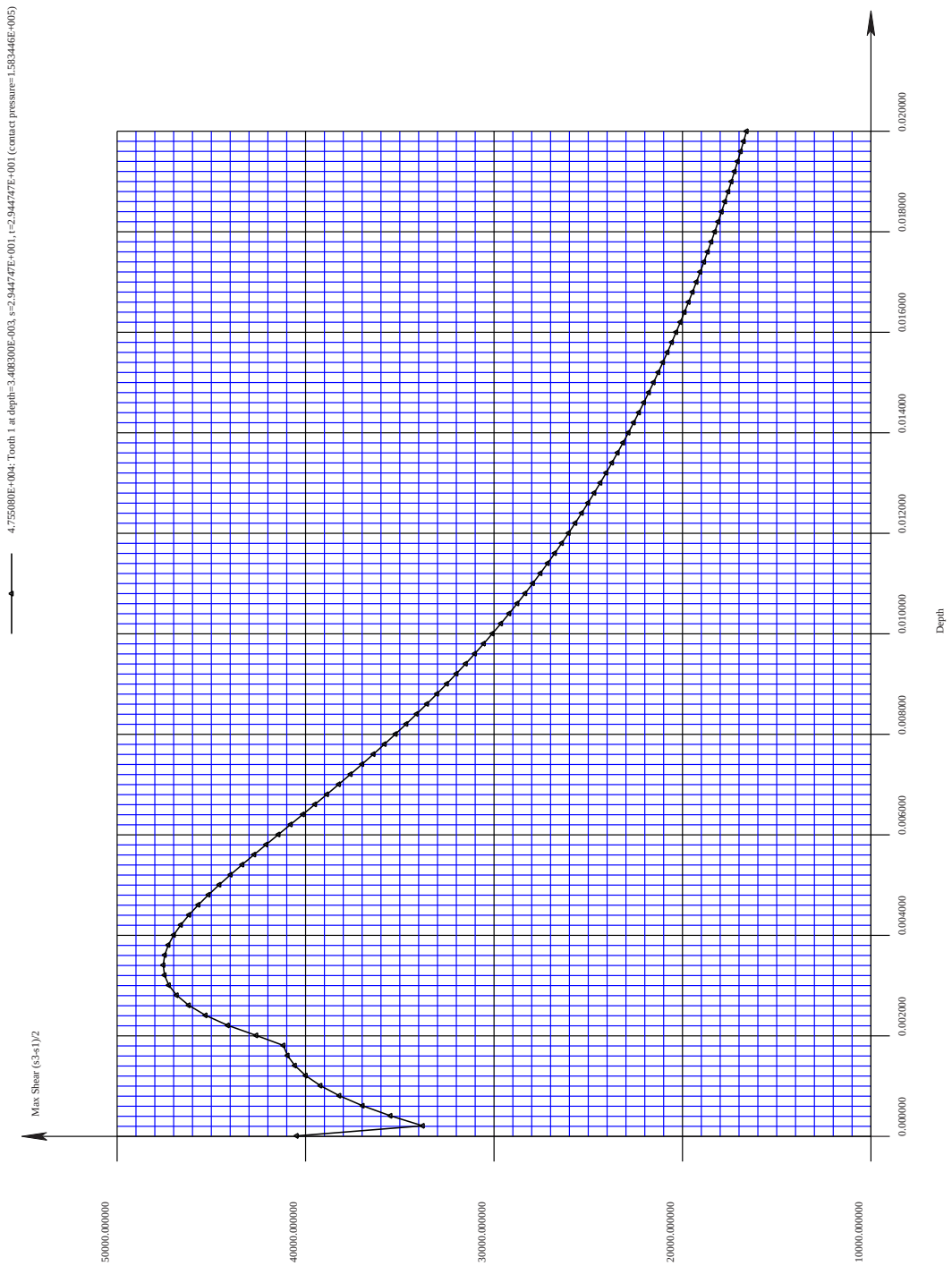

Figure 3.2: Graph of sub-surface max. shear stress as a function of depth at pinion tooth no.1.The contact is at the pitch point.

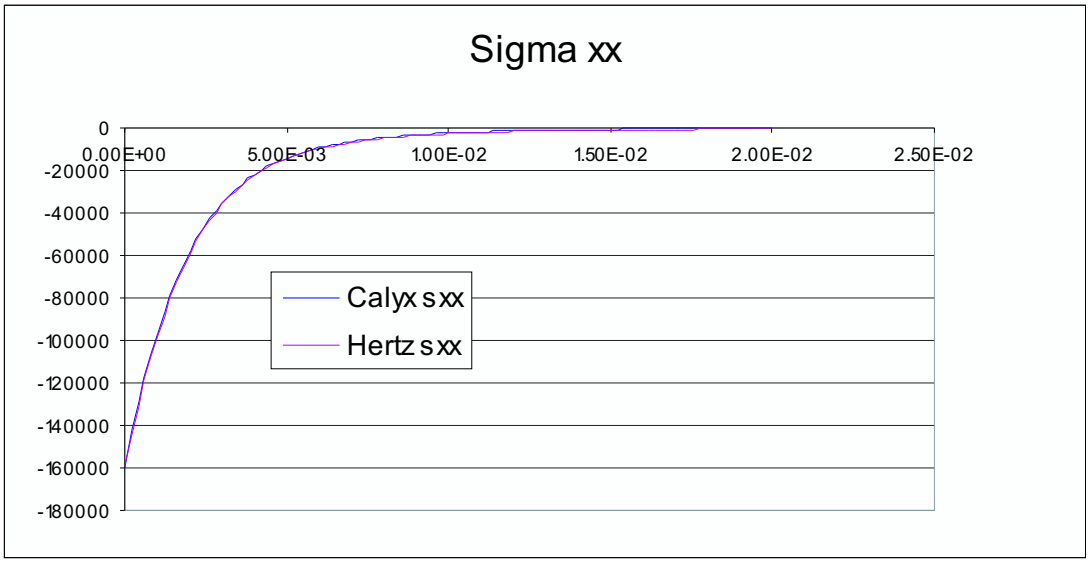

Figure 3.3: Comparison of sub-surface σ_{xx} predicted by Calyx with that computed by the theory of elasticity (K. L. Johnson [20]).

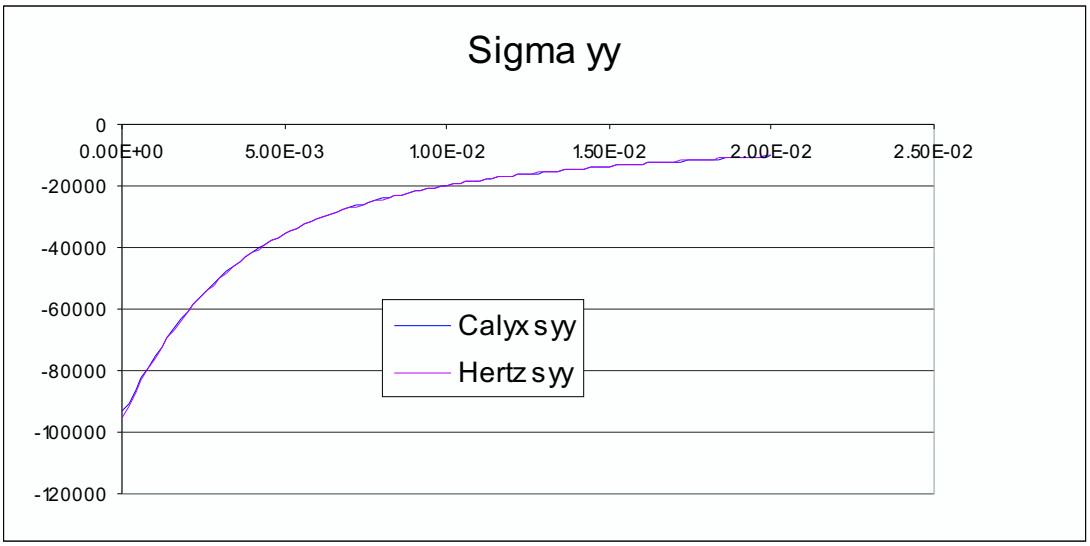

Figure 3.4: Comparison of sub-surface σ_{yy} predicted by Calyx with that computed by the theory of elasticity (K. L. Johnson [20]).

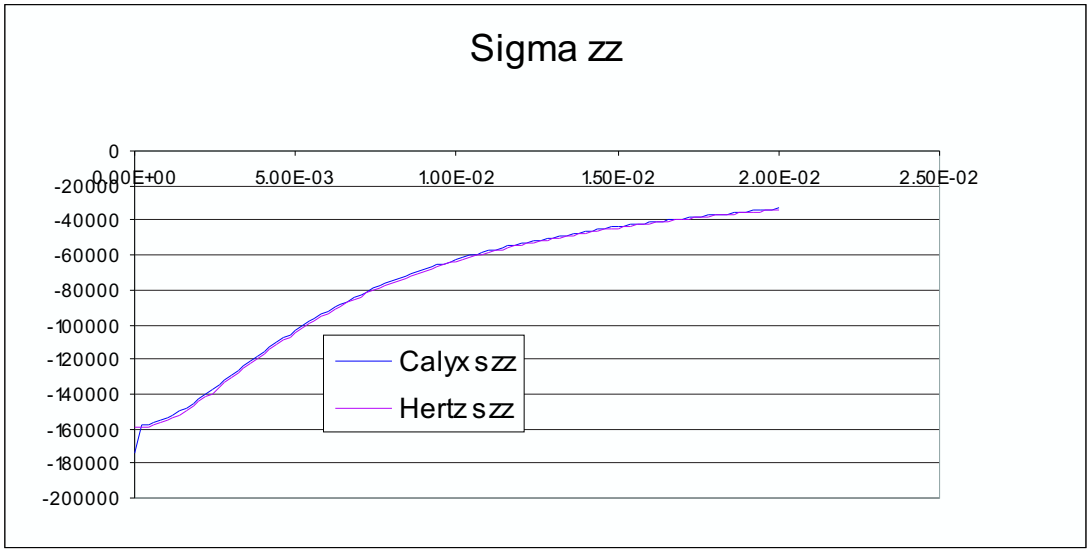

Figure 3.5: Comparison of sub-surface σ_{zz} predicted by Calyx with that computed by the theory of elasticity (K. L. Johnson [20]).

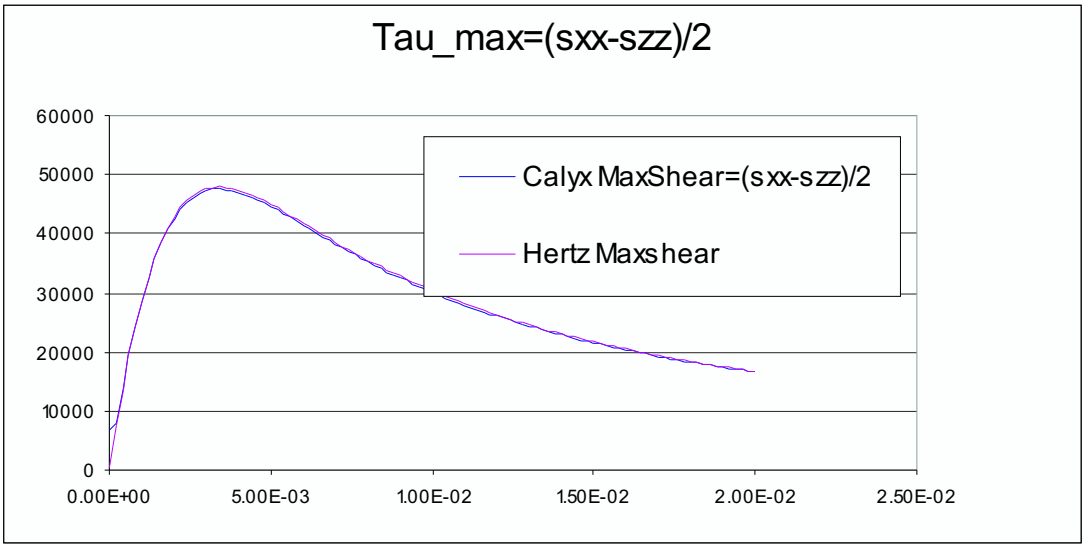

Figure 3.6: Comparison of sub-surface $\tau_{max} = (\sigma_{xx} - \sigma_{zz})/2$ predicted by Calyx with that computed by the theory of elasticity (K. L. Johnson [20]).

Chapter 4

Calculation of transmission error for a spur and helical gear model using Calyx

4.1 Introduction

Gear noise is mainly characterized by components at the gear mesh frequency and its multiples. The gear mesh frequency is the inverse of the time period between consecutive tooth contact and may be computed multiplying the number of teeth on the gear by its rotational velocity. Other frequency components can also occur, but they are usually secondary with respect to the mesh frequency. The most important exciters of the gear forces, which are periodic at the gear mesh frequency are:

- Transmission error
- Mesh stiffness changes

If gears were perfect involutes, absolutely rigid and correctly spaced, there would be no vibration generated when meshing. In practice, for a variety of reasons, this does not occur and the idea of transmission error came into existence. The transmission error is defined as the difference between the current position of the output gear and the position it would occupy if it were perfectly conjugated with the input gear. For unloaded gears, transmission error is the result of surface modifications and manufacturing inaccuracies such as profile errors, spacing errors and runout. For loaded gears, the teeth deflection due to the mesh stiffness variation, superimposed to the unloaded gear errors, is the cause of the transmission error.

A vibration transmission path starts from a combination of manufacturing errors and tooth and gear deflections to generate the transmission error. The transmission error is then the source of vibration and it drives the internal dynamics of the gears to give vibration forces through the bearing supports. In turn, these bearing forces drive the external gear case vibration or, via any isolation mounts, drive the external structure to find the sound radiating panel which transmits noise. In a vehicle, after the vibration has travelled from the gear box through the engine main casting to the support mounts and hence to the structure, it may travel several meters in the body before exciting a panel to emit sound that annoys the occupants.

Table 4.1: Data for low contact ratio spur gear

Item	Pinion	Gear
NUMBER OF TEETH	20	119
TRANSVERSE DIAM. PITCH (in^{-1})	7.8	7.8
TRANSVERSE PRESSURE ANGLE (deg)	20.0	20.0
CENTER DISTANCE (in)	8.9102	8.9102
OPERATING PITCH DIAM. (in)	2.56409	15.2563
OUTSIDE PITCH DIAM. (in)	2.82050	15.4927
ROOT DIAM. (in)	2.19486	14.8671
INNER DIAM. (in)	1.20	13.90
FACE WIDTH (in)	1.0	1.0
STANDARD PITCH RADIUS (in)	0.201382	0.19410
OPERATING PITCH RADIUS (in)	0.201382	0.19410
CONTACT RATIO	1.6443	1.6443
TORQUE ($lbf - in$)	1000	5950

4.2 Measuring the transmission error using calyx

A. Singh [22] in his Masters thesis made a comparison between the transmission error values predicted by the Contact Analysis Program Package called CAPP and the Load Distribution Program called LDP developed at The Ohio State University. In this chapter we have compared the transmission error values obtained from *Calyx* with these results.

4.2.1 Comparison of transmission error values obtained from Calyx and LDP for Spur gears

Two sets of spur gears are analysed. The first is a low contact ratio spur gear and is described in Table 4.1. Load the file `tespurlowcr.ses` from the `TRANSERROR` directory in the Working directory(`WORKDIR`). Figure 4.1 shows the transmission error curves obtained from LDP and CAPP for this gear set. Figure 4.2 shows the transmission error plot for the gear set obtained using *Calyx*. This plot is obtained using the BODYDEFLECTION command in the postprocessing menu. The peak to peak transmission error(T.E) which is the difference in the maximum deflection and the minimum deflection in the Z-direction is $1.50132 \times 10^{-4} rads = 180.86 \mu in$ (Using a base radius value of $1.204728 in$). Figure 4.3 shows the same T.E curve in μin. The sign used for the transmission error is opposite to that used in Figure 4.1. LDP predicts a peak to peak T.E value of $190 \mu in$. CAPP predicts a peak to peak T.E of $150 \mu in$.

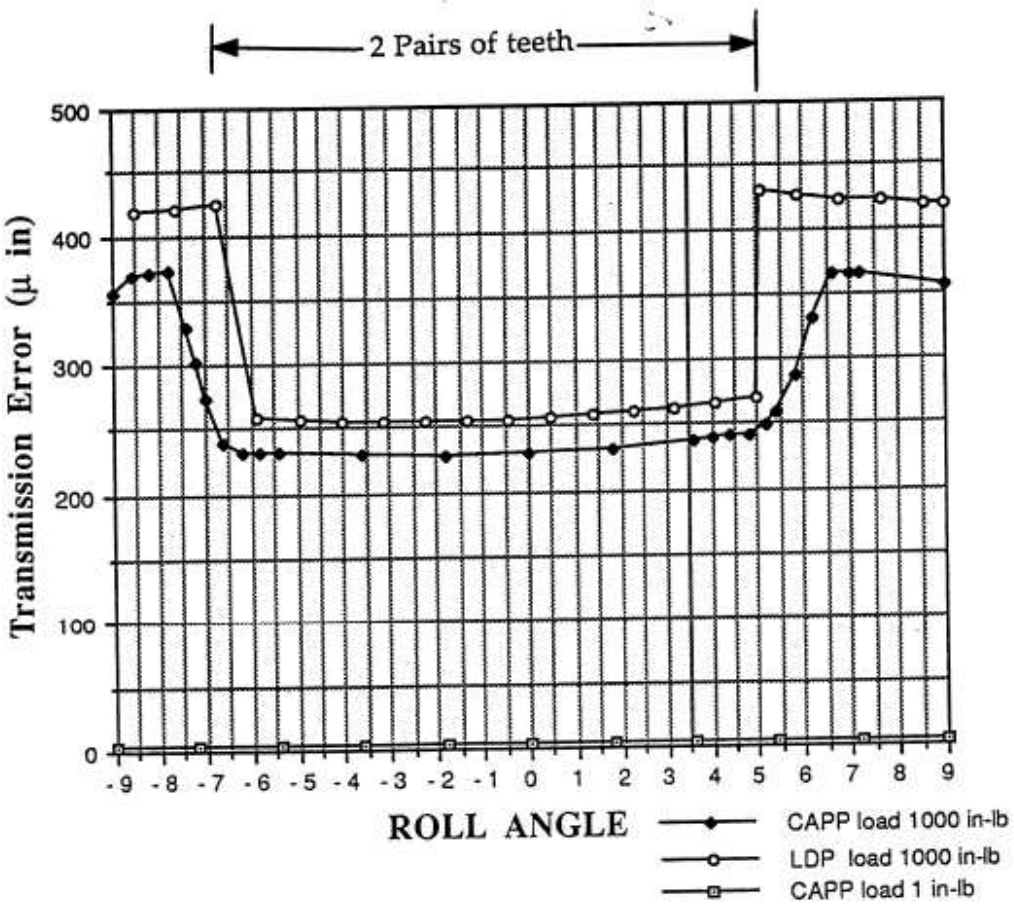

Figure 4.1: Comparison of transmission error predicted by LDP and CAPP for a low contact ratio spur gear model under a load of $1000lbf - in$. Peak to Peak transmission error obtained from LDP is about $190\mu in$. CAPP predicts a peak to peak T.E of $150\mu in$. (From "Analysis of spur and helical gears using a combination of finite element and surface integral techniques", M.S. Thesis by Avinashchandra Singh at The Ohio State University).

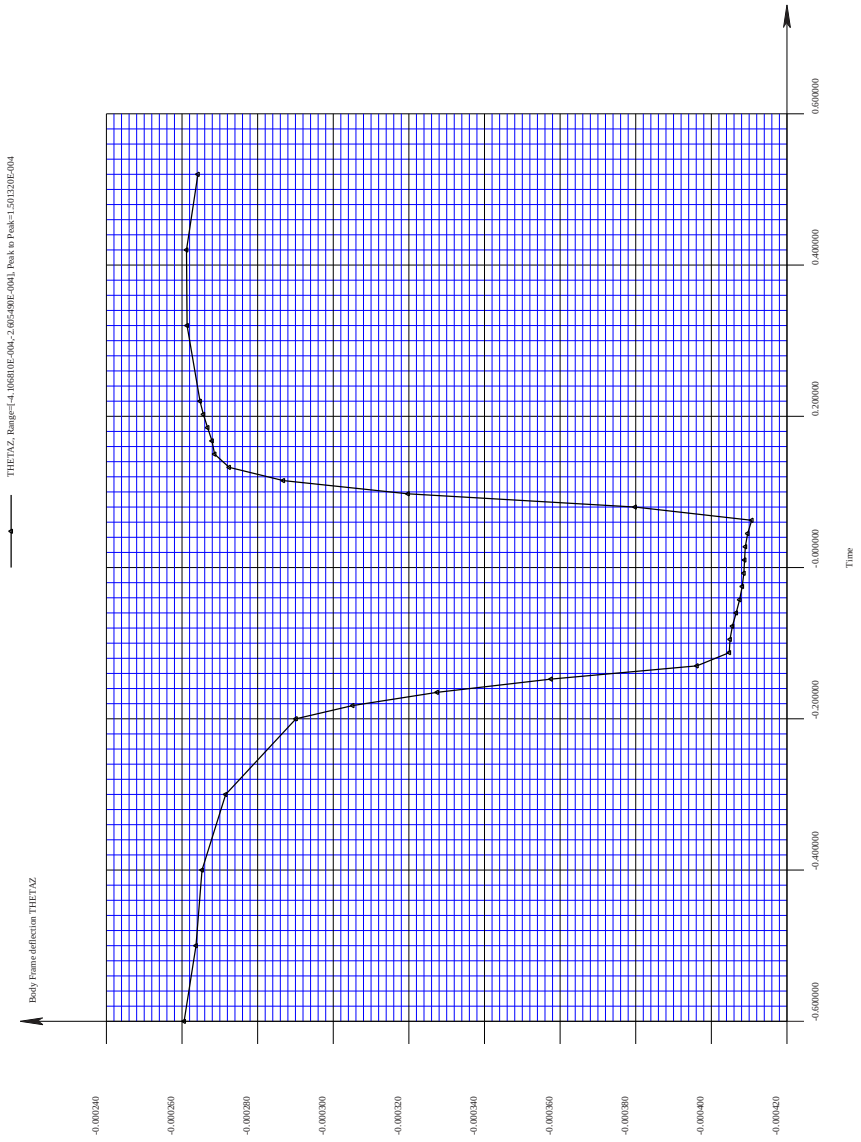

Figure 4.2: Transmission error predicted by Calyx for a low contact ratio spur gear model under a load of $1000lbf-in$. Peak to Peak transmission error predicted by Calyx is $1.50132\times10^{-4}rads$.

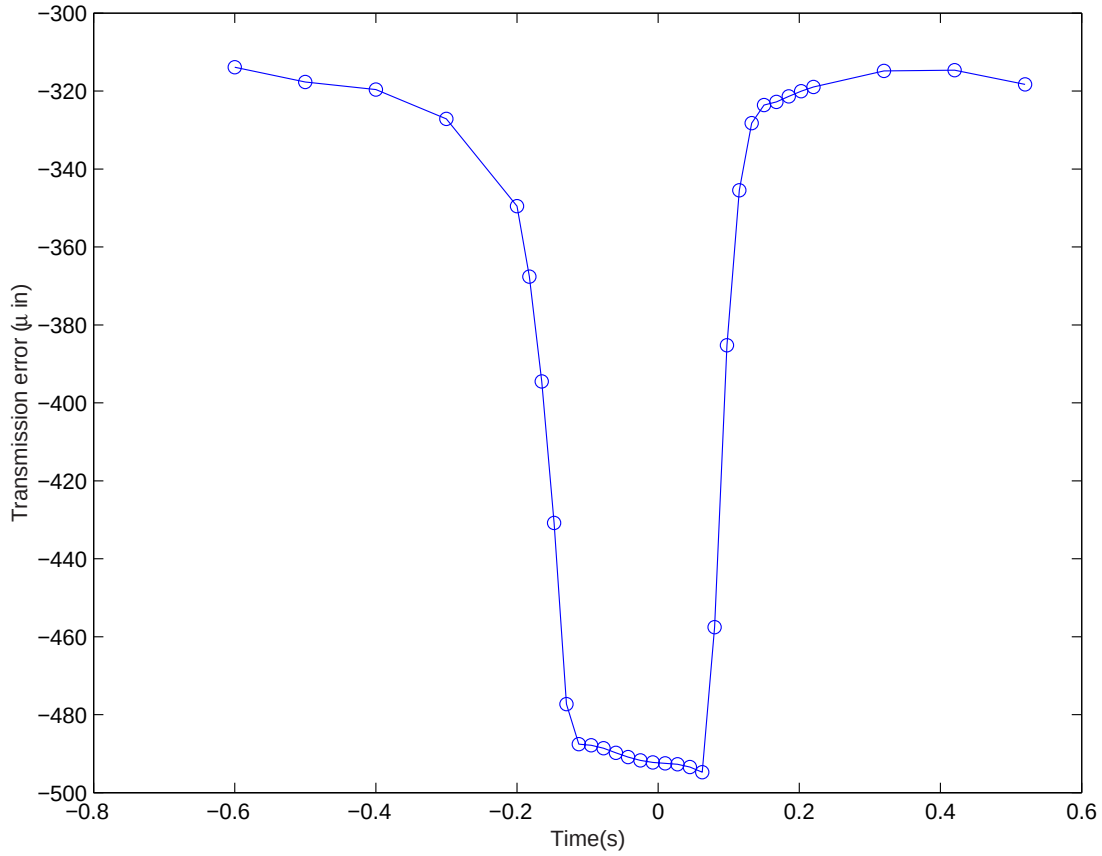

Figure 4.3: Transmission error predicted by Calyx for a low contact ratio spur gear model under a load of $1000lbf - in$. Peak to Peak transmission error obtained from Calyx is about $180\mu in$.

Table 4.2: Data for a high contact ratio spur gear

Item	Pinion	Gear
NUMBER OF TEETH	27	34
TRANSVERSE DIAM. PITCH (in^{-1})	10.233	10.233
TRANSVERSE PRESSURE ANGLE (deg)	20.811	20.811
CENTER DISTANCE (in)	2.980	2.980
OPERATING PITCH DIAM. (in)	2.63803	3.32197
OUTSIDE PITCH DIAM. (in)	2.885	3.622
ROOT DIAM. (in)	2.320	3.039
INNER DIAM. (in)	1.5	2.0
FACE WIDTH (in)	1.152	1.152
STANDARD PITCH RADIUS (in)	0.142	0.160
OPERATING PITCH RADIUS (in)	0.142159	0.160203
CONTACT RATIO	2.17	2.17
TORQUE ($lbf - in$)	900	1133.33

The data for a high contact ratio spur gear is described in Table 4.2. Load the file `tespurhighcr.ses` from the `TRANSERROR` directory in the Working directory(`WORKDIR`). Figure 4.4 shows the transmission error curves obtained from LDP and CAPP for this gear set. Figure 4.5 shows the T.E curve in μin obtained from *Calyx*. The peak to peak T.E predicted by CAPP is approximately $35\mu in$. LDP predicts approximately $50\mu in$. *Calyx* predicts a peak to peak T.E of $37.4\mu in$ with a base radius of $1.232959in$.

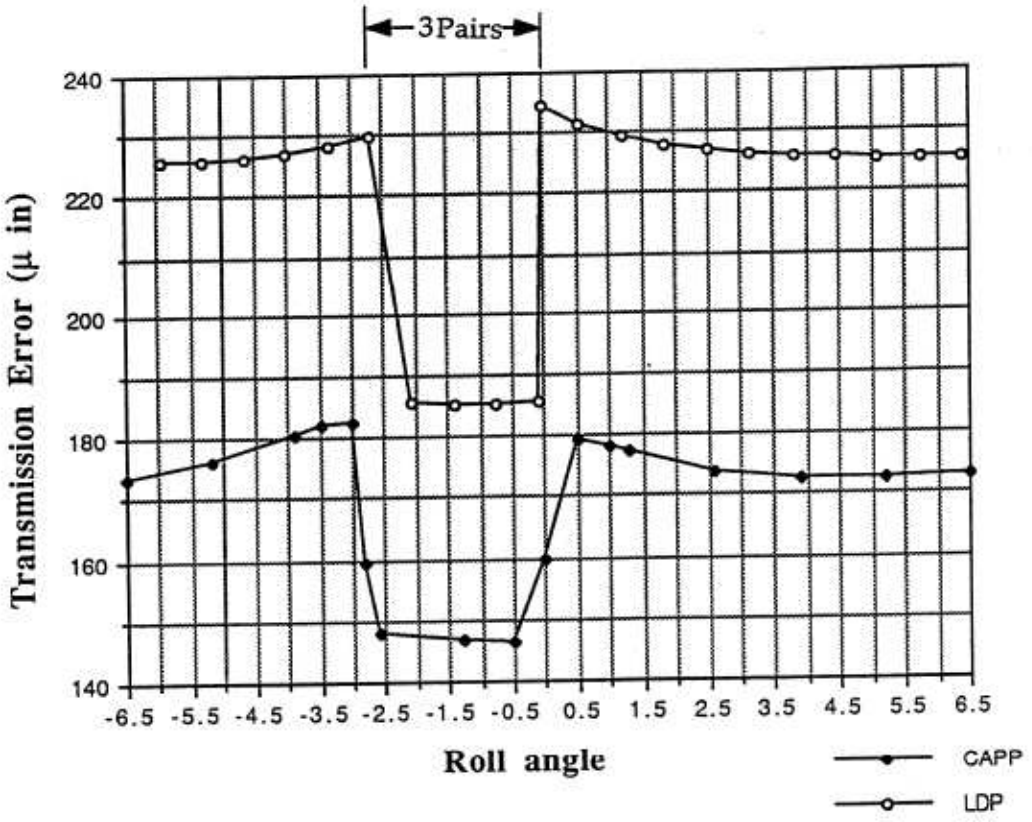

Figure 4.4: Comparison of transmission error predicted by LDP and CAPP for a high contact ratio spur gear model under a load of $900lbf - in$. Peak to Peak transmission error obtained from LDP is about $50\mu in$. (From "Analysis of spur and helical gears using a combination of finite element and surface integral techniques", M.S. Thesis by Avinashchandra Singh at The Ohio State University).

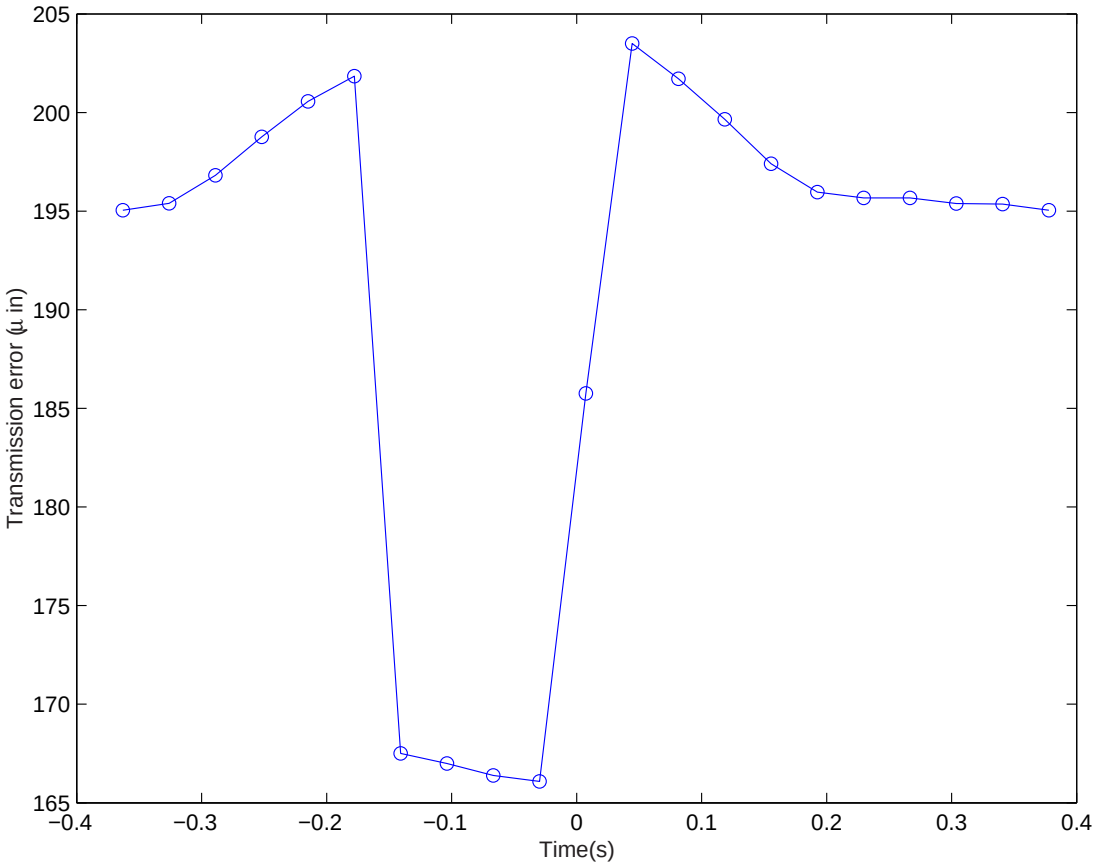

Figure 4.5: Transmission error predicted by Calyx for a low contact ratio spur gear model under a load of $900lbf - in$. Peak to Peak transmission error obtained from Calyx is $37.411\mu in$.

Table 4.3: Data for a helical gear set

Item	Pinion	Gear
NUMBER OF TEETH	13	127
NORMAL DIAM. PITCH (in^{-1})	6.173435	6.173435
TRANSVERSE DIAM. PITCH (in^{-1})	5.29167	5.29167
TRANSVERSE PRESSURE ANGLE (deg)	23.00704	23.00704
NORMAL PRESSURE ANGLE (deg)	20.0	20.0
HELIX ANGLE (deg)	31.00	31.00
CENTER DISTANCE (in)	13.22835	13.22835
PITCH DIAM. (in)	2.4567	24.00
OUTSIDE DIAM. (in)	2.9637	24.2278
ROOT DIAM. (in)	2.1202	23.3842
INNER DIAM. (in)	0.90	22.00
FACE WIDTH (in)	2.00	2.00
TRANSVERSE CIRCULAR THICKNESS (in)	0.341357	0.234960
FACE CONTACT RATIO	2.0242	2.0242
TRANSVERSE CONTACT RATIO	1.3944	1.3944
TORQUE ($lbf - in$)	8040.0	78544.6

4.2.2 Comparison of transmission error values obtained from Calyx and LDP for Helical gears

The data for a helical gear set is described in Table 4.3. Load the file `tehelical.ses` from the `TRANSERROR` directory in the Working directory(`WORKDIR`). Figure 4.6 shows the transmission error curves obtained from LDP and CAPP for this gear set. The T.E curve obtained from CAPP in Figure 4.6 seems to be wrong. Figure 4.7 shows the T.E curve obtained from a more recent run made with CAPP. Note that the sign convention used for this model is opposite to that shown in Figure 4.6. Figure 4.8 shows the T.E curve in μin obtained from *Calyx*. The peak to peak T.E predicted by CAPP is $23.40\mu in$. LDP predicts aproximately $40\mu in$. *Calyx* predicts a peak to peak T.E of $27.745\mu in$ with a base radius of $1.130643in$.

4.3 Conclusion

The deflection curve obtained from *Calyx* closely matches with that obtained from LDP and CAPP. LDP does not predict the premature contact of the gear teeth due to deflection under load because of the assumption of contact along the line of action. The contact ratio obtained from LDP is the theoretical contact ratio. So, the transmission error obtained from LDP has a sudden jump when the gears go from one pair of teeth to two pairs of teeth in contact. But the T.E curve obtained from CAPP and *Calyx* has a smooth transition from one pair of teeth to two pairs of teeth in contact. Thus *Calyx* gives a reasonably correct representation of transmission error for both spur and helical gears.

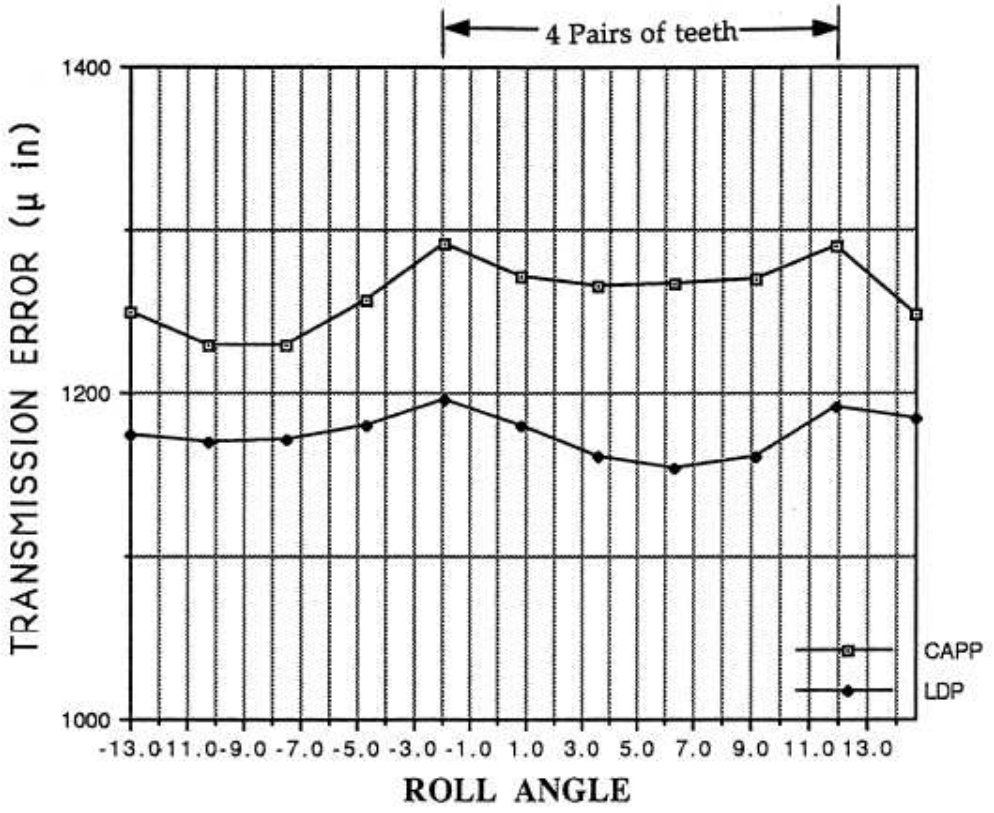

Figure 4.6: Comparison of transmission error predicted by LDP and CAPP for a helical gear model under a load of $8040.0 lbf-in$. Peak to Peak transmission error obtained from LDP is about $40 \mu in$. (From "Analysis of spur and helical gears using a combination of finite element and surface integral techniques", M.S. Thesis by Avinashchandra Singh at The Ohio State University).

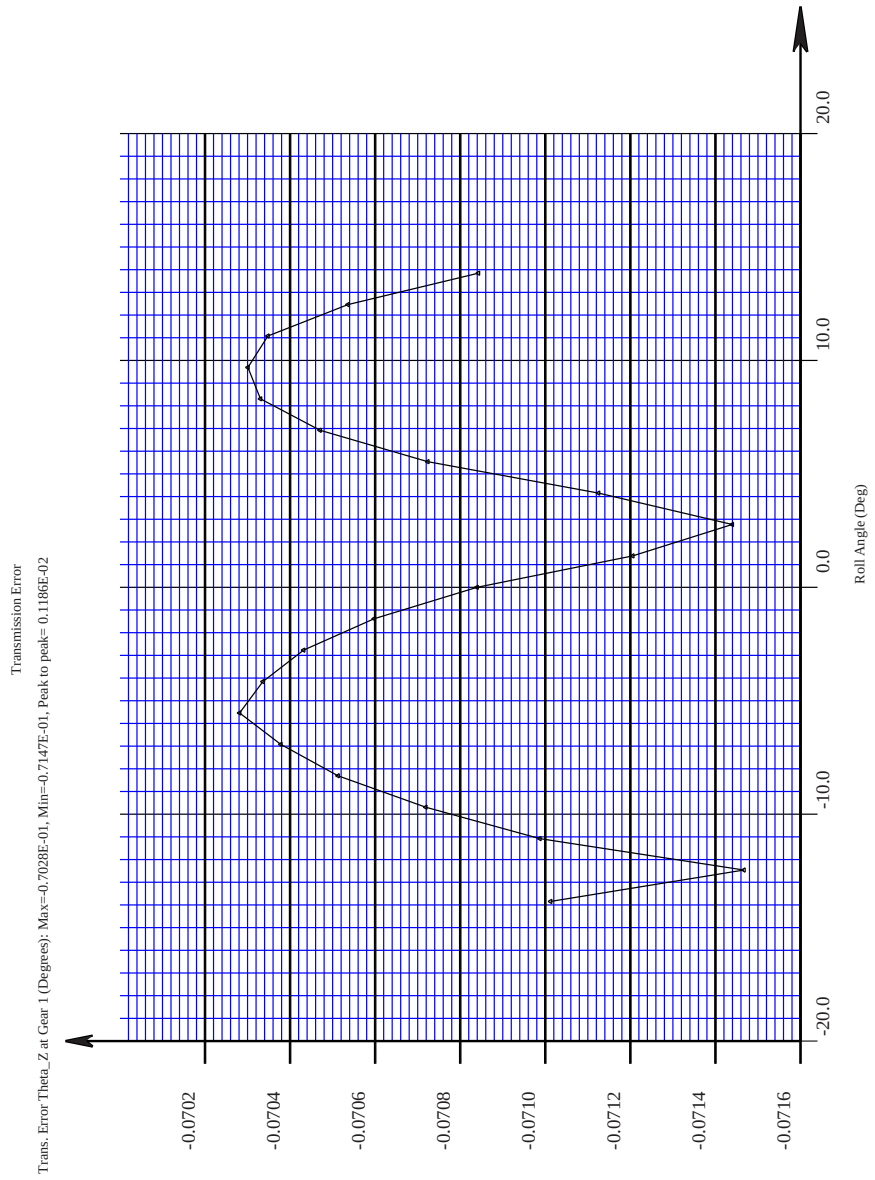

Figure 4.7: Transmission error predicted by CAPP for a helical gear model under a load of $8040lbf - in$. Peak to Peak transmission error obtained from CAPP is $23.40\mu in$.

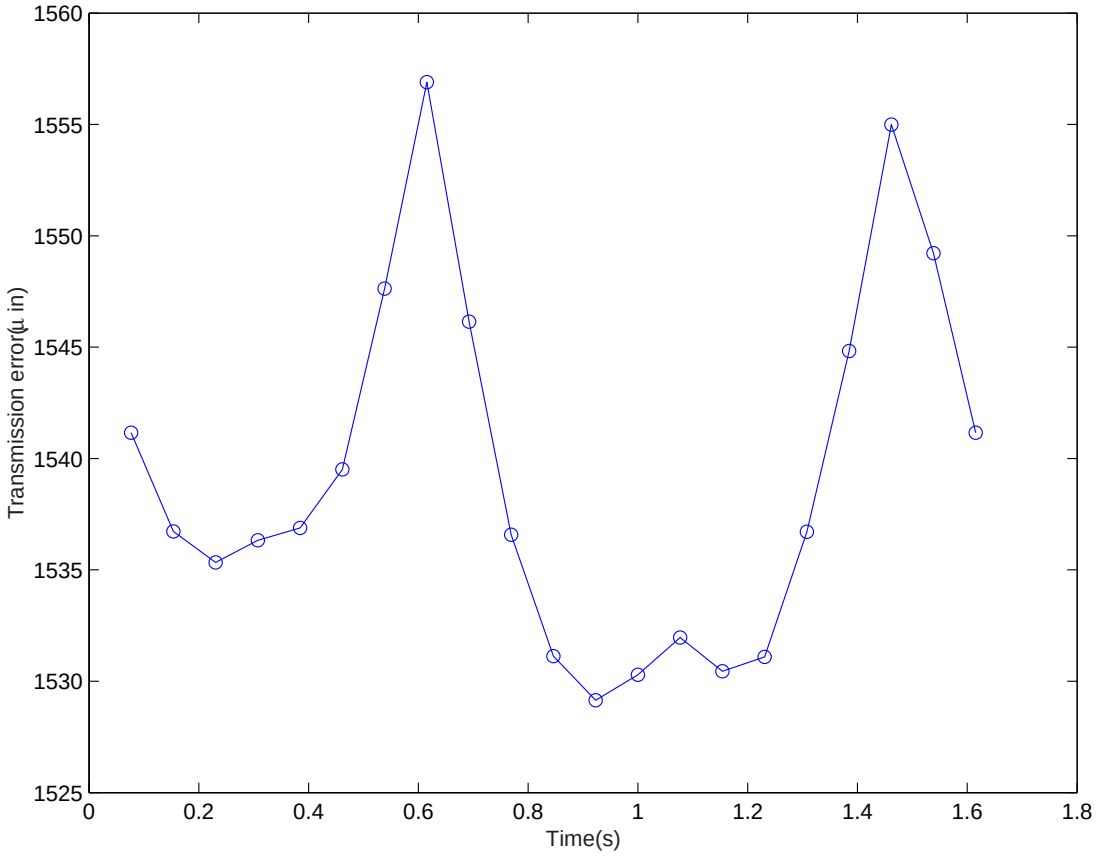

Figure 4.8: Transmission error predicted by Calyx for a low contact ratio spur gear model under a load of $8040lbf - in$. Peak to Peak transmission error obtained from Calyx is $27.75\mu in$.

Chapter 5

Internal helical gear pair example

The internal helical gear set example will help the user model an internal helical gear pair using the Helical3D program. Figure 5.1 shows the finite element model of a internal helical gear set.

5.1 The example file

Load the file `internal.ses` from the `EXAMPLES` directory under the `SAMPLES` directory.

The example model does not have any tooth modifications on the pinion or the gear.

Tables 5.2 through 5.11 show the data to be entered in the EDIT menu for running the internal gear model. No assembly errors are considered for the pinion and the ring/gear. Also there are no bearings in the model.

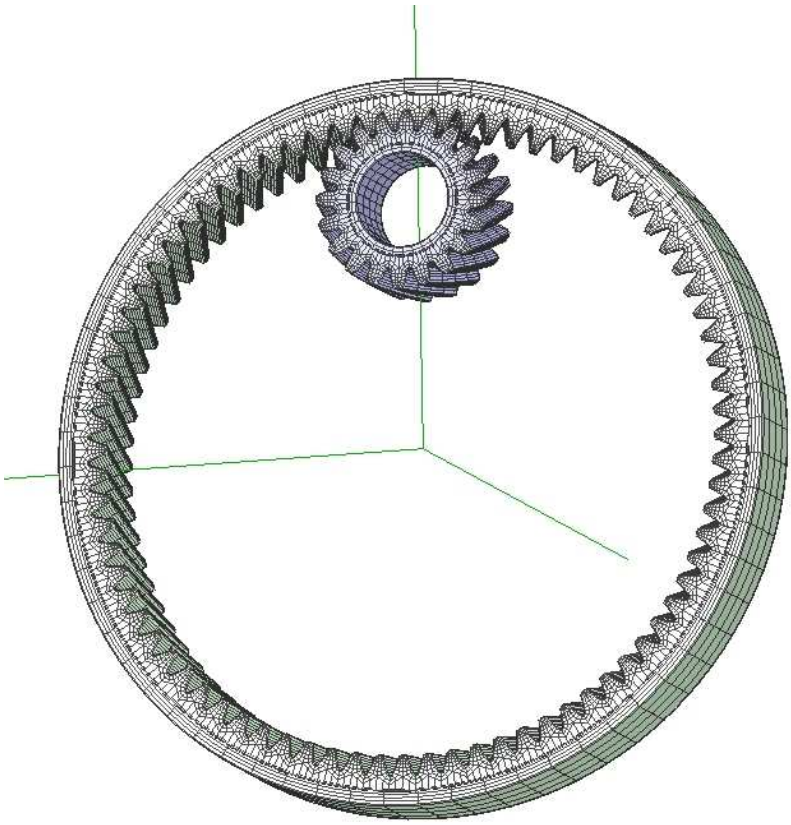

Figure 5.1: Finite element model of an internal helical gear set

Table 5.1: Units used for the internal helical gear set

Physical quantity	English
LENGTH	in
TIME	secs
ANGLE	deg or rad
MASS	lbf.s^2/in
MOMENT OF INERTIA	lbf.s^2.in
STIFFNESS	lbf/in
SPEED	RPM or rad/sec
TORQUE	lbf.in
YOUNGS MODULUS	lbf/in^2
DENSITY	lbf.s^2/in^4
LOAD	lbf
STRESSES	psi

Table 5.2: System configuration parameters

Item	Description
MESHTYPE	CALYX3D
CENTERDIST	3.02
OFFSET	0.00
ROTX	0.00
ROTY	0.00
INPUT	PINION
TORQUEINPUT	1000.00
RPMINPUT	-3.00
MU	0.00
MAGRUNOUTGEAR	0.00
ANGRUNOUTGEAR	0.00
MAGRUNOUTPINION	0.00
ANGRUNOUTPINION	0.00
BACKSIDECONTACT	FALSE

Table 5.3: Pinion data

Item	Description
LUMPMASS	0.00
LUMPMOMINERTIA	0.00
LUMPALPHA	0.00

Table 5.4: Pinion tooth data

Item	Description
NTEETH	20
NFACEELEMS	4
COORDORDER	10
DISPLORDER	3
PLANE	TRANSVERSE
XVERSEDIAMPITCH	10
XVERSEPRESSANGLE	20
XVERSETHICK	0.15708
FACEWIDTH	1
HAND	LEFT
HELIXANGLE	20.00
RACKTIPRAD	0.02
OUTERDIA	2.18
ROOTDIA	1.70
RIMDIA	1.40
YOUNGSMOD	$3x10^7$
POISSON	0.3
MSHFILE	pinion.msh
TPLFILE	medium.tpl

Table 5.5: Pinion rim data

Item	Description
RIMTYPE	SIMPLE
RIMDIA	1.40
INNERDIA	1.20
WIDTH	1.00
OFFSET	0.00
AXIALORDER	2
CIRCORDER	8
ELEMTYPE	LINEAR
NDIVSRADIAL	2
NTHETA	32
NDIVSWIDTH	4

Table 5.6: Pinion bearing menu

Item	Description
RIGIDRACE	FALSE
CIRCORDER	8
AXIALORDER	2
BEARING	FALSE

Table 5.7: Gear data

Item	Description
TYPE	INTERNAL
LUMPMASS	0.00
LUMPMOMINERTIA	0.00
LUMPALPHA	0.00

Table 5.8: Gear tooth data

Item	Description
NTEETH	80
NFACEELEMS	4
COORDORDER	10
DISPLORDER	3
PLANE	TRANSVERSE
XVERSEDIAMPITCH	10
XVERSEPRESSANGLE	20
XVERSETHICK	0.14
FACEWIDTH	1
HAND	LEFT
HELIXANGLE	20.00
RACKTIPRAD	0.04
OUTERDIA	7.80
ROOTDIA	8.30
RIMDIA	8.65
YOUNGSMOD	$3x10^7$
POISSON	0.3
MSHFILE	gear.msh
TPLFILE	medium.tpl

Table 5.9: Gear rim data

Item	Description
RIMTYPE	SIMPLE
RIMDIA	8.65
OUTERDIA	9.00
WIDTH	1.00
OFFSET	0.00
AXIALORDER	2
CIRCORDER	16
ELEMTYPE	QUADRATIC
NDIVSRADIAL	4
NTHETA	64
NDIVSWIDTH	4

Table 5.10: Gear bearing menu

Item	Description
RIGIDRACE	FALSE
CIRCORDER	16
AXIALORDER	2
BEARING	FALSE

Table 5.11: Setup data

Item	Description
SEPTOL	0.01
NPROFDIVS	8
NFACEDIVS	12
DSPROF	0.001
ZEROINITIAL	TRUE
INITIALTIME	-0.5
NRANGES	1
RANGE	1
SOLMETHOD	STATIC
NTIMESTEPS	11
DELTATIME	0.1
STARTSPEEDFACTOR	1.0
STARTTORQUEFACTOR	1.0
ENDTORQUEFACTOR	1.0
SAVEPERIODICALLY	FALSE
OUTPUTRESTART	FALSE
POSTPROCWRITE	TRUE
POSTFILENAME	postproc.dat
NSTEPSWRITE	1

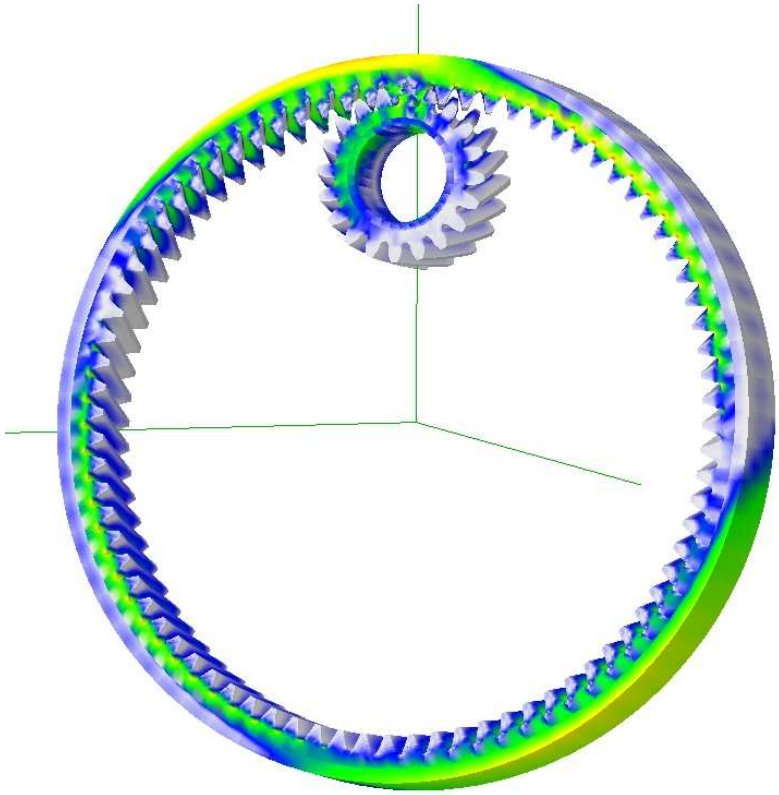

Figure 5.2: Maximum principal normal stress contour for an internal helical gear set

5.2 Results

After the analysis is complete a postprocessing file is created in the working directory. Figure 5.2 shows the maximum principal normal stress contour for the internal helical gear pair.

Chapter 6

Internal helical gear with webbed rim

Figure 6.1 shows the finite element model of a internal helical gear set with webbed rim .

6.1 The example file

Load the file `internalwebbed.ses` from the `EXAMPLES` directory.

The data is similar to the previous example except for the rim menu. The example model does not have any tooth modifications on the pinion or the gear.

6.2 Modeling the rim

The purpose of including a rim model is to apply the correct boundary conditions to the tooth model. This is important because the boundary conditions can have a significant effect on the load and stress distribution.

The webbed rim is composed of an arbitrary number of 'segments'(in this case 4). The position of the first segment cannot be changed. As discussed in the Users manual each of the remaining segments can be placed in four different positions(AHEAD, BEHIND, INSIDE and OUTSIDE) relative to the previous segment.

Table 6.1 shows the data common to all the segments for the webbed rim for the internal gear. Table 6.2 show the radial and axial coordinates for each segment and their respective positions relative to the previous segment.

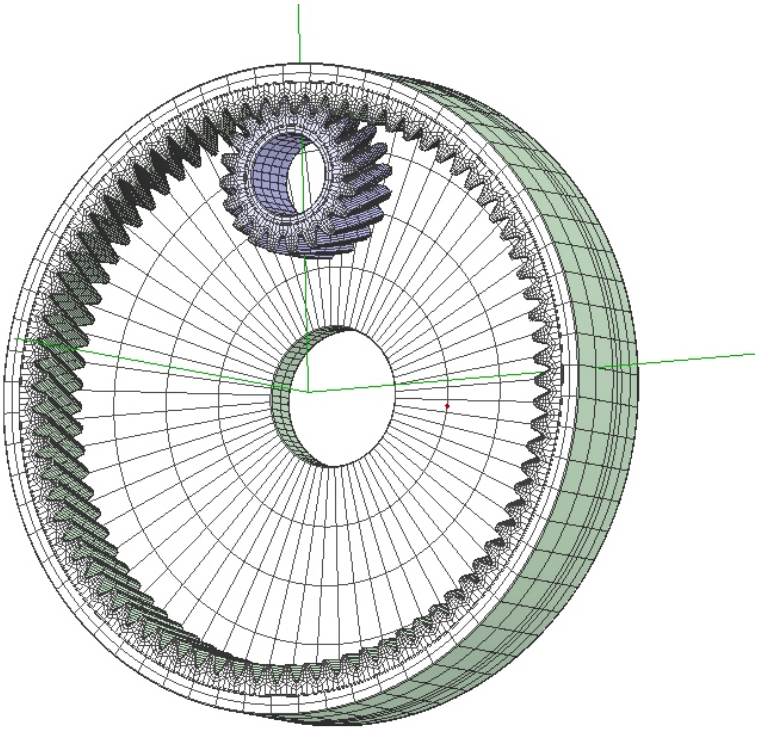

Figure 6.1: Finite element model of an internal helical gear set with a webbed rim

Table 6.1: Webbed rim data common to all segments

Item	Description
RIMTYPE	WEBBED
RIMDIA	8.65
NTHETA	64
ELEMTYPE	QUADRATIC
AXIALORDER	2
CIRCORDER	16
NSEGS	4
NETA	2
NZETA	2

Table 6.2: Data for each segment of the webbed rim

ISEG	POSITION	RA	RB	ZA	ZB
1	OUTSIDE	4.575	4.575	-0.50	0.50
2	BEHIND	4.325	4.575	-0.75	-0.75
3	BEHIND	4.325	4.575	-1.25	-1.25
4	INSIDE	1.00	1.00	-1.25	-0.75

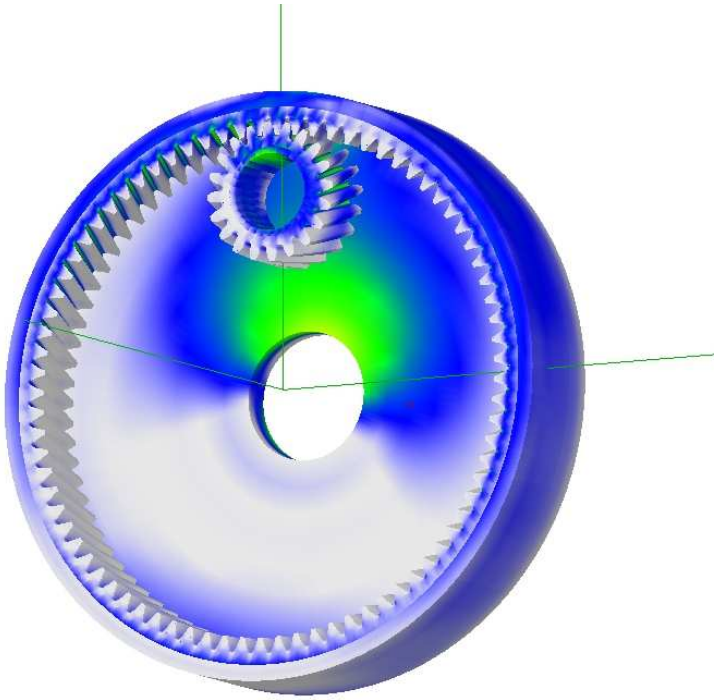

Figure 6.2: Maximum principal normal stress contour for an internal helical gear set with a webbed rim

6.3 Results

After the analysis is complete a postprocessing file is created in the working directory. Figure 6.2 shows the maximum principal normal stress contour for the internal helical gear pair.

Chapter 7

Modeling splines using the Helical 3D program

Using the Helical3D program external splines or internal splines can be used with external or internal gears. Thus it is possible to model four different combinations of gears and splines.

7.1 Internal splines on external gear

The following example has internal splines on an external gear(Pinion). Figure 7.1 shows the model of a internal helical gear set with splines on the inner diameter of the Pinion .

7.1.1 The example file

Load the file `extgearintsplines.ses` from the `EXAMPLES` directory.

The data is similar to the Internal helical gear pair example except for the pinion rim menu. The example model does not have any tooth modifications on the pinion or the gear.

7.1.2 Modeling the splines

The INTERNALSPLINED option in the Rim menu refers to the internal splines. The pinion rim data to model the internal splines on the pinion is shown in Table 7.1. All the splines are evenly spaced along the inner diameter of the pinion.

7.1.3 Results

After the analysis is complete a postprocessing file is created in the working directory. Figure 7.2 shows the maximum principal normal stress contour for the internal helical gear pair. Figure 7.3 shows the load distribution on the pinion and the splines.

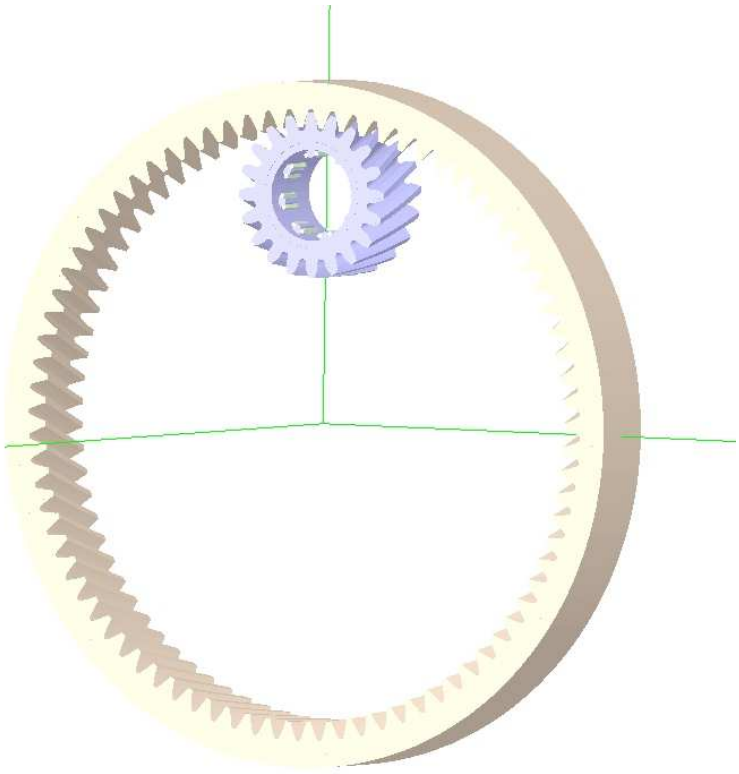

Figure 7.1: An internal helical gear set with internal splines on the external gear

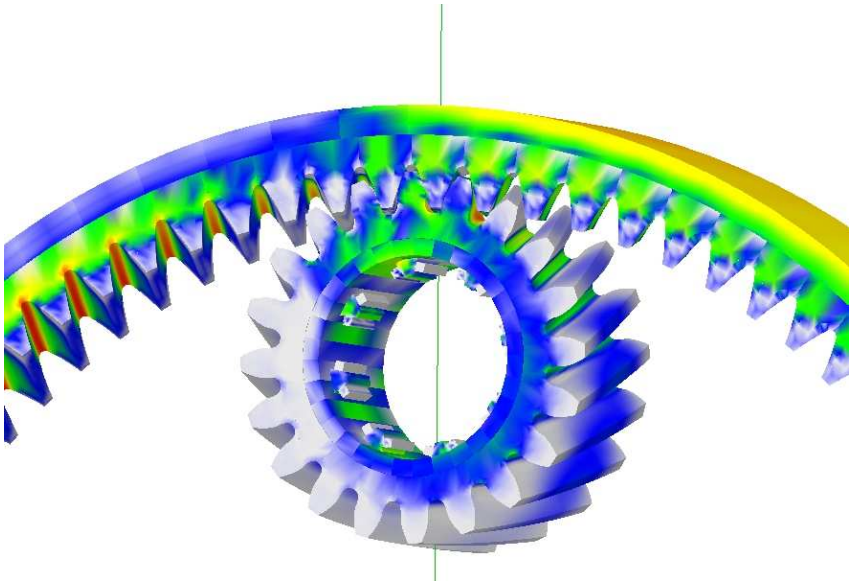

Figure 7.2: Maximum principal normal stress contour for an internal helical gear set with internal splines on the pinion

Table 7.1: Pinion rim menu to model the internal splines

Item	Description
RIMTYPE	INTERNALSPLINED
TYPE	DOUBLESIDED
BACKLASH	0.00
RIMDIA	1.40
INNERDIA	1.20
RIMWIDTH	1.00
RIMOFFSET	0.00
AXIALORDER	2
CIRCORDER	8
ELEMTYPE	LINEAR
NDIVSRADIAL	2
NTHETA	32
NDIVSWIDTH	4
NSPLINES	8
PRESSANGLE	10
SPLINEWIDTH	0.15
SPLINEHEIGHT	0.10
SPLINELENGTH	0.35
SPLINEOFFSET	0.15
EVEN	TRUE
ANGPOSNFIRSTSPLIN	0.00
SPLINEELEMTYPE	QUADRATIC
NDIVSSPLINEWIDTH	2
NDIVSSPLINEHEIGHT	2
NDIVSSPLINELENGTH	2

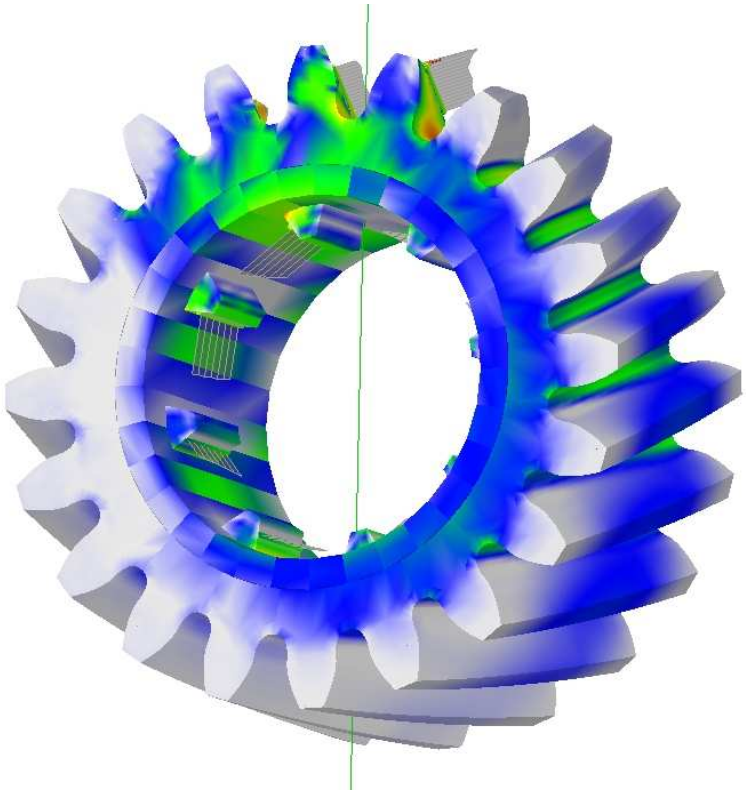

Figure 7.3: Load distribution on the pinion and the splines

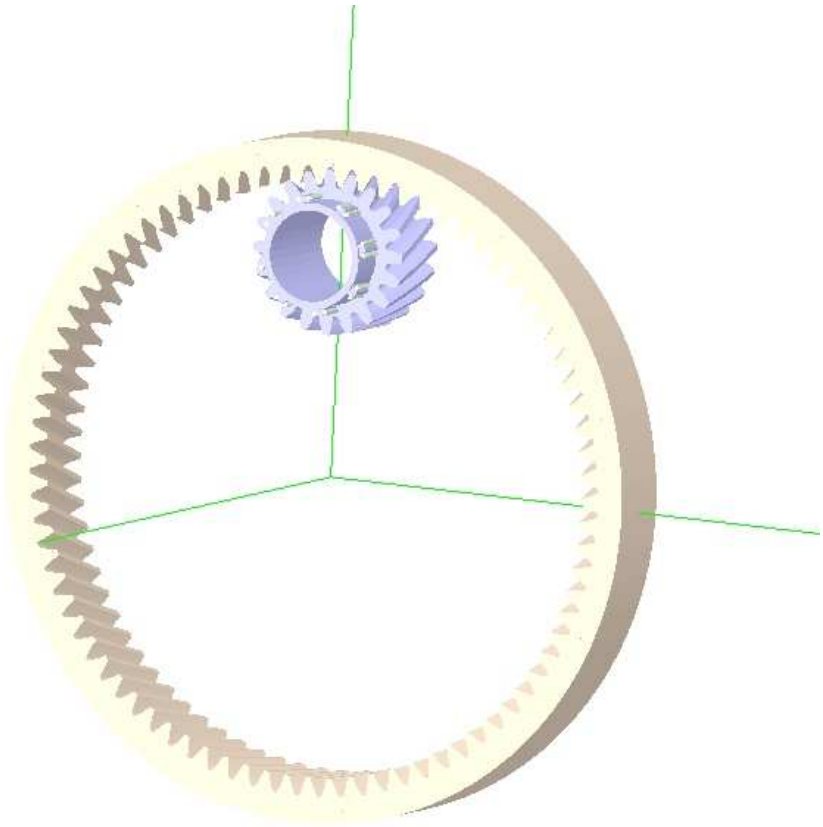

Figure 7.4: An internal helical gear set with external splines on the external gear

7.2 External splines on external gear

The following example has external splines on an external gear(Pinion). Figure 7.4 shows the model of a internal helical gear set with external splines on the Pinion .

7.2.1 The example file

Load the file `extgearextsplines.ses` from the `EXAMPLES` directory.

The data is similar to the Internal helical gear pair example except for the pinion rim menu. The example model does not have any tooth modifications on the pinion or the gear.

7.2.2 Modeling the splines

The EXTERNALSPLINED option in the Rim menu refers to the external splines. The pinion rim data to model the external splines on the pinion is shown in Table 7.2. All the splines are evenly spaced along the rim diameter of the pinion.

Table 7.2: Pinion rim menu to model the external splines

Item	Description
RIMTYPE	EXTERNALSPLINED
TYPE	DOUBLESIDED
BACKLASH	0.00
RIMDIA	1.40
INNERDIA	1.20
RIMWIDTH	1.50
RIMOFFSET	0.25
AXIALORDER	2
CIRCORDER	8
ELEMTYPE	LINEAR
NDIVSRADIAL	2
NTHETA	32
NDIVSWIDTH	4
NSPLINES	8
PRESSANGLE	10
SPLINEWIDTH	0.15
SPLINEHEIGHT	0.10
SPLINELENGTH	0.35
SPLINEOFFSET	0.80
EVEN	TRUE
ANGPOSNFIRSTSPLIN	0.00
SPLINEELEMTYPE	QUADRATIC
NDIVSSPLINEWIDTH	2
NDIVSSPLINEHEIGHT	2
NDIVSSPLINELENGTH	2

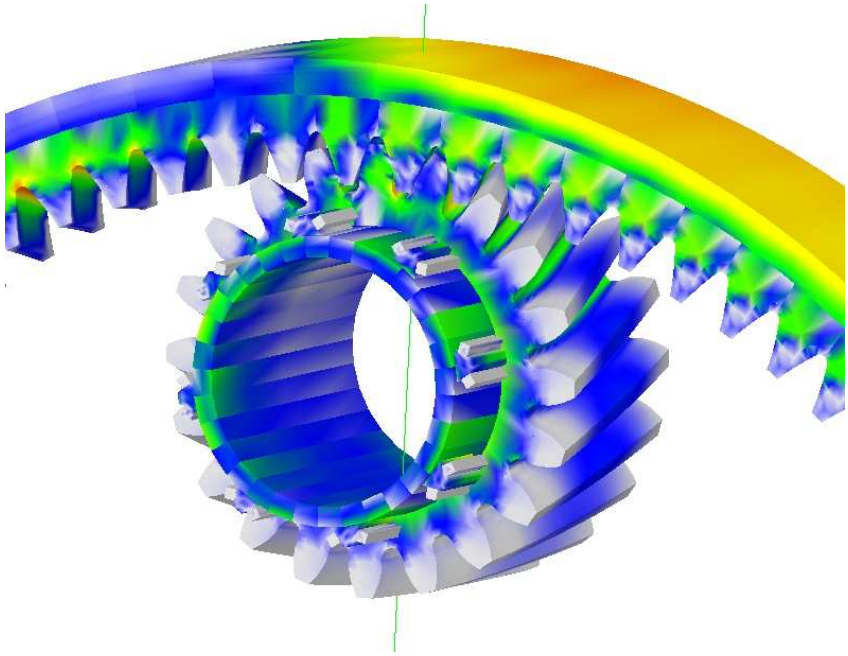

Figure 7.5: Maximum principal normal stress contour for an internal helical gear set with external splines on the pinion

7.2.3 Results

After the analysis is complete a postprocessing file is created in the working directory. Figure 7.5 shows the maximum principal normal stress contour for the internal helical gear pair. Figure 7.6 shows the load distribution on the pinion and the splines.

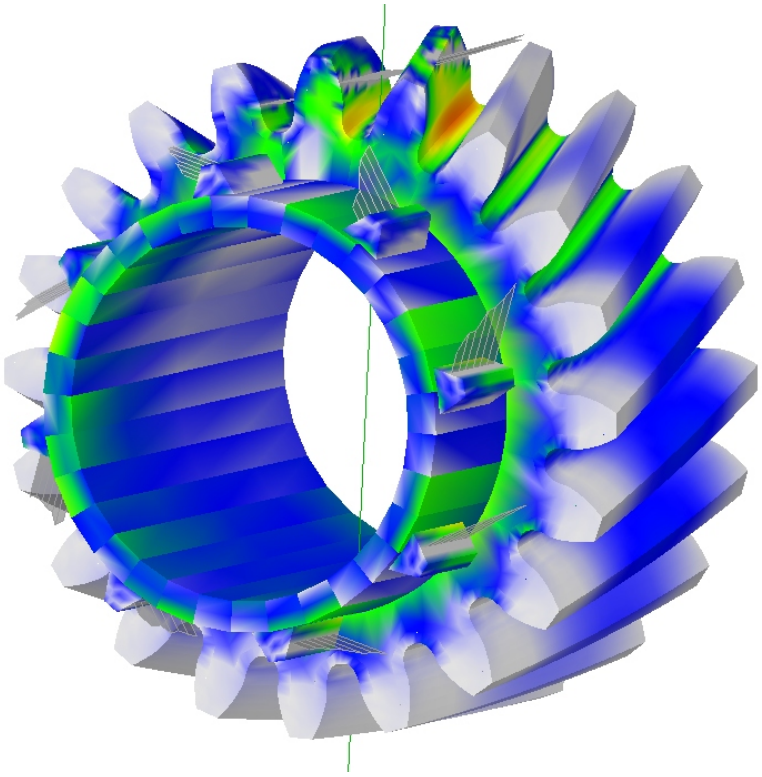

Figure 7.6: Load distribution on the pinion and the splines

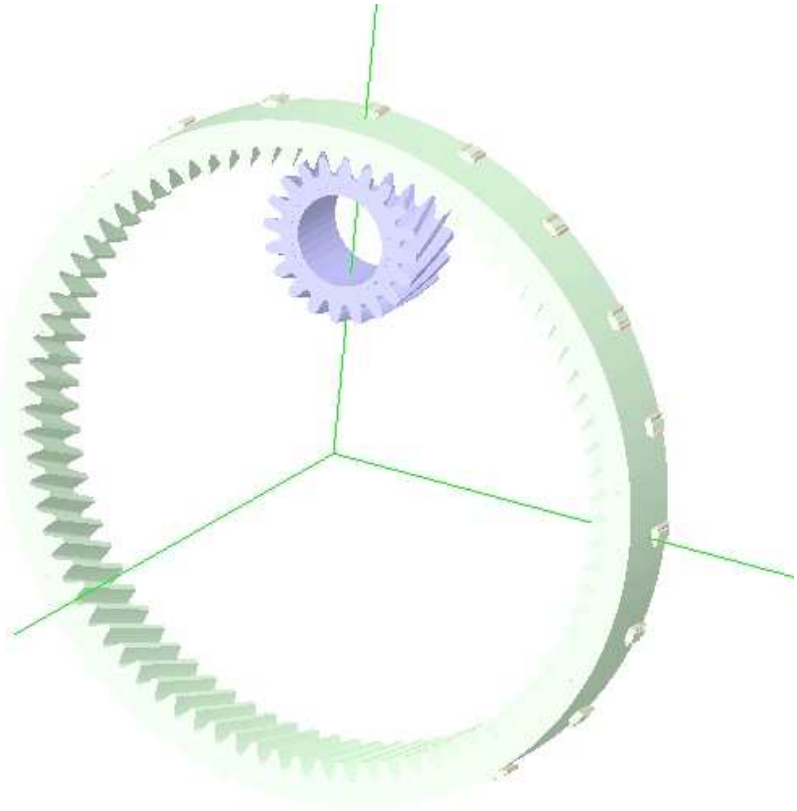

Figure 7.7: An internal helical gear set with external splines on the internal gear

7.3 External splines on internal gear

The following example has external splines on an internal gear. Figure 7.7 shows the model of an internal helical gear set with external splines on the Ring(internal) gear.

7.3.1 The example file

Load the file `intgearextsplines.ses` from the `EXAMPLES` directory.

The data is similar to the Internal helical gear pair example except for the pinion rim menu. The example model does not have any tooth modifications on the pinion or the gear.

7.3.2 Modeling the splines

The EXTERNALSPLINED option in the Rim menu refers to the external splines. The Gear rim data to model the external splines on the internal gear is shown in Table 7.3. All the splines are evenly spaced along the outer diameter of the gear.

Table 7.3: Gear rim menu to model the external splines

Item	Description
RIMTYPE	EXTERNALSPLINED
TYPE	DOUBLESIDED
BACKLASH	0.00
RIMDIA	8.65
OUTERDIA	9.00
RIMWIDTH	1.00
RIMOFFSET	0.00
AXIALORDER	2
CIRCORDER	16
ELEMTYPE	QUADRATIC
NDIVSRADIAL	4
NTHETA	64
NDIVSWIDTH	4
NSPLINES	20
PRESSANGLE	25
SPLINEWIDTH	0.20
SPLINEHEIGHT	0.10
SPLINELENGTH	0.30
SPLINEOFFSET	-0.25
EVEN	TRUE
ANGPOSNFIRSTSPLIN	0.00
SPLINEELEMTYPE	QUADRATIC
NDIVSSPLINEWIDTH	2
NDIVSSPLINEHEIGHT	2
NDIVSSPLINELENGTH	2

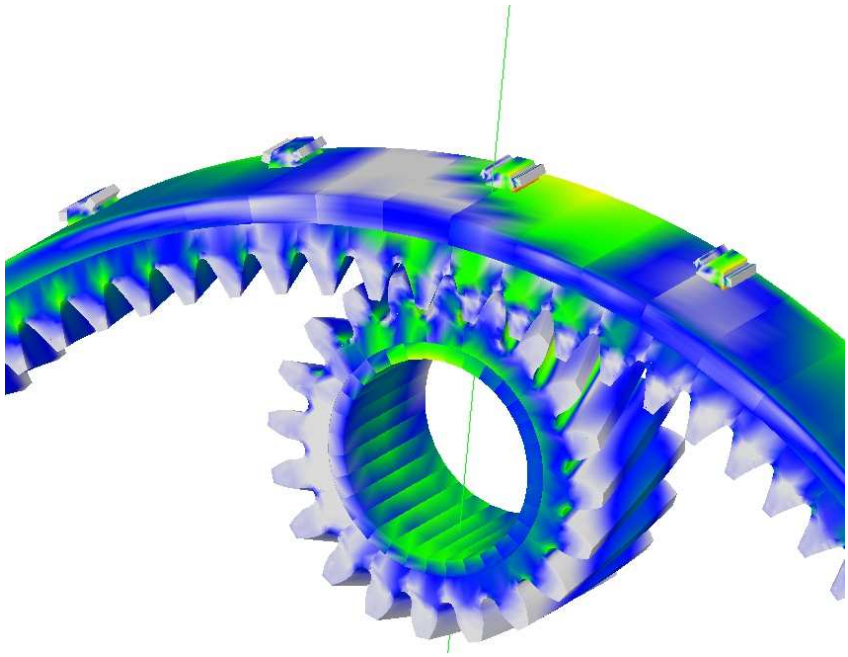

Figure 7.8: Maximum principal normal stress contour for an internal helical gear set with external splines on the internal gear

7.3.3 Results

After the analysis is complete a postprocessing file is created in the working directory. Figure 7.8 shows the maximum principal normal stress contour for the internal helical gear pair. Figure 7.9 shows the contact pressure distribution on the gear and the splines.

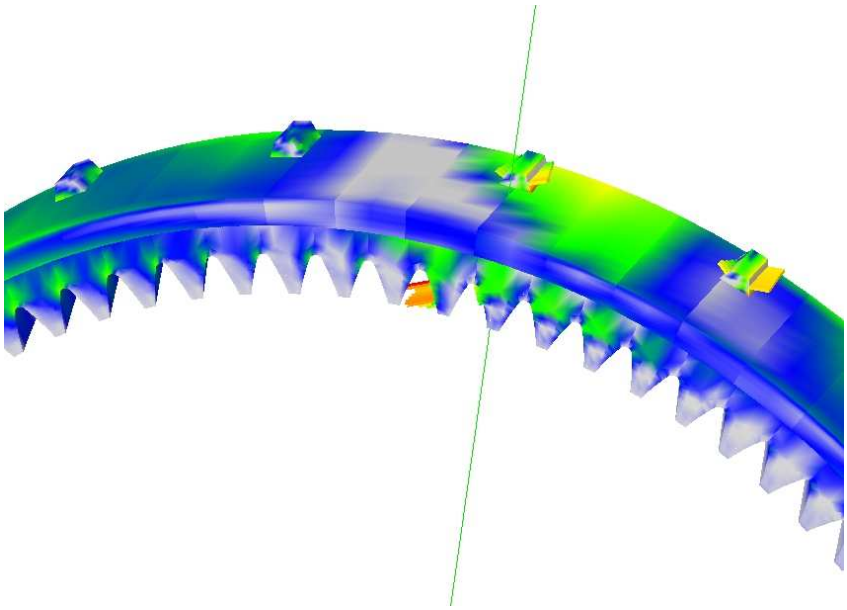

Figure 7.9: Contact pressure distribution for an internal helical gear set with external splines on the internal gear

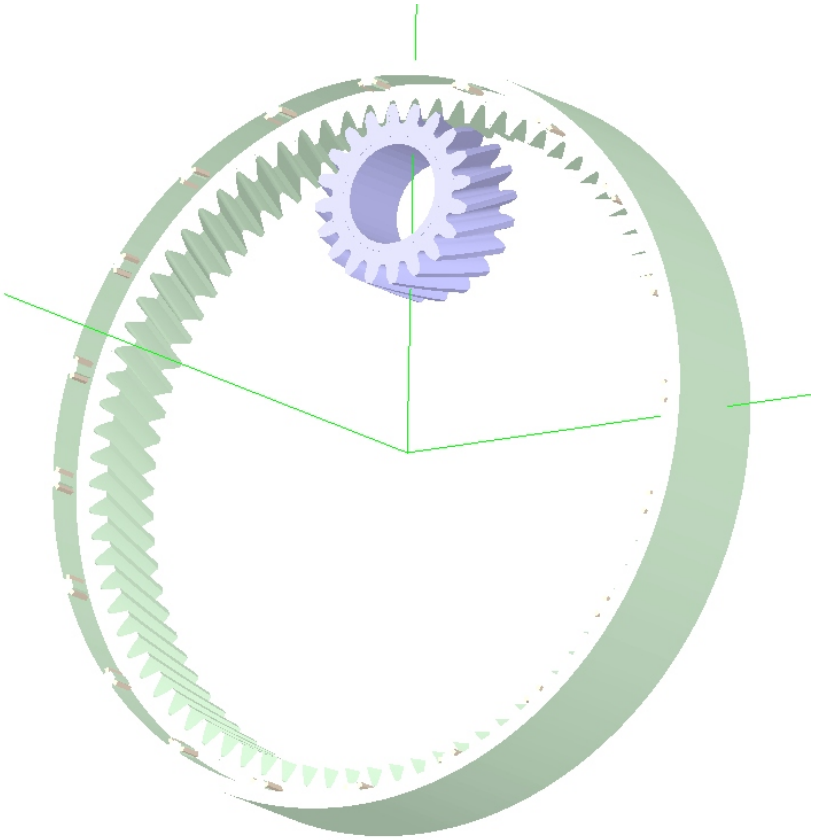

Figure 7.10: An internal helical gear set with internal splines on the internal gear

7.4 Internal splines on internal gear

The following example has internal splines on an internal gear. Figure 7.10 shows the model of an internal helical gear set with internal splines on the Ring(internal) gear.

7.4.1 The example file

Load the file `intgearintsplines.ses` from the `EXAMPLES` directory.

The data is similar to the Internal helical gear pair example except for the gear rim menu. The example model does not have any tooth modifications on the pinion or the gear.

7.4.2 Modeling the splines

The INTERNALSPLINED option in the Rim menu refers to the internal splines. The Gear rim data to model the internal splines on the internal gear is shown in Table 7.4. All the splines are evenly spaced along the rim diameter of the gear.

Table 7.4: Gear rim menu to model the internal splines

Item	Description
RIMTYPE	INTERNALSPLINED
TYPE	DOUBLESIDED
BACKLASH	0.00
RIMDIA	8.65
OUTERDIA	9.00
RIMWIDTH	1.50
RIMOFFSET	0.25
AXIALORDER	2
CIRCORDER	16
ELEMTYPE	QUADRATIC
NDIVSRADIAL	4
NTHETA	64
NDIVSWIDTH	4
NSPLINES	20
PRESSANGLE	25
SPLINEWIDTH	0.20
SPLINEHEIGHT	0.10
SPLINELENGTH	0.30
SPLINEOFFSET	0.85
EVEN	TRUE
ANGPOSNFIRSTSPLIN	0.00
SPLINEELEMTYPE	QUADRATIC
NDIVSSPLINEWIDTH	2
NDIVSSPLINEHEIGHT	2
NDIVSSPLINELENGTH	2

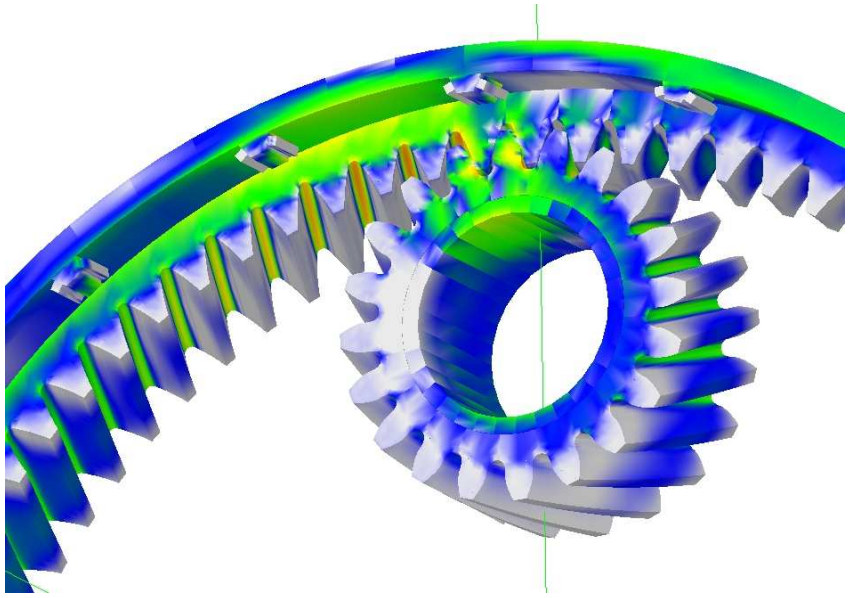

Figure 7.11: Maximum principal normal stress contour for an internal helical gear set with internal splines on the internal gear

7.4.3 Results

After the analysis is complete a postprocessing file is created in the working directory. Figure 7.11 shows the maximum principal normal stress contour for the internal helical gear pair. Figure 7.12 shows the contact pressure distribution on the gear and the splines.

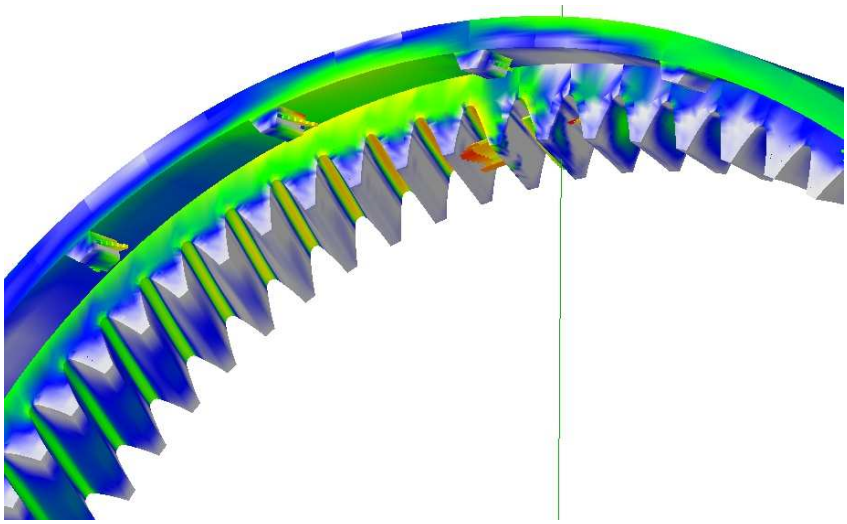

Figure 7.12: Contact pressure distribution for an internal helical gear set with internal splines on the internal gear

Chapter 8

Example of topographic modification

Using the Helical3D program topographic modifications can be applied on to the gear tooth. Following example shows how to model a pinion tooth with topographic modification. Figure 8.1 shows a finite element model of a helical gear set in the preprocessing view.

8.1 The example file

Load the file `topomod.ses` from the `TOPOMODFN` directory located in the `SAMPLES` directory .

The data is similar to the no tooth modification gear pair example except for the pinion tooth modification menu. The example model does not have any tooth modifications on the gear. We have specified a helix angle of 20 for both pinion and gear tooth. We run the analysis for one tooth cycle.

8.2 Applying topographic modifications on the pinion tooth

A surface modification that is an arbitrary function of both the roll angle and zeta can be specified using the topographic modification option. The TOPOMOD command in the tooth data menu leads to the topographic modification menu. The modification is specified at an arbitrary number of ζ and roll angle values. The magnitude is specified for each pair of these values. Bilinear interpolation is used between them.

The modification data is specified in the TOPOMOD menu using the script file topomod.txt located in the working directory(WORKDIR). Figure 8.2 shows the rollangles in degrees along the profile and zeta values along the facewidth at which modification is applied. For the present example the contact for tooth no.1 of the pinion starts at a roll angle(degrees) of 11.84 near the root region. We assume that the modification is applied between the roll angles(deg) 11.84 and 14.85 in the root region and between the roll angles 29.40 and 33.67 near the tip region.

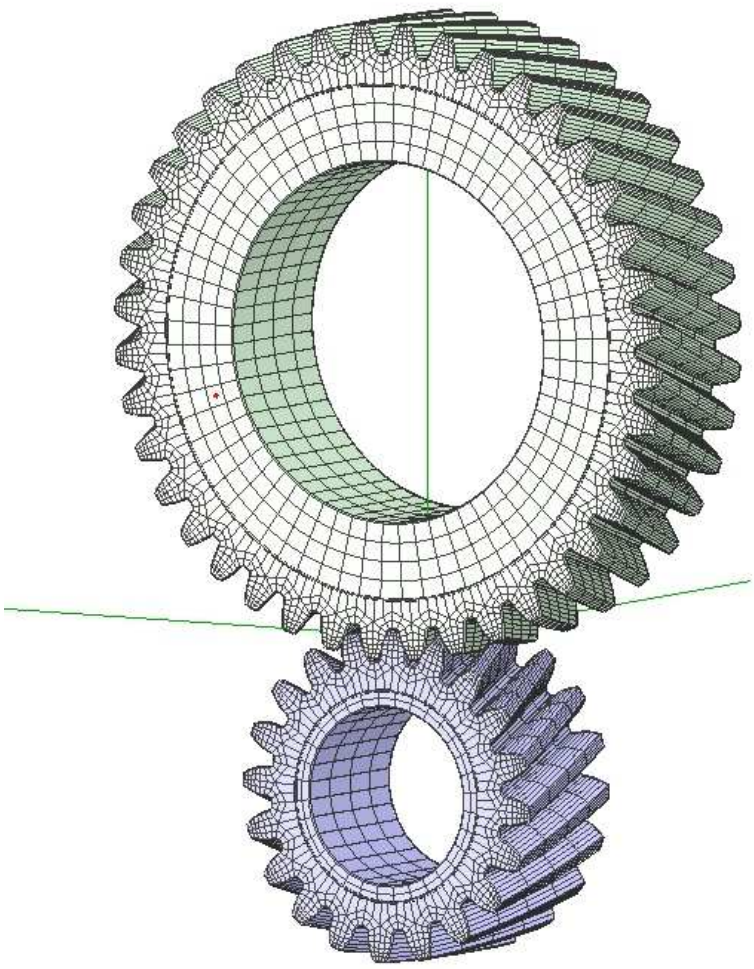

Figure 8.1: An external helical gear set with topographical modifications applied on to the pinion tooth

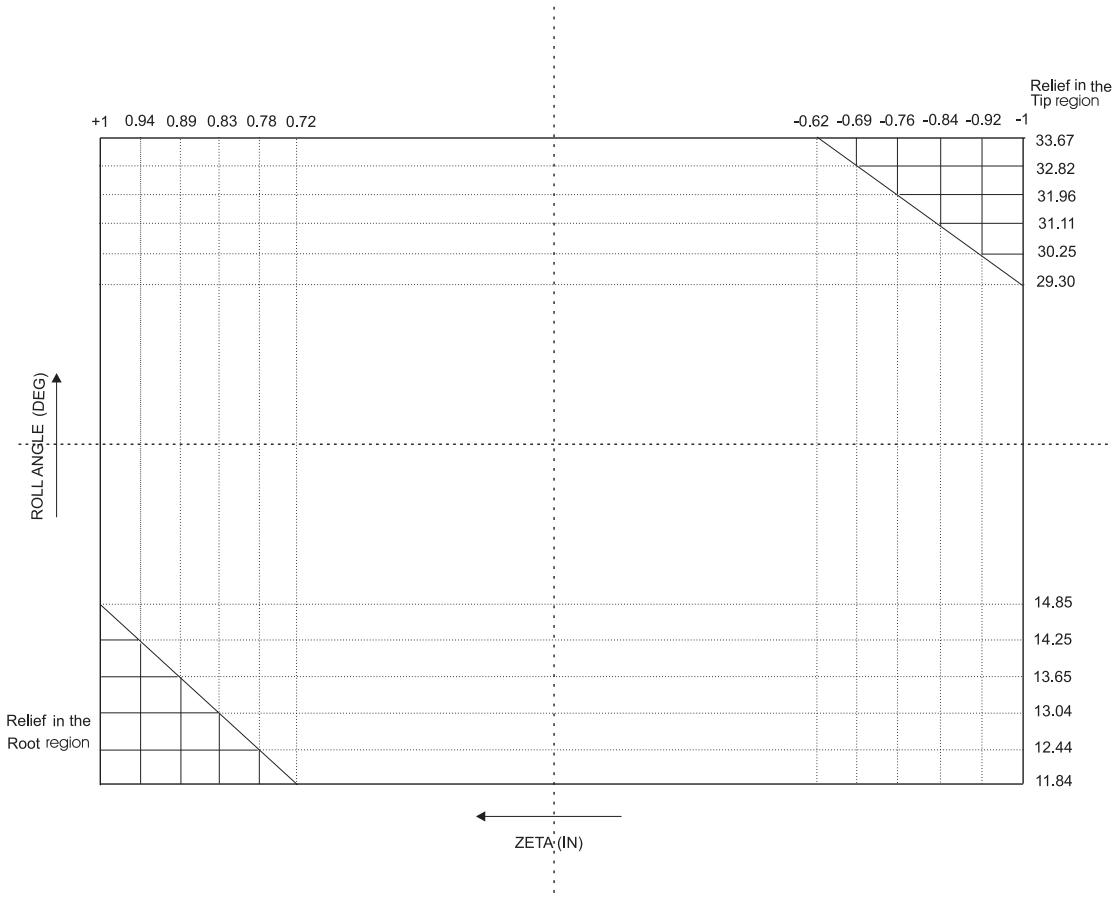

Figure 8.2: Roll angle and zeta values for which modification is applied

The zeta extension for modification is found using the following:

From the Pinion tooth geometry data:

$$\begin{aligned}
\text{Pitch diam}(D_p) &= 2in \\
\text{Helix angle}(\psi) &= 20^o \\
\text{Facewidth}(W) &= 1in \\
\text{Lead}(L) &= \frac{\pi D_p}{tan\psi} \\
&= 17.2629in
\end{aligned}$$

In the root region :

$$\begin{aligned}
\text{Distance of modfn along the profile in roll angle}(\theta) &= 14.85 - 11.84 \\
&= 3.01^o \\
\text{Distance of modification along the profile in inches} &= r_b \times \theta(rads) \\
&= 0.9395 \times 0.0525 \\
&= 0.049in \\
\text{Distance of modification along the width in inches} &= \frac{0.049 \times L}{2\pi} \\
&= 0.135in.
\end{aligned}$$

Note that the ZETA along the facewidth goes from -1 to +1.

The corresponding Zeta distance of modification along the facewidth is 0.135 × 2 = 0.27in.

In the tip region :

$$\begin{aligned}
\text{Distance of modfn along the profile in roll angle}(\theta) &= 33.67 - 29.40 \\
&= 4.27^o \\
\text{Distance of modification along the profile in inches} &= r_b \times \theta(rads) \\
&= 0.9395 \times 0.0745 \\
&= 0.07in \\
\text{Distance of modification along the width in inches} &= \frac{0.07 \times L}{2\pi} \\
&= 0.192in.
\end{aligned}$$

The corresponding Zeta distance of modification along the facewidth is 0.192 × 2 = 0.384in.

For this example we have considered 6 points along the modified profile and width in both the root and the tip region as shown in Figure 8.2. In the root region, maximum modification magnitude of $0.0005in$ is applied at Rollangle(deg) and zeta(in) value of 11.84 and +1 respectively. In the tip region, maximum modification magnitude of $0.0005in$ is applied at Rollangle(deg) and zeta(in) value of 33.67 and -1 respectively. We reduce the modification magnitude in steps of $0.0001in$ as we go away from the root and the tip regions. The modification at roll angles(deg) 14.85 and 29.30 is $0.00in$. Refer to the text file `topomod.txt` for further details.

8.3 Results

After the analysis is complete a postprocessing file is created in the working directory. Figure 8.3 shows the contact pattern plot for pinion tooth with topographical modification. The relieved tip region at $Zeta = -1$ and root region at $Zeta = 1$ can be clearly seen in this plot. Figure 8.4 shows the contact pattern plot for pinion tooth without any modifications. Figure 8.5 shows the body deflection plot for pinion tooth with topographical modification. The transmission error for the gear model with modification is $1.953 \times 10^{-5} rads = 1.8348 \times 10^{-5} in$. Figure 8.6 shows the body deflection plot for pinion tooth without any modifications. The transmission error for the Helical gear set without any modification is $2.508 \times 10^{-}5 rads = 2.356 \times 10^{-}5 in$.

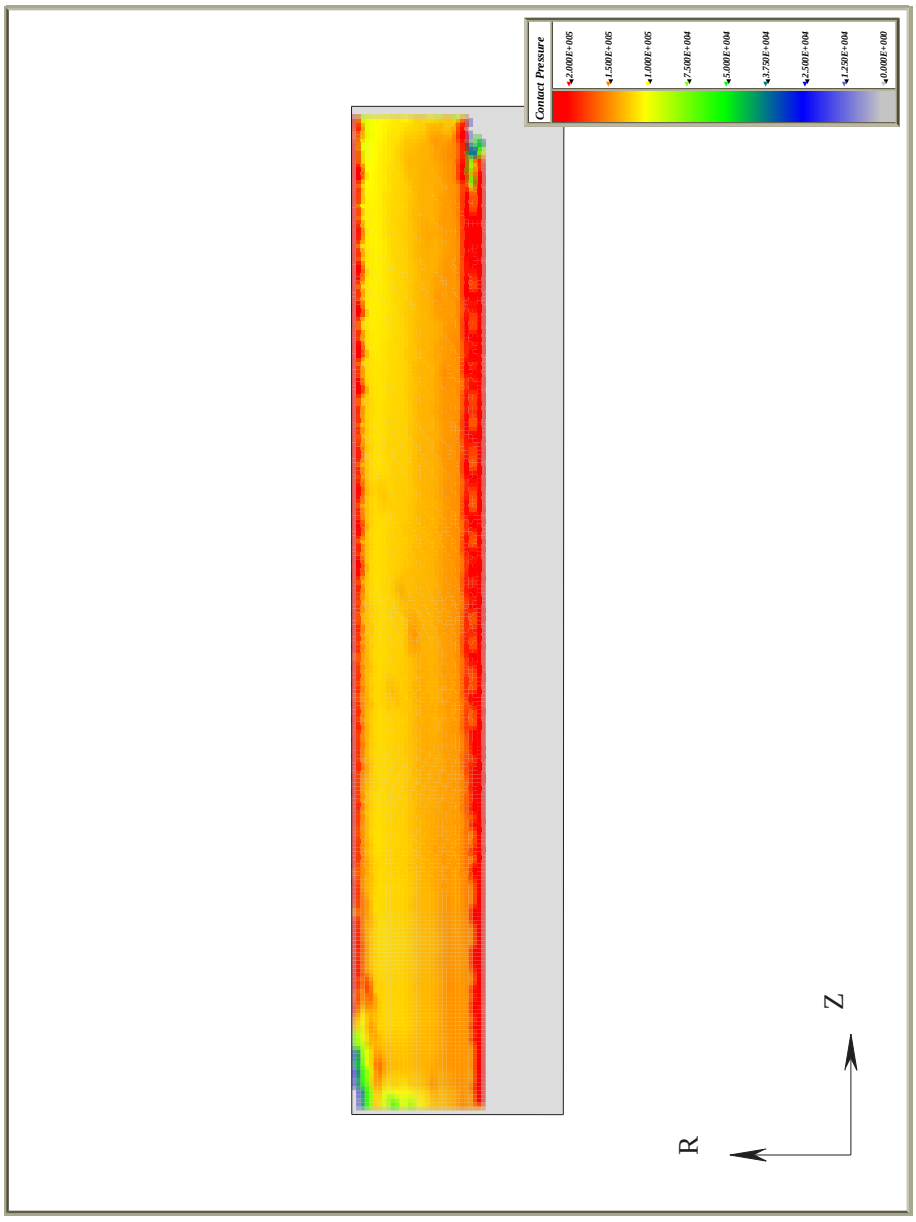

Figure 8.3: Contact pattern for pinion tooth with topographical modifications

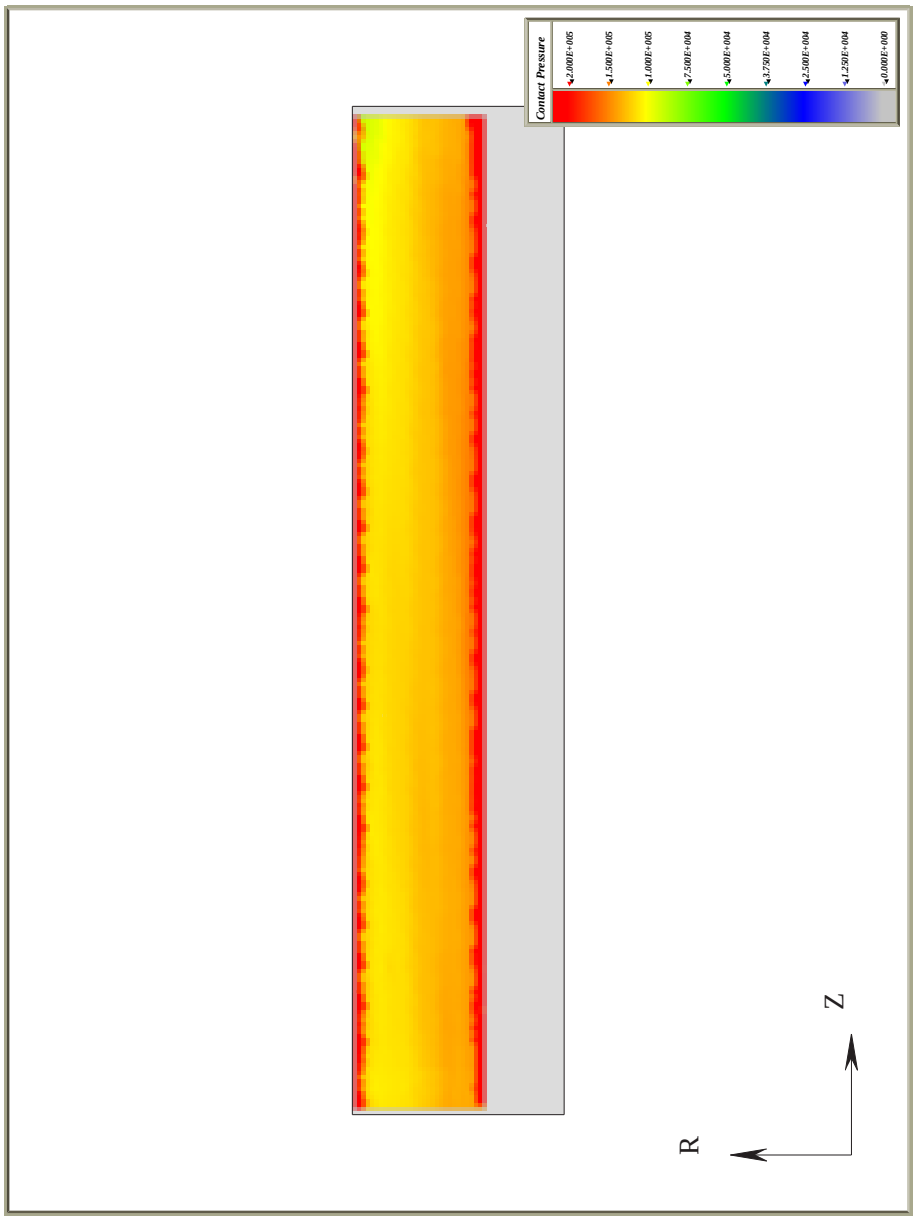

Figure 8.4: Contact pattern for pinion tooth without any modifications

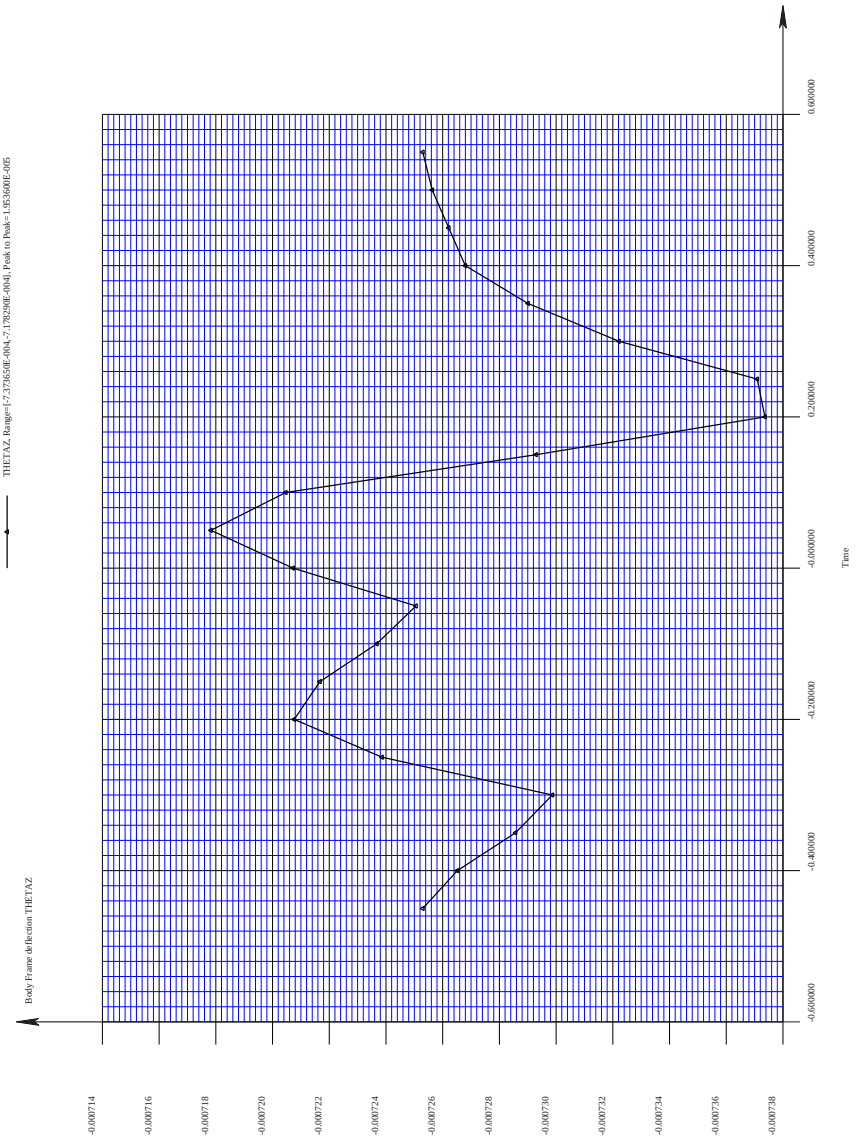

Figure 8.5: Body deflection plot showing the transmission error for pinion tooth with topographical modifications

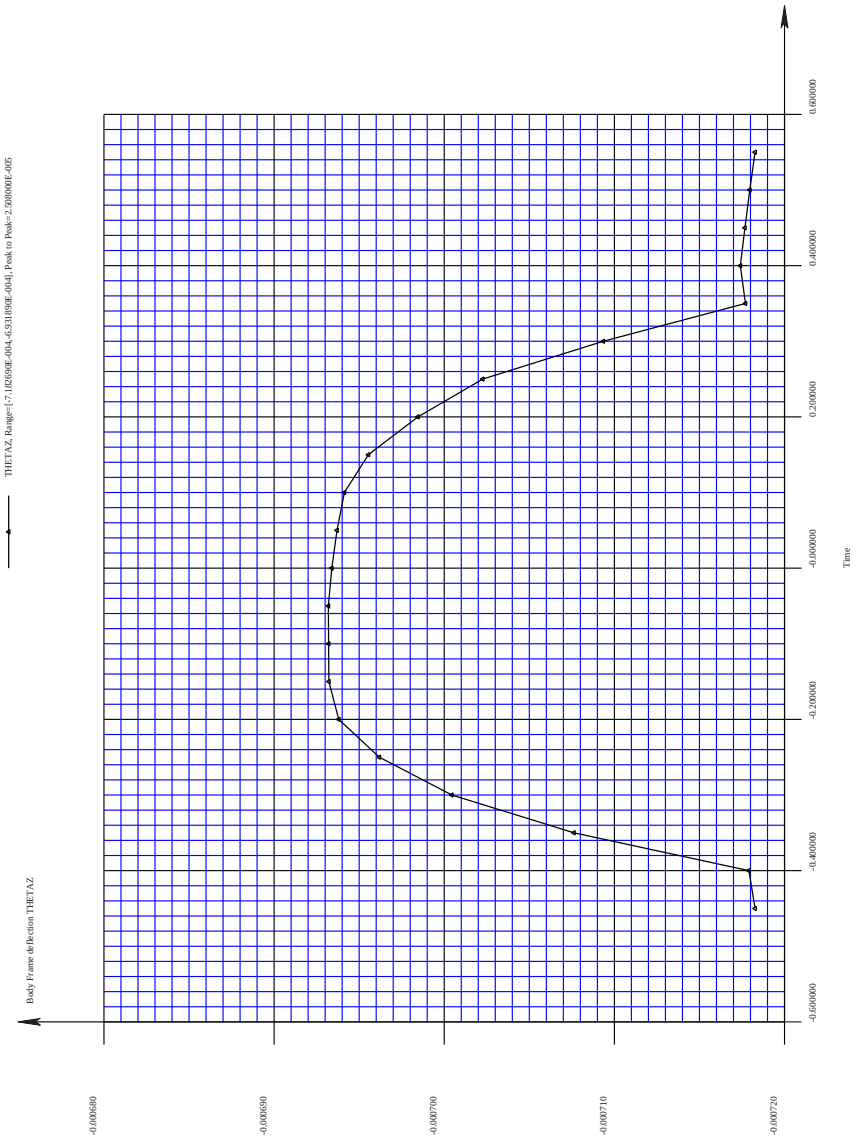

Figure 8.6: Body deflection plot showing the transmission error for pinion tooth without any modifications

Chapter 9

Convergence study

The following test cases are meant to study the effect of various parameters such as tip radius, thickness, nfaceelems and displorder on the maximum principle normal stress for a helical pinion and also the convergence of the stress values for different types of mesh templates.

9.1 Effect of Tip radius on the max ppl normal stress

9.1.1 The example file

Load the file `convergence.ses` from the `CONVERGENCE` directory located in the `SAMPLES` directory.

Tables 9.1 through 9.10 show the data to be entered in the EDIT menu for running the analysis. No assembly errors are considered for the pinion and the gear. Also there are no bearings in the model. In order to study the effect of tip radius on the stress values we run the analysis for different tip radii for all the mesh templates. We vary the tip radius from $0.01in$ to $0.045in$ in steps of $0.005in$.

Table 9.1: System configuration parameters

Item	Description
MESHTYPE	CALYX3D
CENTERDIST	3.00
OFFSET	0.00
ROTX	0.00
ROTY	0.00
INPUT	PINION
TORQUEINPUT	1000.00
RPMINPUT	-3.00
MU	0.00
MAGRUNOUTGEAR	0.00
ANGRUNOUTGEAR	0.00
MAGRUNOUTPINION	0.00
ANGRUNOUTPINION	0.00
BACKSIDECONTACT	FALSE

Table 9.2: Pinion data

Item	Description
LUMPMASS	0.00
LUMPMOMINERTIA	0.00
LUMPALPHA	0.00

Table 9.3: Pinion tooth data

Item	Description
NTEETH	20
NFACEELEMS	4
COORDORDER	10
DISPLORDER	3
PLANE	TRANSVERSE
XVERSEDIAMPITCH	10
XVERSEPRESSANGLE	20
XVERSETHICK	0.15708
FACEWIDTH	1
HAND	LEFT
HELIXANGLE	0.00
RACKTIPRAD	0.02
OUTERDIA	2.18
ROOTDIA	1.76
RIMDIA	1.40
YOUNGSMOD	$3x10^7$
POISSON	0.3
MSHFILE	pinion.msh
TPLFILE	medium.tpl

Table 9.4: Modification menu for the pinion tooth

Item	Description
QUADTIPMOD	TRUE
ROLLQUADTIPMOD	27.25
MAGQUADTIPMOD	0.0005
LEADCROWN	0.0005

Table 9.5: Pinion rim data

Item	Description
RIMTYPE	SIMPLE
RIMDIA	1.40
INNERDIA	1.20
WIDTH	1.00
OFFSET	0.00
AXIALORDER	2
CIRCORDER	8
ELEMTYPE	LINEAR
NDIVSRADIAL	2
NTHETA	32
NDIVSWIDTH	4

Table 9.6: Gear data

Item	Description
TYPE	EXTERNAL
LUMPMASS	0.00
LUMPMOMINERTIA	0.00
LUMPALPHA	0.00

Table 9.7: Gear tooth data

Item	Description
NTEETH	40
NFACEELEMS	4
COORDORDER	10
DISPLORDER	3
PLANE	TRANSVERSE
XVERSEDIAMPITCH	10
XVERSEPRESSANGLE	20
XVERSETHICK	0.15708
FACEWIDTH	1
HAND	RIGHT
HELIXANGLE	0.00
RACKTIPRAD	0.02
OUTERDIA	4.18
ROOTDIA	3.78
RIMDIA	3.40
YOUNGSMOD	$3x10^7$
POISSON	0.3
MSHFILE	gear.msh
TPLFILE	medium.tpl

Table 9.8: Modification menu for the gear tooth

Item	Description
QUADTIPMOD	TRUE
ROLLQUADTIPMOD	19.60
MAGQUADTIPMOD	0.0005
LEADCROWN	0.0005

Table 9.9: Gear rim data

Item	Description
RIMTYPE	SIMPLE
RIMDIA	3.40
INNERDIA	2.40
WIDTH	1.00
OFFSET	0.00
AXIALORDER	2
CIRCORDER	16
ELEMTYPE	QUADRATIC
NDIVSRADIAL	4
NTHETA	64
NDIVSWIDTH	4

Table 9.10: Setup data

Item	Description
SEPTOL	0.01
NPROFDIVS	8
NFACEDIVS	12
DSPROF	0.001
ZEROINITIAL	TRUE
INITIALTIME	0.0
NRANGES	1
RANGE	1
SOLMETHOD	STATIC
NTIMESTEPS	11
DELTATIME	0.1
STARTSPEEDFACTOR	1.0
STARTTORQUEFACTOR	1.0
ENDTORQUEFACTOR	1.0
SAVEPERIODICALLY	FALSE
OUTPUTRESTART	FALSE
POSTPROCWRITE	TRUE
POSTFILENAME	postproc.dat
NSTEPSWRITE	1

Table 9.11: Searchstress data

Item	Description
COMPONENT	MAXPPLSTRESS
XAXIS	TIME
BEGINSTEP	1
ENDSTEP	10
BODY	PINION
SURFACE	FILLET1
TOOTHBEGIN	20
TOOTHEND	2
SEPTEETH	TRUE
SPROFBEGIN	0.00
SPROFEND	16.00
NUMSPROF	51
TFACEBEGIN	-1.00
TFACEEND	1.00
NUMTFACE	51
DEPTHBEGIN	0.00
DEPTHEND	0.00
NUMDEPTH	1
DISTMIN	0.05
OUTPUTTOFILE	TRUE
FILENAME	out.txt
APPEND	TRUE

9.1.2 Results and discussion

A graph for the maximum principal normal stress against time for tooth numbers 20, 1 and 2 in the fillet region of the pinion obtained from the searchstress menu is shown in Figure 9.1.

The maximum stress in this case is $5.230x10^4 psi$ for tooth no.1. The searchstress data to extract this graph is shown in Table 9.11.

The stress values hence obtained are shown in Table 9.12. Figure 9.2 shows a plot of Tip radius against the Max ppl normal stress. It can be concluded from the graph that as you increase the tip radius, the stress decreases. From the graph it can be seen that the variation in the results for the three templates is 3.7% at a tip radius of $0.01in$. The difference in the results between fineroot and finest templates is about 2.7% at $0.01in$ tip radius. The agreement is better for larger values of tip radius. For a radius of $0.045in$ the variation between the templates is less than 1.3% and the difference between the fineroot and finest templates is about 0.5%.

The time required to run the analysis for each case with the medium, fineroot and finest templates was about $20mins$, $1hr$ and $5hrs$ respectively on a Intel $pentium4$, $1700MHz$ CPU.

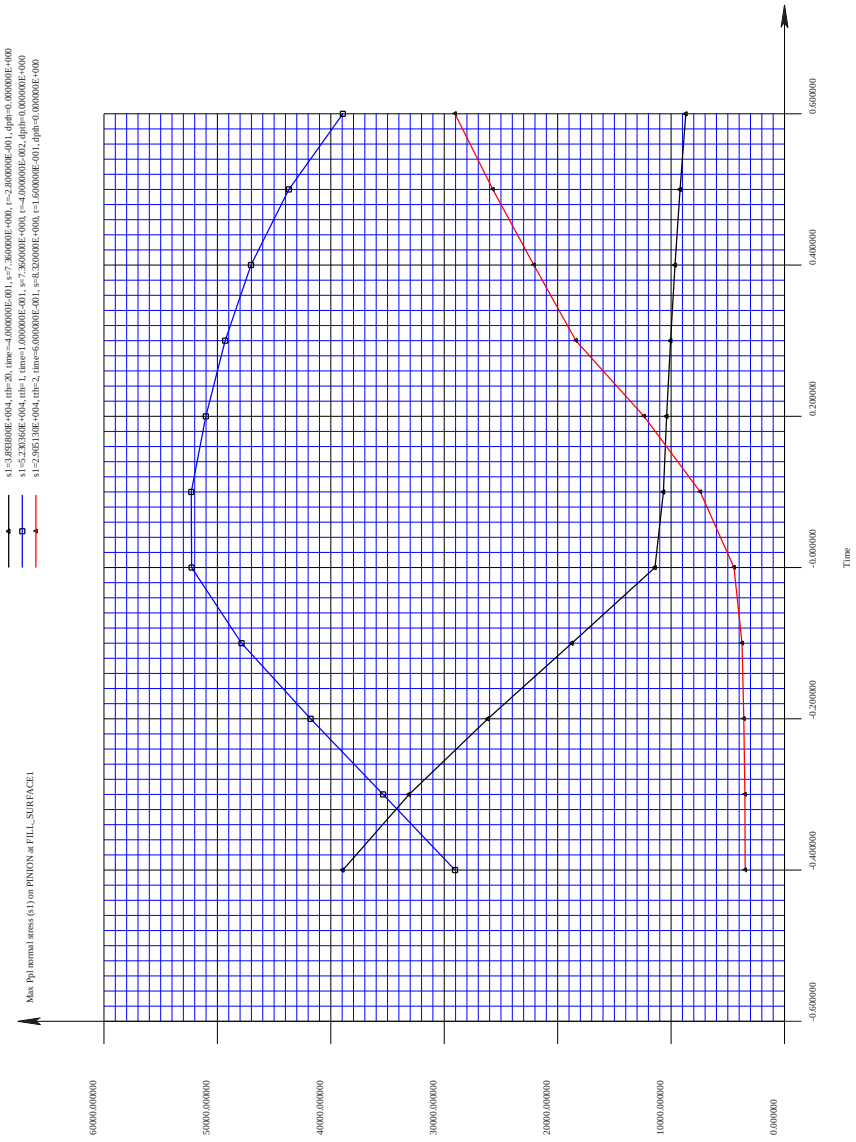

Figure 9.1: Graph of Max ppl normal stresses against time for pinion tooth nos.20,1 and 2, for a tip radius 0.02in with a medium template

Table 9.12: Max ppl normal stress values for different radii

Tip radius	Stress with medium.tpl	Stress with fineroot.tpl	Stress with finest.tpl
0.010	56644.23	54495.34	56025.16
0.015	53667.44	52024.40	53145.63
0.020	51024.51	49802.44	50643.22
0.025	48973.85	48006.89	48604.28
0.030	47156.78	46325.61	46724.35
0.035	45678.29	44922.02	45235.11
0.040	44217.18	43564.49	43795.09
0.045	42940.21	42361.25	42556.73

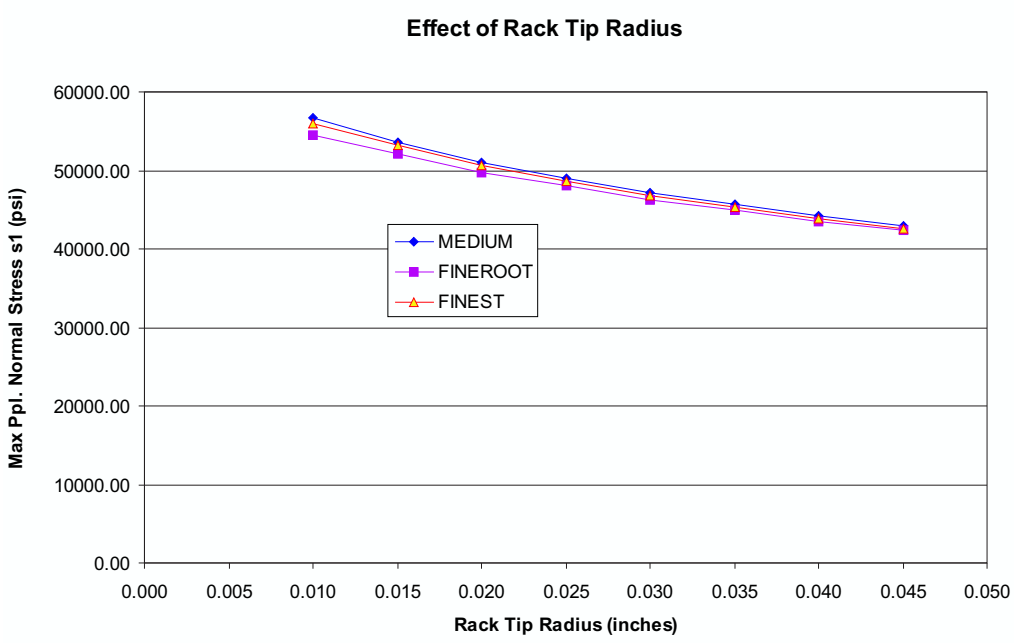

Figure 9.2: Graph of Max ppl normal stresses against tip radii (0.010 in-0.045 in) for medium, fineroot and finest templates

9.2 Effect of Tooth thickness on the max ppl normal stress

To study the effect of tooth thickness on the stress values we run the analysis for different tooth thicknesses for all the mesh templates. We vary the thickness from $0.1in$ to $0.16in$ in steps of $0.005in$. The tip radius for all the tooth thickness values is $0.02in$. The stress values hence obtained are shown in Table 9.13. Figure 9.3 shows a plot of the Max ppl normal stress against tooth thickness. It can be concluded from the graph that as you go on decreasing the thickness, the stress increases. From the graph it can be seen that the variation in the results for all the templates is about 2.6% at $0.16in$ tooth thickness. The difference between the fineroot and finest templates is about 1.8%.

Table 9.13: Max ppl normal stress values for different tooth thicknesses

Tooth thickness	Stress with medium.tpl	Stress with fineroot.tpl	Stress with finest.tpl
0.100	75526.61	75884.99	75106.59
0.105	73026.86	72687.67	72284.21
0.110	70465.08	69862.45	69704.46
0.115	67918.90	67124.32	67122.06
0.120	65388.86	64575.92	64655.39
0.125	62853.14	62149.01	62179.37
0.130	60491.53	59888.73	60158.73
0.135	58420.23	57747.31	58252.61
0.140	56632.43	55717.01	56339.82
0.145	54886.12	53905.71	54455.09
0.150	53197.34	52162.69	52668.94
0.155	51711.23	50566.00	51306.36
0.160	50316.66	48970.18	49904.44

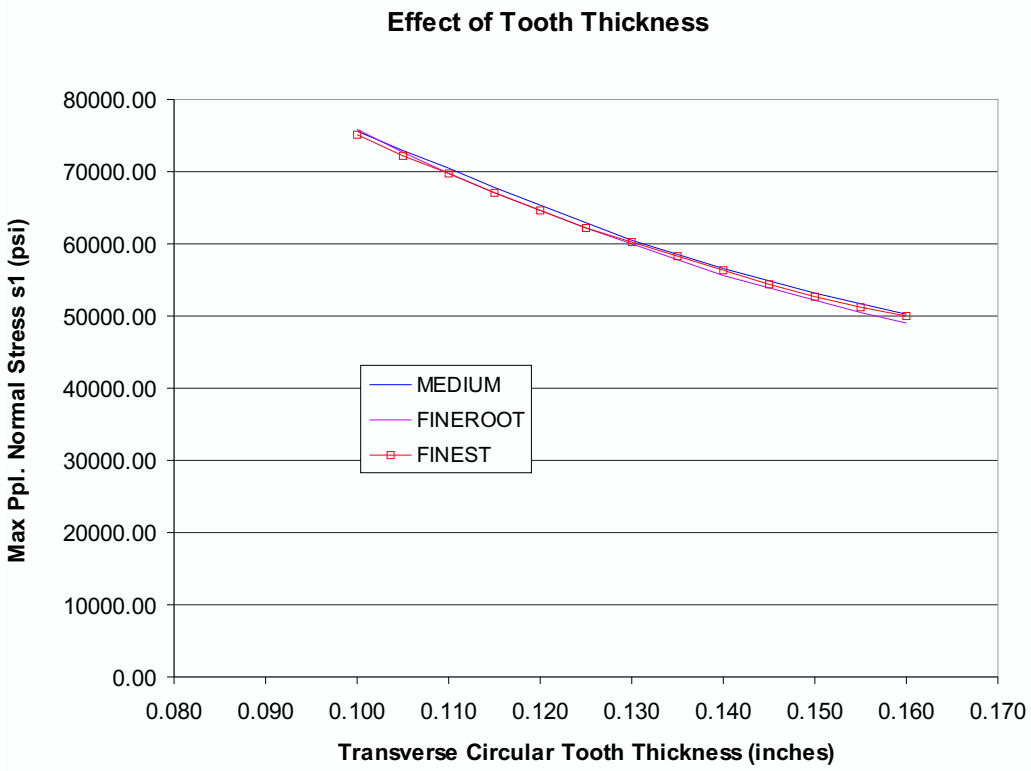

Figure 9.3: Graph of Max ppl normal stresses against tooth thickness (0.10in-0.16in) for medium, fineroot and finest templates

9.3 Effect of number of elements in the face direction on the max ppl normal stress

To study the effect of number of elements along the face width on the stress values we run the analysis for different NFACEELEMS for all the mesh templates. The polynomial order of the elements DISPLORDER is maintained at 3. We vary the NFACEELEMS parameter from 2 to 10 in steps of 2. The tip radius and the tooth thickness values for all the test cases are $0.02in$ and $0.15708in$ respectively. The stress values hence obtained are shown in Table 9.14. Figure 9.4 shows a plot of the Max ppl normal stress against the no. of face elements for the medium and fineroot templates. Results for higher elements with the finest mesh could not be obtained due to CPU limitations. As expected the stress values converge for higher number of elements. For the fineroot template, the difference between 2 elements and 10 elements is less than 0.1%. This implies that the stress variation in the face direction in the fillet can be well approximated even with 4 elements when a polynomial order of 3 is used along the face width.

Table 9.14: Max ppl normal stress values for different number of elements along the face width

Nfaceelems	Stress with medium.tpl	Stress with fineroot.tpl	Stress with finest.tpl
2	51107.14	49911.72	50799.47
4	51024.51	49802.44	50643.22
6	51084.53	49867.04	-
8	51082.93	49865.59	-
10	51079.74	49862.72	-

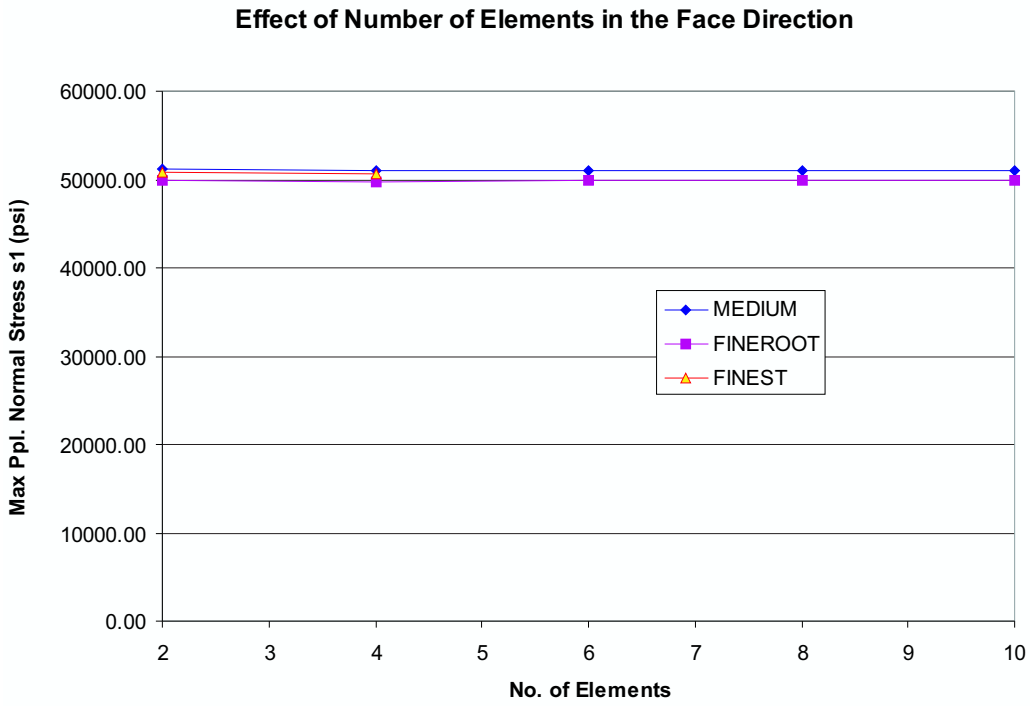

Figure 9.4: Graph of Max ppl normal stresses against No.of elements along the face width for medium and fineroot templates

Table 9.15: Max ppl normal stress values for different Displ. order

Displ.order	Stress with medium.tpl	Stress with fineroot.tpl	Stress with finest.tpl
3	51024.51	49802.44	50643.22
4	51087.63	49868.23	50643.22
5	51080.99	49863.92	-
6	51081.50	49864.99	-

9.4 Effect of displacement order on the max ppl normal stress

In order to study the effect of the element polynomial order DISPLORDER on the stress values we run the analysis for different DISPLORDER for all the mesh templates. With 4 elements along the face width, we vary the DISPLORDER parameter from 3 to 6 in steps of 1. The tip radius and the tooth thickness values for all the test cases are $0.02in$ and $0.15708in$ respectively. The stress values hence obtained are shown in Table 9.15. Figure 9.5 shows a plot of the Max ppl normal stress against the displacement order for the medium and fineroot templates. Results for higher order with the finest mesh could not be obtained due to CPU limitations. The results converge for higher order as expected. For the fineroot template, the difference in stress between order 6 and and order 3 is about 0.1%. It is evident that in this example, the variation of stress in the face direction is gradual enough that order 3 interpolation is sufficient when 4 elements are used to span the face width.

9.5 Conclusions

The stress values have been shown to converge with increasing refinement of the finite element mesh. For typical gears with a full fillet radius, this convergence study shows that we have a discretization error of about 1.0% in the coarsest mesh generated by using the medium template. When a very small fillet radius ($0.01in.$) was used, we observed the discretization error climb to 4.0%. The stress values converge with higher number of elements along the face direction and also with a higher polynomial order.

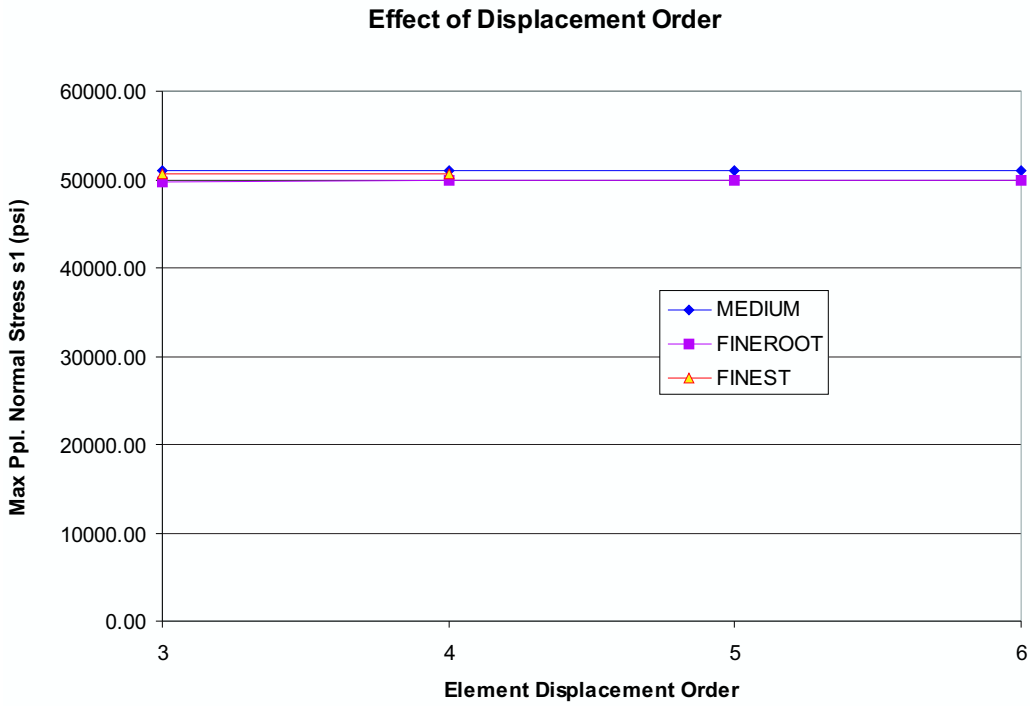

Figure 9.5: Graph of Max ppl normal stresses against displacement order for medium and fineroot templates

Chapter 10

Fatigue theory and life prediction using the Helical gear program

10.1 Introduction

Most engineering design projects involve machine parts subjected to fluctuating or cyclic loads. Such loading induces fluctuating or cyclic stresses that often result in failure by fatigue. Materials fracturing under repeated loadings were found to exhibit no gross deformation and gave the appearance of having suddenly snapped. It is difficult to detect the progressive changes in the material properties that occur during fatigue stressing and failure may therefore occur with little or no warning. Also, periods of rest, with the fatigue stress removed, do not lead to any measurable healing or recovery from the effects of prior cyclic stressing. Thus the damage done during the fatigue process is cumulative and generally unrecoverable.

With the increasing demand for more efficient and economic components and structures operation at higher speeds with minimum weight design the number of failures by fatigue has continued to increase. It is by far the most common cause of failure of load carrying metallic parts operating at or close to room temperature.

10.2 Fatigue characteristics

Fatigue may be characterised as a progressive failure phenomenon that proceeds by the initiation and propagation of cracks to an unstable size. Fatigue crack nuclei, from which crack grows and often propagate to failure, are thought to be formed through the movements of dislocations that produce fine slip bands at the crystal surfaces. Under cyclic loading these fine slip bands ultimately turn out to be the regions in which fatigue cracks are initiated. Further, the fatigue slip bands gives rise to intrusions as a result of reversed slip in adjacent slip planes caused by load reversal. Once formed, these intrusions grow in depth by reverse slip process, and their growth may well constitute a major portion of the fatigue of the metal. Crack propagation and hence fatigue are affected by various factors such as material composition, grain size and grain direction, heat treatment, welding, geometrical discontinuities, surface conditions, size, residual surface stresses, corrosion, fretting, operating temperature, operating speed, etc.

A term called fatigue limit(endurance limit) is very commonly used while studying fatigue failure. It is the stress level below which an infinite number of cycles can be sustained without failure. To characterize the failure response of components in the finite life range, the term fatigue strength at a specified life, S_N is used. The term fatigue strength identifies the stress level at which failure will occur at specified life.

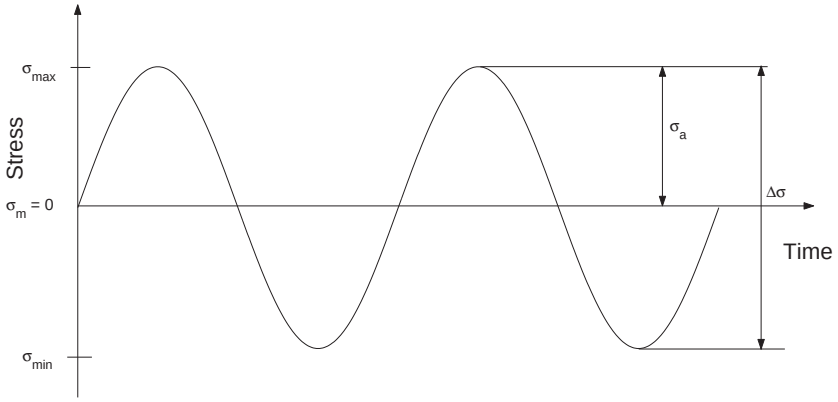

Figure 10.1: Completely reversed cyclic stress plot

10.3 Low and High cycle fatigue

It is observed that the fatigue process embraces two domains of cyclic stressing or straining that are significantly different in character, and in each of which failure is probably produced by different physical mechanisms. One domain of cyclic loading is that for which significant plastic strains occur during each cycle. This domain is associated with high loads and short lives, or low number of cycles to produce fatigue failure, and is commonly referred to as low cycle fatigue.

The other domain of cyclic loading is that for which the strain cycles are largely confined to the elastic range. This domain is associated with lower loads and long lives, or high number of cycles to produce fatigue failure, and is commonly referred to as high cycle fatigue. Low-cycle fatigue is typically associated with cycle lives up to about 10^4 or 10^5 cycles, and high cycle fatigue for lives greater than about 10^4 or 10^5 cycles. In most gearing applications fatigue failure is associated with high cycle fatigue. Hence we address the helical fatigue failure problem based on the theory related to the high cycle fatigue.

10.4 Fatigue loading

As discussed earlier fatigue failure is caused in materials or components when subjected to cyclic or alternating stress. A simple example of a fatigue stress spectrum to which an element may be subjected could be a zero-mean sinusoidal stress-time pattern of constant amplitude and fixed frequency, applied for a specified number of cycles. Such a stress-time pattern, often referred to as a completely reversed cyclic stress is shown in Figure 10.1.

Using the figure we define the following terms and symbols so as to calculate the fatigue strength or fatigue life for a helical gear set.

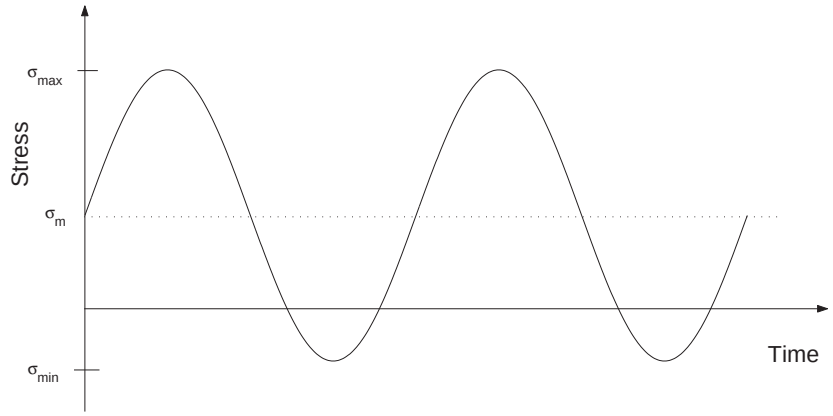

Figure 10.2: Nonzero mean stress-time pattern

$$\sigma_{max} = \text{Maximum Stress in the cycle} \tag{10.1}$$

$$\sigma_{min} = \text{Minimum Stress in the cycle} \tag{10.2}$$

$$\sigma_m = \text{Mean Stress} = \frac{\sigma_{max} + \sigma_{min}}{2} \tag{10.3}$$

$$\sigma_a = \text{Alternating Stress amplitude} = \frac{\sigma_{max} - \sigma_{min}}{2} \tag{10.4}$$

$$\Delta\sigma = \text{Range of Stress} = \sigma_{max} - \sigma_{min} \tag{10.5}$$

$$R = \text{Stress Ratio} = \frac{\sigma_{min}}{\sigma_{max}} \tag{10.6}$$

$$A = \text{Amplitude Ratio} = \frac{\sigma_a}{\sigma_m} \tag{10.7}$$

Some of the examples of Stress-time patterns are shown in Figures 10.2 through 10.7.

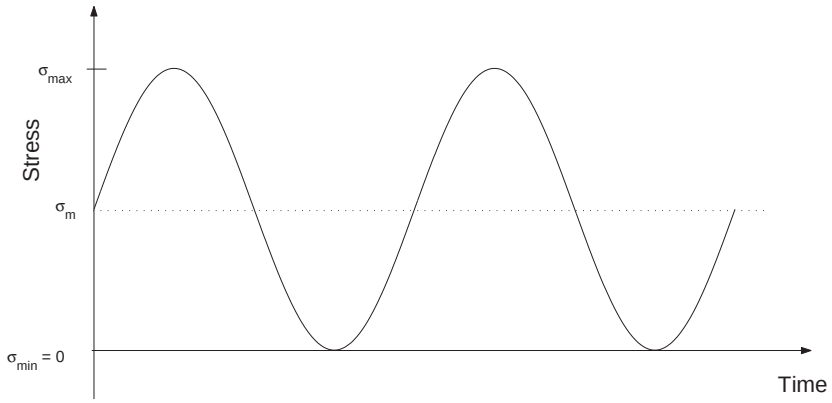

Figure 10.3: Released tension, R=0, stress-time pattern

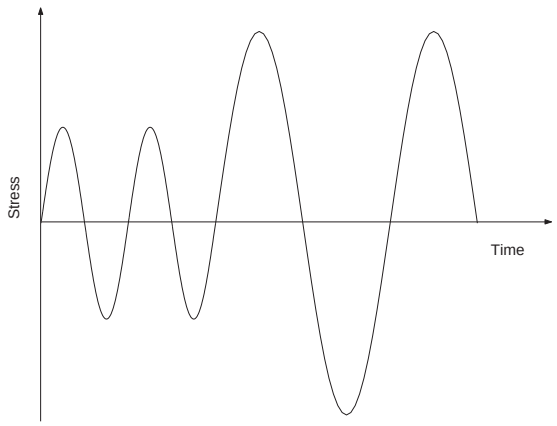

Figure 10.4: Changing amplitude stress-time pattern

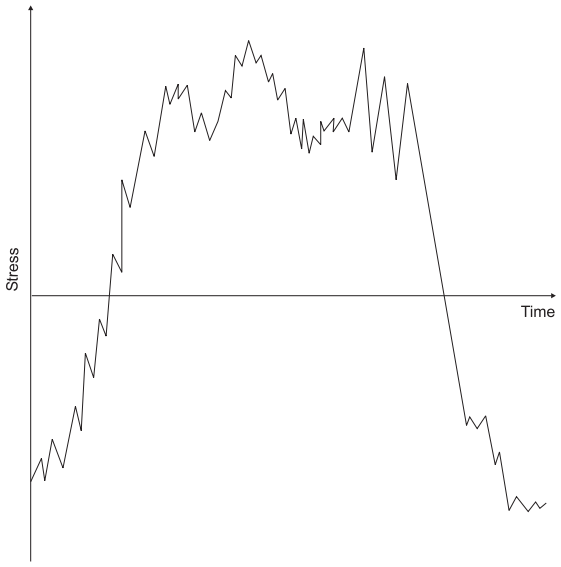

Figure 10.5: Quasi-random stress-time pattern

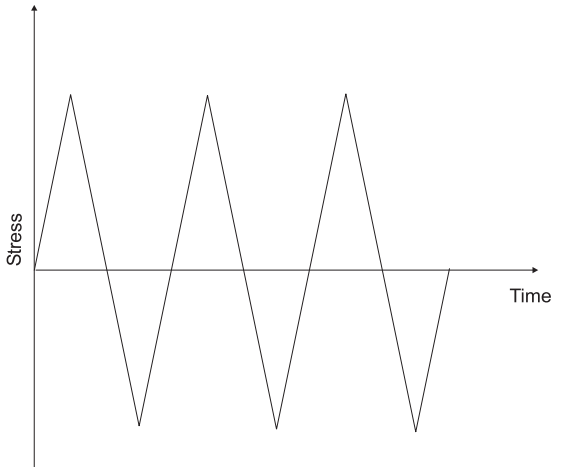

Figure 10.6: Completely reversed ramp stress-time pattern

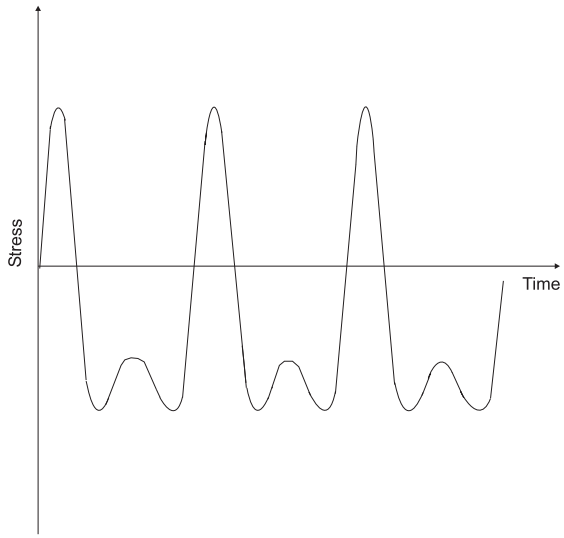

Figure 10.7: Stress-time pattern with distorted peaks

10.5 Example of a laboratory fatigue testing

Designing machine parts or structures that are subjected to fatigue loading is usually based on the results of laboratory fatigue tests using specimens of the material of interest. An example of a laboratory fatigue testing called as the rotating bending machine of the constant bending moment type is shown in Figure 10.8.

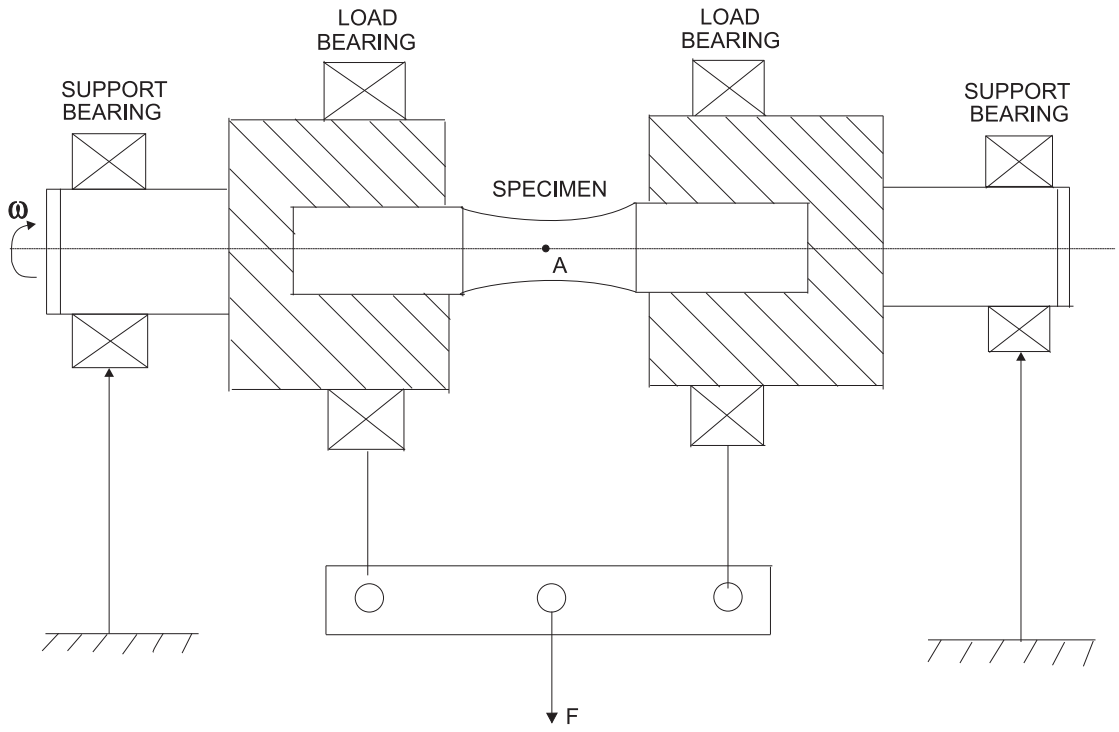

Figure 10.8: Schematic of the rotating-bending fatigue testing machine of the constant bending moment type

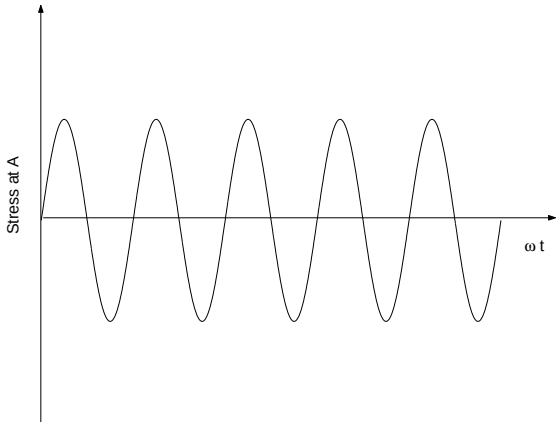

Figure 10.9: Stress-time pattern for point A at the surface of the critical section

With this type of device the region of the rotating beam between the inboard bearings is subjected to a constant bending moment all along its length. While under the influence of this constant moment, the specimen is caused to rotate with the drive spindles about the longitudinal axis. Any point on the surface is thereby subjected to a completely reversed stress-time pattern, as can be deduced by following the stress history of a point as it rotates from maximum compression at the top position down through zero stress when at the side through maximum tension at the bottom, and then back through zero to maximum compression at the top again. The stress-time pattern for a point on the surface of the critical section is shown in Figure 10.9.

10.6 Gear fatigue failure

Gears may fail by wear and scuffing but the main causes of failure are bending fatigue leading to breakage at the root of the tooth and surface contact fatigue leading to pitting. Fatigue failure in gears can be broadly classified in to two types:

- Those arising from a **tensile fatigue** failure of the material at the root of a gear tooth i.e. away from the area of contact between intermeshing teeth.
- Those arising from **compressive stresses** on the working surface of the gear tooth, where it is in contact with the intermeshing gear.

Tensile fatigue failure occurs in materials subjected to fluctuating stresses where the continuously repeated stress is much lower than the static tensile strength of the material. This type of high cycle fatigue failure generally depends upon the number of stress cycles rather than on the total time under load and does not occur below a certain stress, called the fatigue and endurance limit. In a homogeneous material tensile fatigue crack always starts at and propagates from the point of maximum stress concentration. Under normal operation and with correct design the point of maximum tensile stress concentration on a gear is at the root of the tooth on the loaded side. The crack progresses through the tooth to the root on the opposite side. During this crack propagation the tooth can bend over and shed the load on to the next tooth which also ultimately fails.

Surface fatigue failure is brought about by cumulative damage to the gear material caused by repeated application of contact stresses. Surface contact fatigue does not usually lead to catastrophic breakage (as in the case of a tensile fatigue failure) but rather to progressive deterioration of the surface by pitting or spalling.

10.7 Running the Helical3D program for fatigue failure

10.7.1 The example file

Load the file `fatigue.ses` from the `FATIGUE` directory located in the `SAMPLES` directory.

The data for the fatigue test model is similar to the data we used for convergence study. We run the analysis for one mesh cycle.

10.7.2 Locating the point of maximum stress

The SEARCHSTRESS menu is used to locate the point of maximum stress on the profile, facewidth and the depth of a tooth. A plot of maximum principal stress against time for Pinion tooth no.1 is shown in Figure 10.10. The legend on the top right corner of the figure shows the location along the profile(s), width(t) and the depth(dpth) of the maximum stress point. The search stress menu used to plot this graph is shown in Table 10.1. The depth on the surface of the tooth is 0.00. As can be seen from the stress results the maximum stress occurs at profile, $s = 7.38$. The involute profile as shown in Figure 10.11 goes from $s = 0$ to $s = 48$. There are 8 elements along the profile(element nos.3 through 10). So each element corresponds to a profile distance of 6 units. From figure 10.11 and figure 10.12 the point of maximum stress lies between the profile, $s = 6$ and $s = 12$. To find the corresponding XI(ξ) co-ordinate we use the following:

$$\frac{\xi - (-1)}{2} = \frac{7.38 - 12}{6 - 12}$$
$$\xi = 0.54$$

The ETA(η) co-ordinate on the surface is 1.00.

Since there are 4 finite elements along the width and the point of maximum stress lies close to $0.00(t = -0.02)$ we are interested in element numbers 40 and 76. The element orientation is shown in Figure 10.12. Refer to the appendix of the Helical Users manual for further details. Note that ZETA(ζ) is along the facewidth direction. So as to locate the exact ζ value we apply FEPROBES close to $\zeta = +1$ for element no.40 and $\zeta = -1$ for element no.76. The FE probe menu for one of the probes is shown in table 10.2. Analysing the FE probe data the co-ordinates of the maximum stress point is found to be (ξ, η, ζ) = (0.54, 1.00, 0.90) on element no.40. For this point the plot of maximum and minimum principal normal stress against time is shown in Figure 10.13.

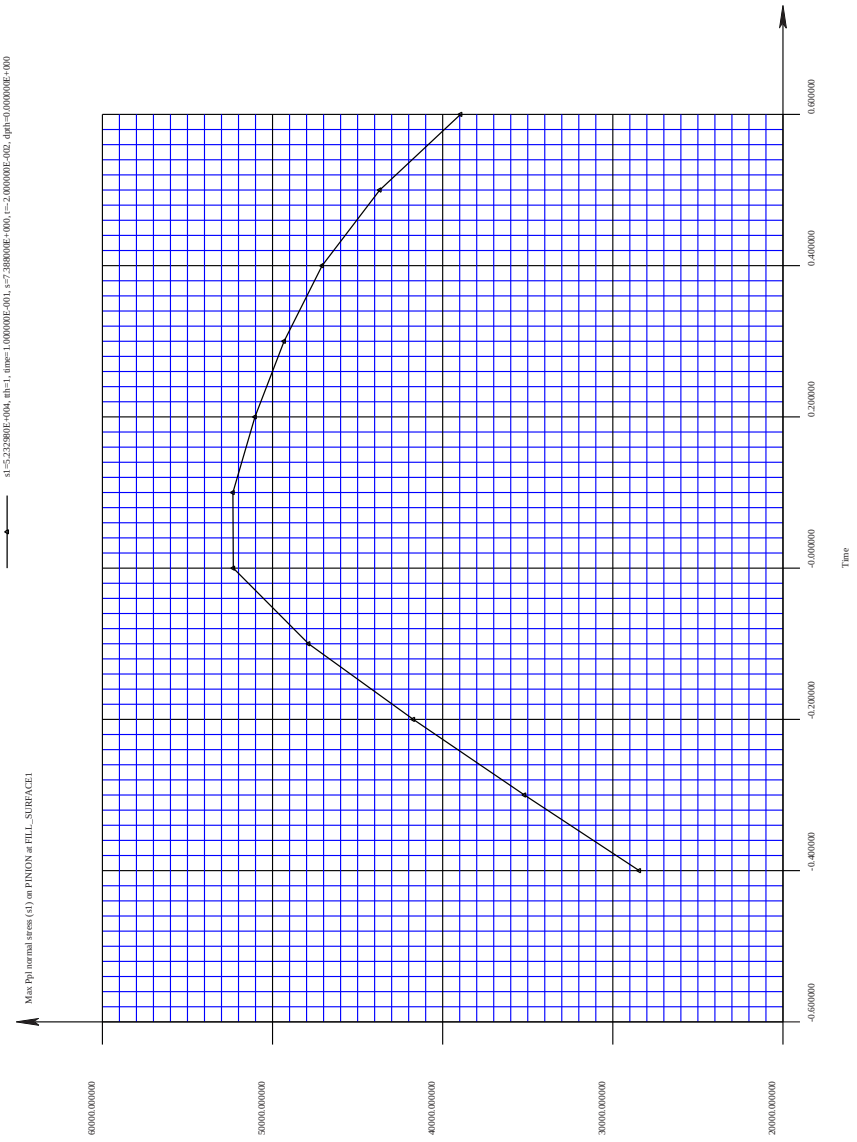

Figure 10.10: Plot of maximum principal normal stress against time for pinion tooth no.1 using the SEARCHSTRESS menu

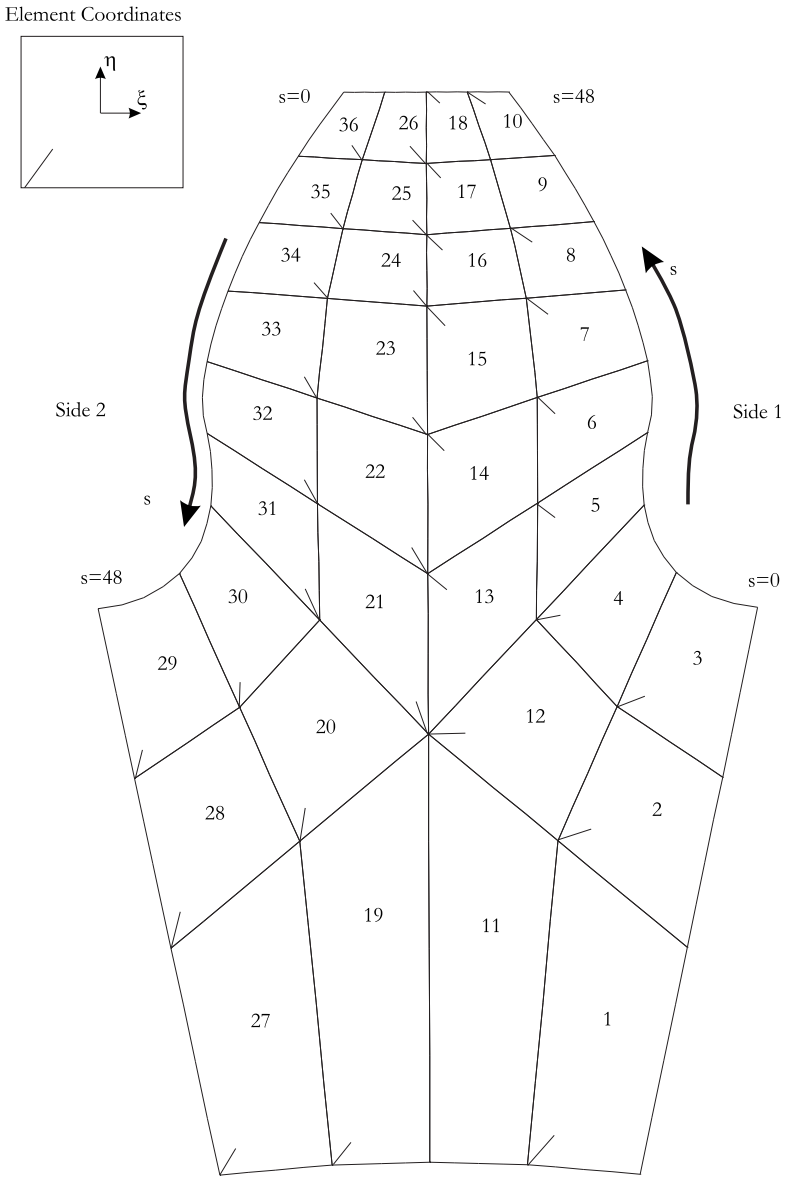

Figure 10.11: The MEDIUM.TPL template file.

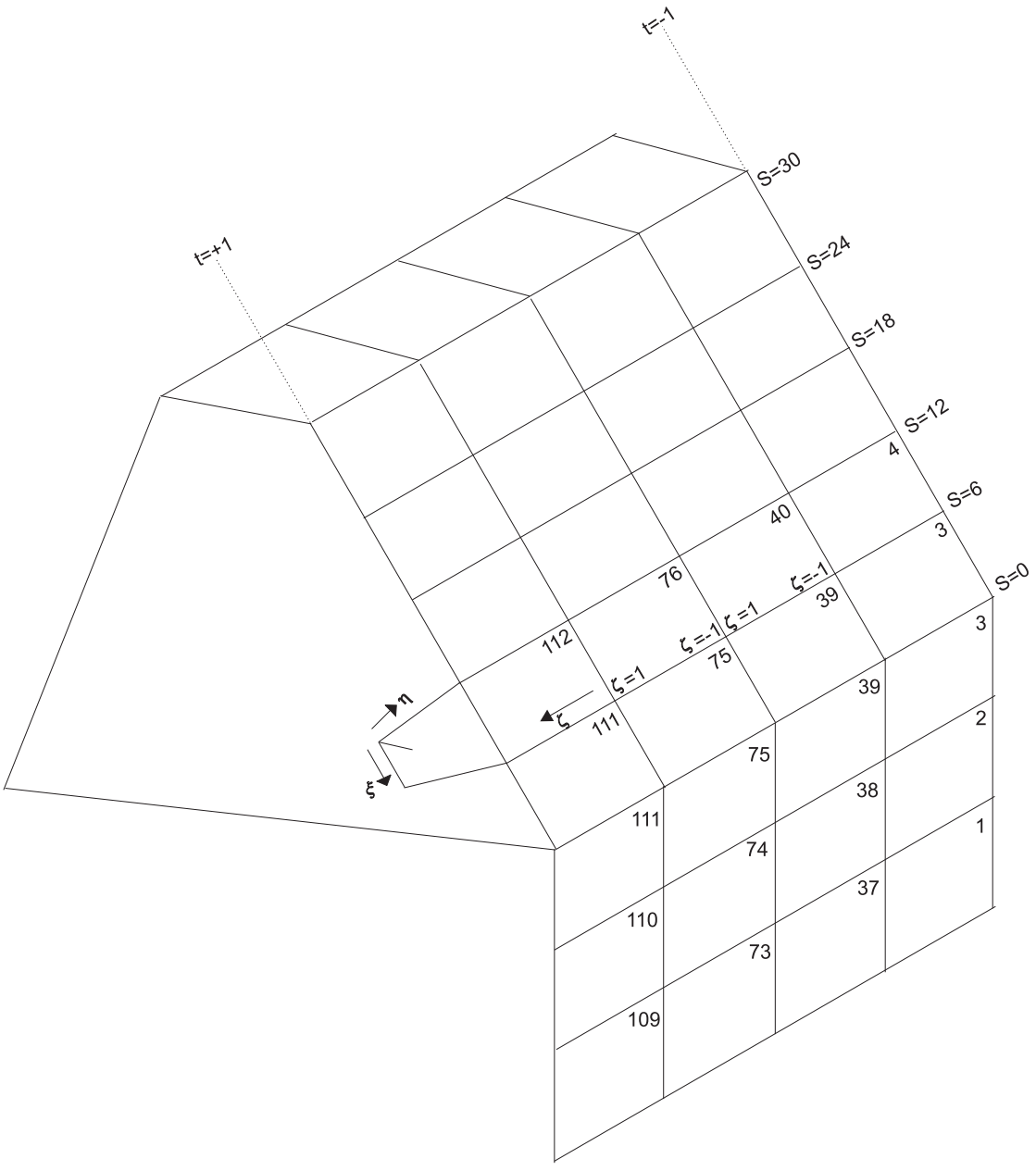

Figure 10.12: Orientation of ξ, η and ζ on the tooth

Table 10.1: Searchstress data

Item	Description
COMPONENT	MAXPPLSTRESS
XAXIS	TIME
BEGINSTEP	1
ENDSTEP	11
BODY	PINION
SURFACE	FILLET1
TOOTHBEGIN	1
TOOTHEND	1
SEPTEETH	TRUE
SPROFBEGIN	6.00
SPROFEND	12.00
NUMSPROF	51
TFACEBEGIN	-0.5
TFACEEND	0.5
NUMTFACE	51
DEPTHBEGIN	0.00
DEPTHEND	0.00
NUMDEPTH	1
DISTMIN	0.05
OUTPUTTOFILE	TRUE
FILENAME	out.txt
APPEND	TRUE

Table 10.2: FE probe data

Item	Description
NPROBES	40
PROBE	1
BODY	PINION
MESH	TOOTH
ELEM	40
XI	0.54
ETA	1.00
ZETA	0.90
COMPONENT	MAXPPLNORMAL
FILENAME	PROBES.DAT

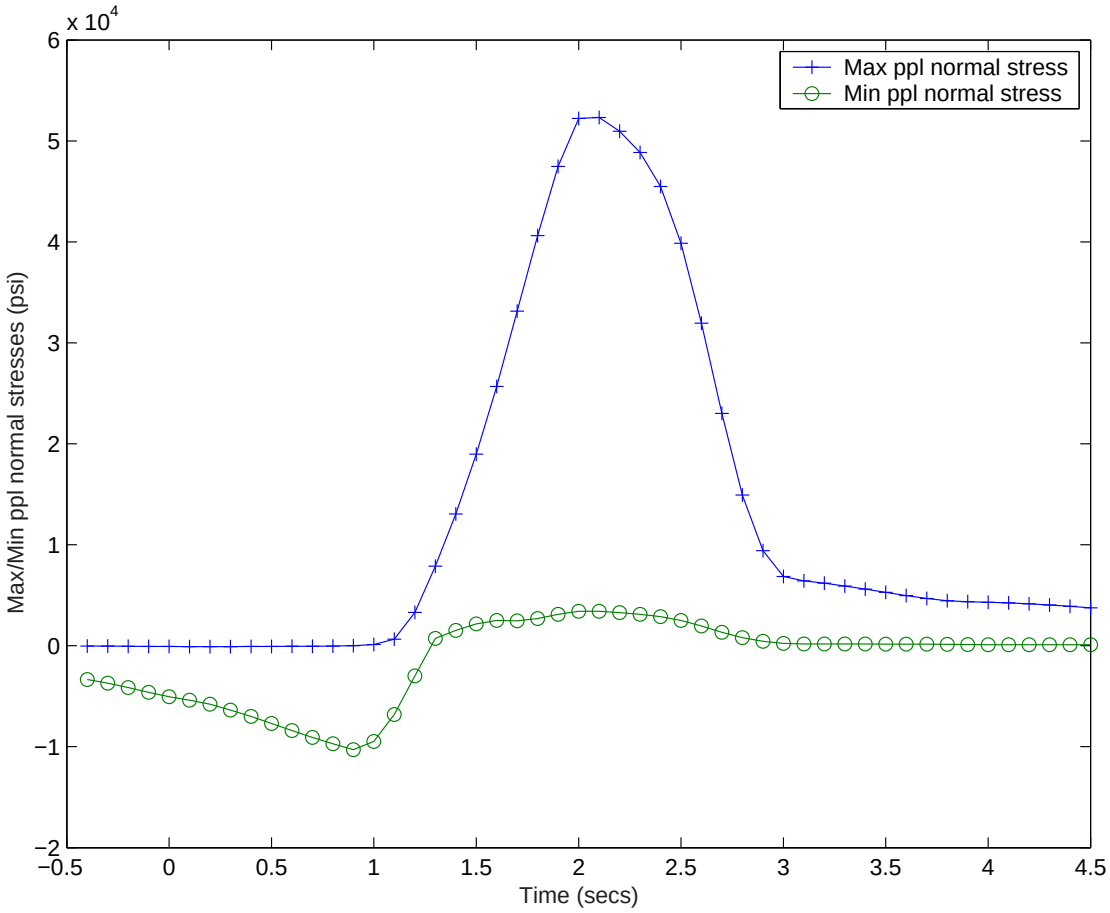

Figure 10.13: Plot of maximum and minimum principal normal stress for a point on the pinion tooth against time

10.7.3 Results

The maximum principal and the minimum principal normal stress plot obtained from the FE probe data is shown in Figure 10.13. The maximum principal normal stress ($\sigma_{\max}$) = $5.2330x10^4 psi$ and the minimum principal normal stress ($\sigma_{\min}$) = $-9.7156x10^3 psi$. Hence, Alternating stress, $\sigma_{\mathrm{a}} = 3.10232x10^4 psi$ and the Mean stress, $\sigma_{\mathrm{m}} = 2.13075x10^4 psi$.

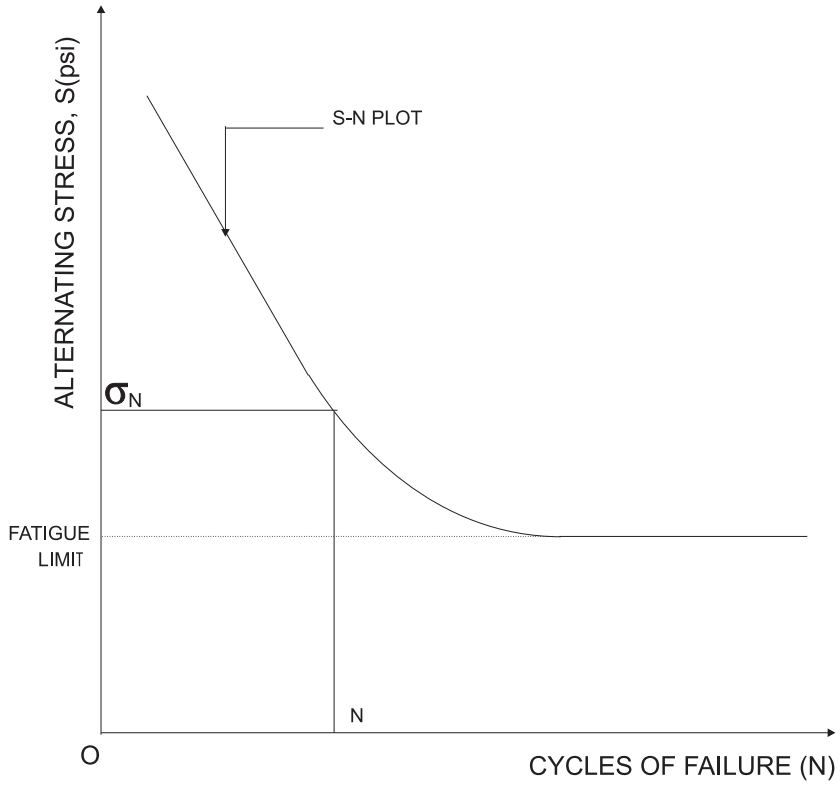

Figure 10.14: An example of an S-N curve for predicting fatigue life

10.8 Calculating the fatigue life

The stress life, S-N, method was the first approach used in an attempt to understand and quantify fatigue life. The S-N approach is still widely used in design applications where the applied stress is primarily within the elastic range of the material and the resultant lives (cycles to failures) are long, such as power transmission shafts. The S-N diagram is a plot of alternating stress, S, versus cycles to failure, N. One of the major drawbacks of the stress-life approach is that it ignores the true stress-strain behavior and treats all strains as elastic. This may be significant since the initiation of fatigue cracks is caused by plastic deformation. The simplifying assumptions of the S-N approach are valid only if the plastic strains are small. At long lives most steels have only a small component of cyclic strain which is plastic and the S-N approach is valid. An example of an S-N plot is shown in Figure 10.14.

The magnitude of mean stress has an important influence on the fatigue behavior of a specimen or a machine part. Most service applications involve nonzero mean cyclic stresses. The present case under consideration also is an example of a nonzero mean cyclic stress. The influence of non-zero mean stress on failure can be estimated by empirical relationships (Figure 10.15) that relate the failure at a given life under non-zero mean conditions to failure at the same life under zero mean cyclic stresses.

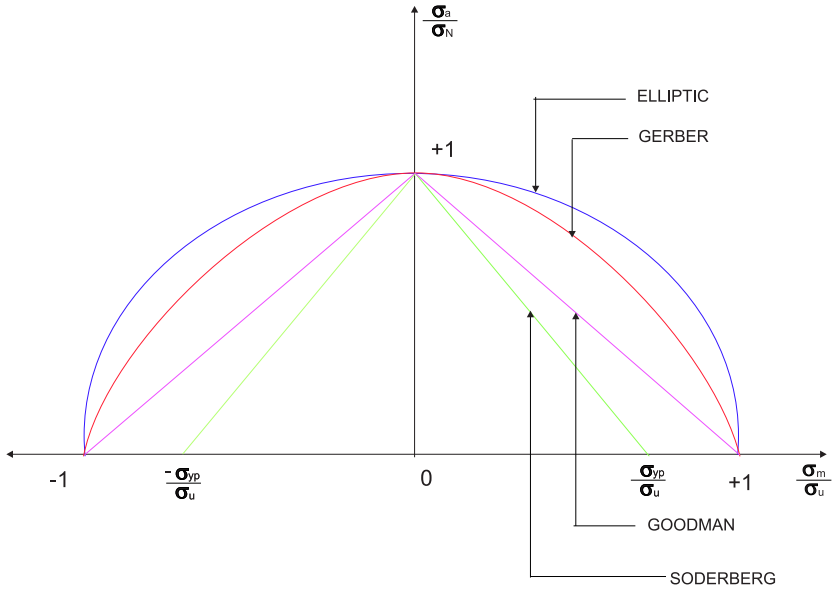

Figure 10.15: Various empirical relationships for estimating the influence of nonzero-mean stress on fatigue failure

10.8.1 Goodman's Linear relationship

Let,

$$\begin{aligned} \sigma_a &= \text{Alternating stress amplitude} \\ \sigma_N &= \text{Fatigue strength} \\ \sigma_m &= \text{Mean stress} \\ \sigma_u &= \text{Ultimate strength} \\ \sigma_{y_p} &= \text{Yield point stress} \end{aligned}$$

`Goodman's linear relationship` states that fatigue failure occurs when

$$\frac{\sigma_a}{\sigma_N} + \frac{\sigma_m}{\sigma_u} \geq 1 \tag{10.8}$$

For G43400 steel [1] with tensile strength 140 kpsi and fatigue limit 71 kpsi, using the results for σ_a and σ_m, the Goodman linear relationship gives

$$\frac{\sigma_a}{\sigma_N} + \frac{\sigma_m}{\sigma_u} = 0.5890$$

10.8.2 Gerber's parabolic relationship

`Gerber's parabolic relationship` states that fatigue failure occurs when

$$\frac{\sigma_a}{\sigma_N} + (\frac{\sigma_m}{\sigma_u})^2 \geq 1 \tag{10.9}$$

For G43400 steel with tensile strength 140 kpsi and fatigue limit 71 kpsi, the Gerber's parabolic relationship gives

$$\frac{\sigma_a}{\sigma_N} + (\frac{\sigma_m}{\sigma_u})^2 = 0.4600$$

10.8.3 Soderberg's linear relationship

`Soderberg's linear relationship` states that fatigue failure occurs when

$$\frac{\sigma_a}{\sigma_N} + \frac{\sigma_m}{\sigma_{y_p}} \geq 1 \tag{10.10}$$

For G43400 steel with yield strength 100 kpsi and fatigue limit 71 kpsi, the Soderberg's linear relationship gives

$$\frac{\sigma_a}{\sigma_N} + \frac{\sigma_m}{\sigma_{y_p}} = 0.6499$$

10.8.4 Elliptic relationship

`Elliptic relationship` states that fatigue failure occurs when

$$(\frac{\sigma_a}{\sigma_N})^2 + (\frac{\sigma_m}{\sigma_u})^2 \geq 1 \tag{10.11}$$

For G43400 steel with tensile strength 140 kpsi and fatigue limit 71 kpsi, the Elliptic relationship gives

$$(\frac{\sigma_a}{\sigma_N})^2 + (\frac{\sigma_m}{\sigma_u})^2 = 0.2140$$

The above theories can be used to find the alternating stress at which fatigue failure will occur. For instance, according to the Goodman's linear relationship, for a steel with tensile strength 80 kpsi, the fatigue stress is 42.285 kpsi. Using an S-N plot for steel shown in Figure 10.16 [2], the corresponding fatigue life is 4.5×10^5 cycles. Note that the S-N plot used in the figure is not a standard curve for gear materials. It is used to demonstrate the ability of the Helical3D program in calculating the fatigue life.

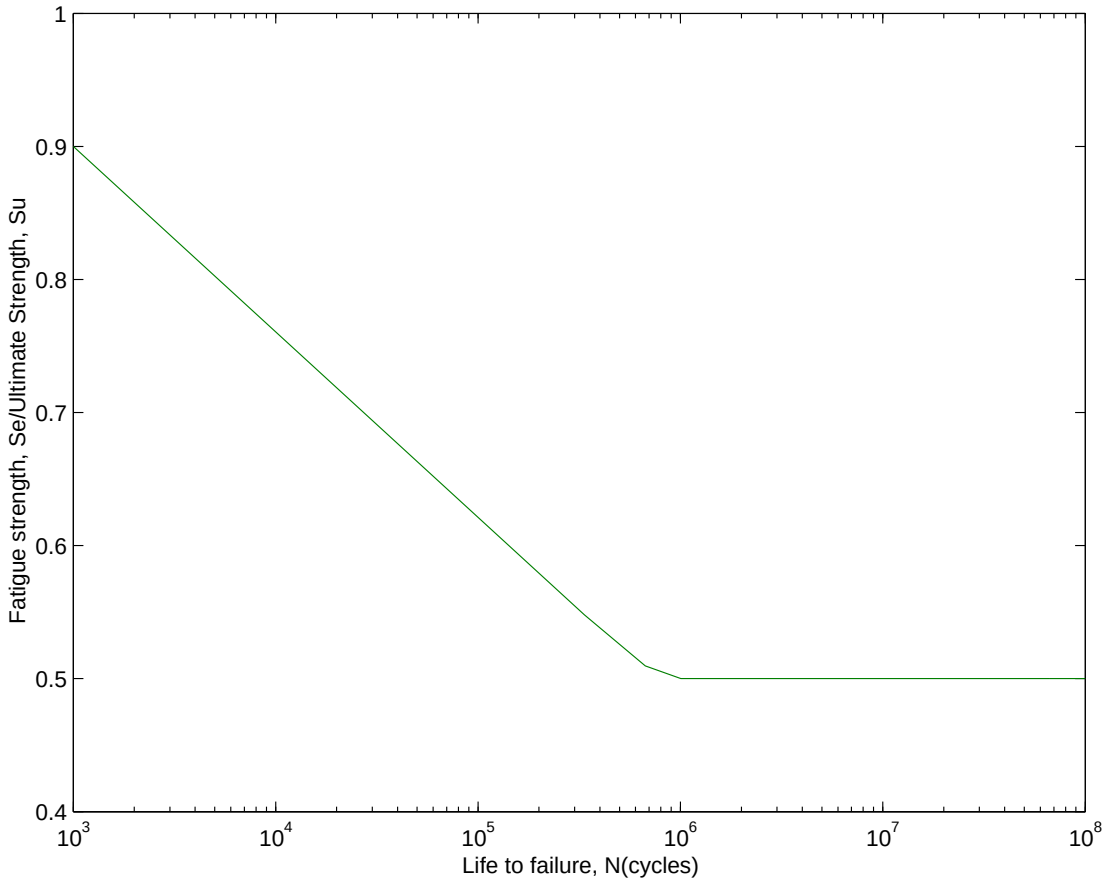

Figure 10.16: Example of an S-N plot for wrought steel

10.9 Effect of rigid internal diameter on fatigue life

So as to study the effect of a different boundary condition on fatigue life we make the inner diameter of the pinion as rigid. Load the file `fatigueinnerdiarigid.ses` located in the `FATIGUE` directory. The BEARING menu data for this case is shown in Table 10.3.

Table 10.3: Bearing menu to specify rigid inner diameter for the pinion

Item	Description
RIGIDRACE	TRUE
BEARING	FALSE

10.9.1 Locating the point of maximum stress

The SEARCHSTRESS menu is used to locate the point of maximum stress on the profile, facewidth and the depth of a tooth. A plot of maximum principal stress against time for Pinion tooth no.1 is shown in Figure 10.17. The legend on the top right corner of the figure shows the profile(s), width(t) and the depth(dpth) data of the maximum stress point. The search stress menu used to plot this graph is shown in Table 10.4. The depth on the surface of the tooth is 0.00. As can be seen from the stress results the maximum stress occurs at profile, $s = 7.30$. Thus the point of maximum stress lies between the profile, $s = 6$ and $s = 12$. To find the corresponding XI(ξ) co-ordinate we use the following:

$$\frac{\xi - (-1)}{2} = \frac{7.30 - 12}{6 - 12}$$
$$\xi = 0.56$$

The ETA(η) co-ordinate on the surface is 1.00.

Since there are 4 finite elements along the width and the point of maximum stress lies close to 0.00($t = 0.04$) we are interested in element numbers 40 and 76. Refer to the appendix of the Helical Users manual for further details. So as to locate the exact ζ value we apply FEPROBES close to $\zeta = +1$ for element no.40 and $\zeta = -1$ for element no.76. The FE probe menu for one of the probes is shown in table 10.5. Analysing the FE probe data the co-ordinates of the maximum stress point is found to be (ξ, η, ζ) = (0.56, 1.00, -0.80) on element no.76. For this point the plot of maximum and minimum principal normal stress against time is shown in Figure 10.18.

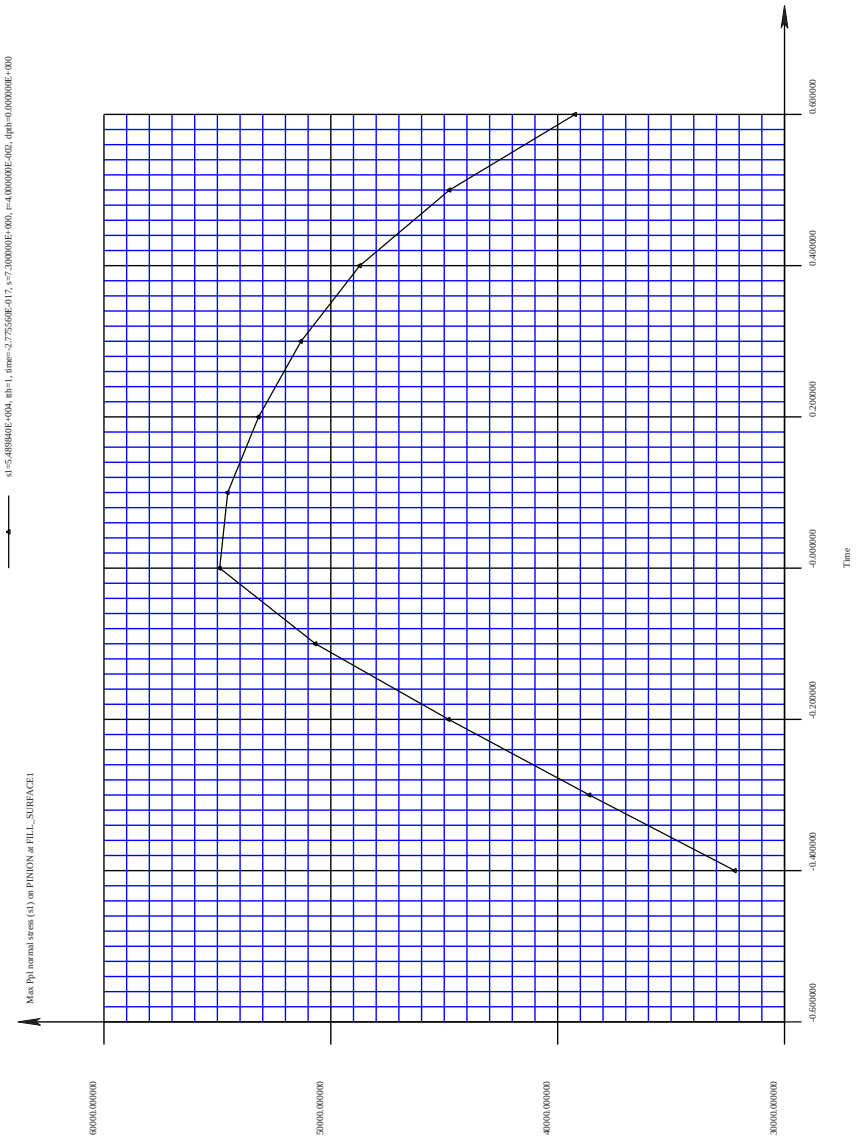

Figure 10.17: Plot of maximum principal normal stress against time for pinion tooth no.1 using the SEARCHSTRESS menu

Table 10.4: Searchstress data

Item	Description
COMPONENT	MAXPPLSTRESS
XAXIS	TIME
BEGINSTEP	1
ENDSTEP	11
BODY	PINION
SURFACE	FILLET1
TOOTHBEGIN	1
TOOTHEND	1
SEPTEETH	TRUE
SPROFBEGIN	6.00
SPROFEND	12.00
NUMSPROF	51
TFACEBEGIN	-0.5
TFACEEND	0.5
NUMTFACE	51
DEPTHBEGIN	0.00
DEPTHEND	0.00
NUMDEPTH	1
DISTMIN	0.05
OUTPUTTOFILE	TRUE
FILENAME	out.txt
APPEND	TRUE

Table 10.5: FE probe data

Item	Description
NPROBES	40
PROBE	1
BODY	PINION
MESH	TOOTH
ELEM	76
XI	0.56
ETA	1.00
ZETA	-0.80
COMPONENT	MAXPPLNORMAL
FILENAME	PROBES.DAT

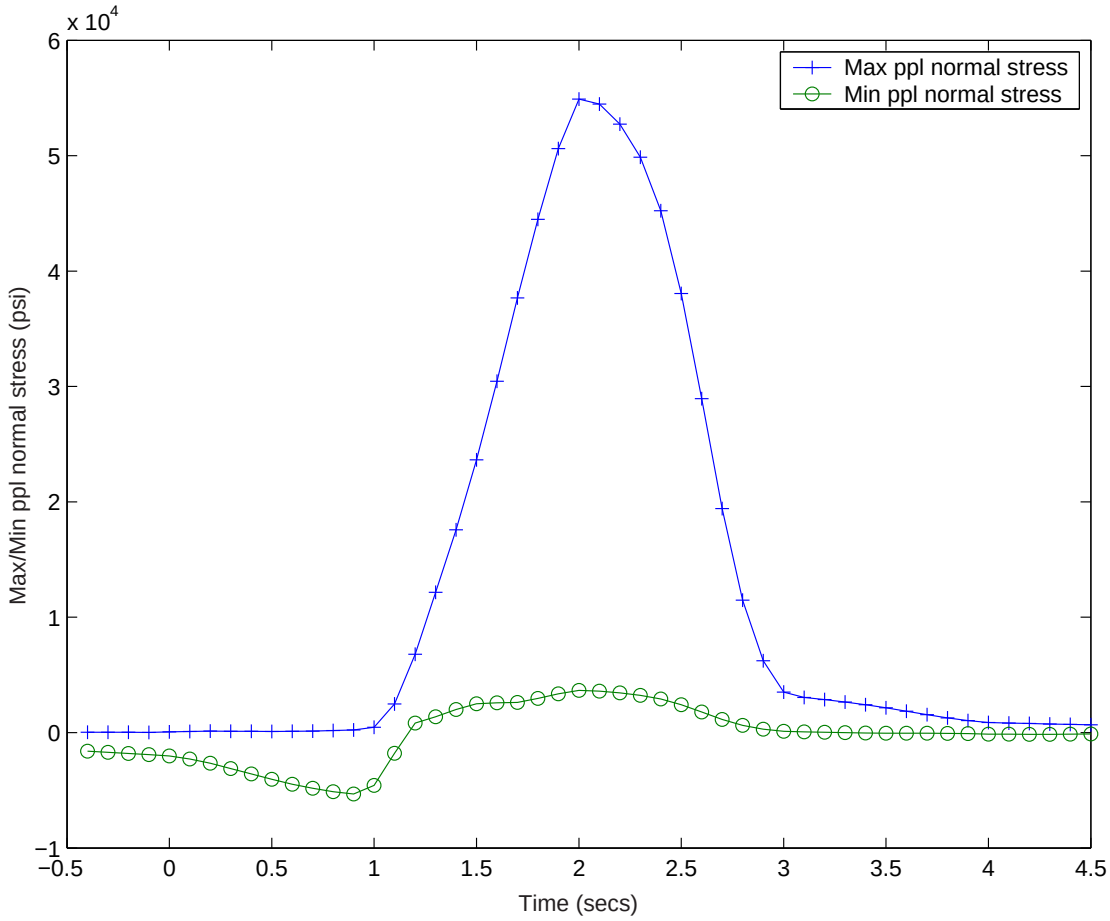

Figure 10.18: Plot of maximum and minimum principal stresses against time for pinion tooth for the case with rigid pinion inner diameter

10.9.2 Results

The maximum principal and the minimum principal normal stress plot obtained from the FE probe data is shown in Figure 10.18. The maximum principal normal stress ($\sigma_{\max}$) = $5.4898x10^4 psi$ and the minimum principal normal stress ($\sigma_{\min}$) = $-5.3251x10^3 psi$. Hence, Alternating stress, $\sigma_a = 3.0111x10^4 psi$ and the Mean stress, $\sigma_m = 2.4786x10^4 psi$.

According to the Goodman's linear relationship, for a steel with tensile strength $80 kpsi$, the fatigue stress using above data is $43.628 kpsi$. Using an S-N plot for steel shown in Figure 10.16, the corresponding fatigue life is 4.30×10^5 cycles. Note that the S-N plot used in the figure is not a standard curve for gear materials. It is used to demonstrate the ability of the $Helical3D$ program in calculating the fatigue life.

10.10 Fatigue life for a thin flexible rim model

Load the file `fatiguethinrim.ses` located in the `FATIGUE` directory. The BEARING menu data for this case is shown in Table 10.6.

Table 10.6: Bearing menu to specify flexible inner diameter for the pinion

Item	Description
RIGIDRACE	FALSE
CIRCORDER	8
AXIALORDER	2
BEARING	FALSE

10.10.1 Locating the point of maximum stress

A plot of maximum principal stress against time for Pinion tooth no.1 is shown in Figure 10.19. Table 10.7 shows the searchstress menu to obtain this plot. Analysing the FE probe data the co-ordinates of the maximum stress point is found to be (ξ, η, ζ) = (0.226, 1.00, 0.70) on element no.40. For this point the plot of maximum and minimum principal normal stress against time is shown in Figure 10.20. An example of a FEPROBE menu is shown in Table 10.8.

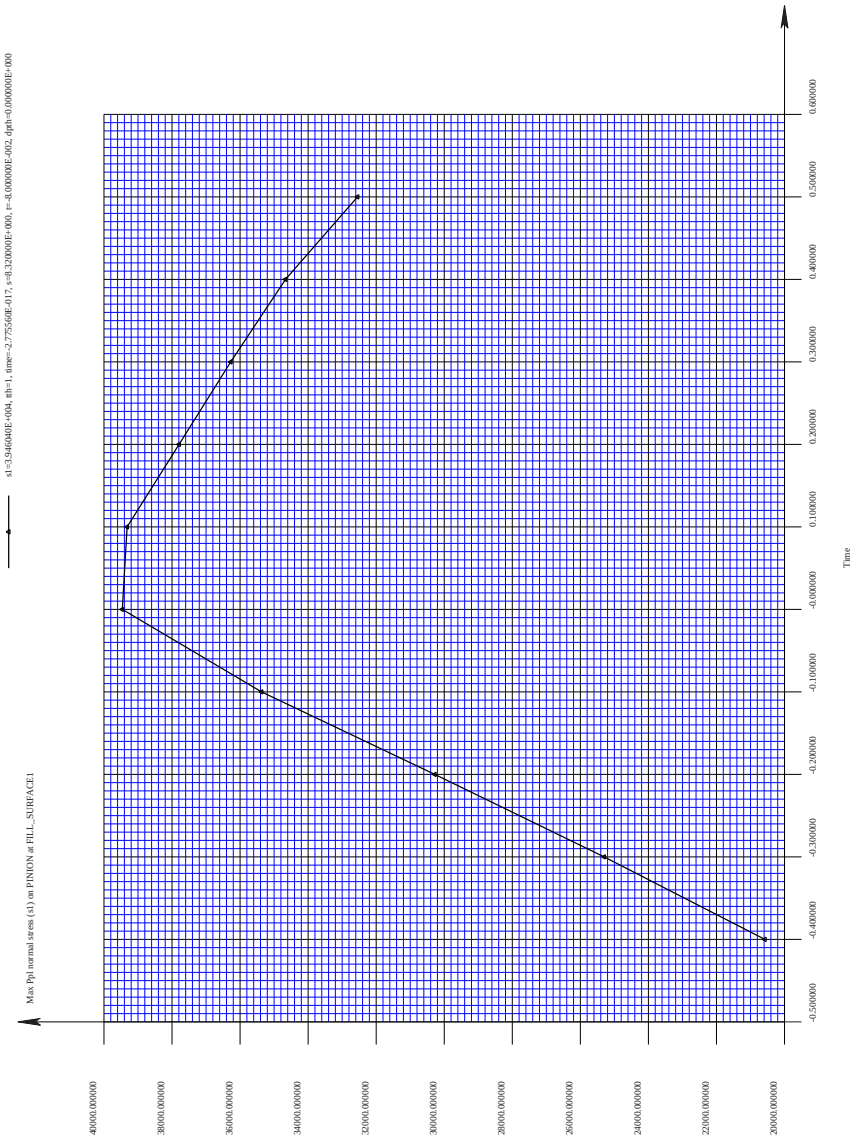

Figure 10.19: Plot of maximum principal normal stress against time for pinion tooth no.1 using the SEARCHSTRESS menu

Table 10.7: Searchstress data

Item	Description
COMPONENT	MAXPPLSTRESS
XAXIS	TIME
BEGINSTEP	1
ENDSTEP	11
BODY	PINION
SURFACE	FILLET1
TOOTHBEGIN	1
TOOTHEND	1
SEPTEETH	TRUE
SPROFBEGIN	6.00
SPROFEND	12.00
NUMSPROF	51
TFACEBEGIN	-0.5
TFACEEND	0.5
NUMTFACE	51
DEPTHBEGIN	0.00
DEPTHEND	0.00
NUMDEPTH	1
DISTMIN	0.05
OUTPUTTOFILE	TRUE
FILENAME	out.txt
APPEND	TRUE

Table 10.8: FE probe data

Item	Description
NPROBES	40
PROBE	1
BODY	PINION
MESH	TOOTH
ELEM	40
XI	0.226
ETA	1.00
ZETA	0.70
COMPONENT	MAXPPLNORMAL
FILENAME	PROBES.DAT

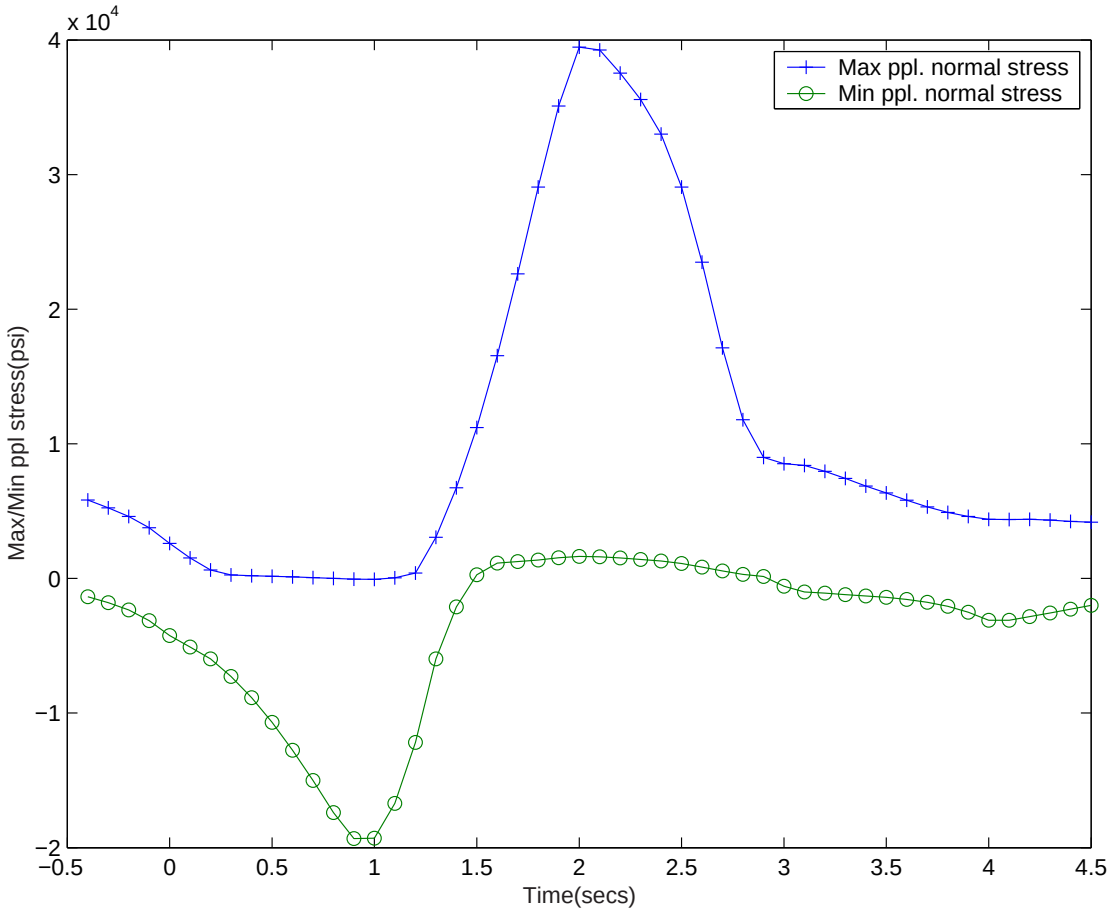

Figure 10.20: Plot of maximum and minimum principal stresses against time for pinion tooth for the case with thin flexible pinion inner diameter

10.10.2 Results

The maximum principal and the minimum principal normal stress plot obtained from the FE probe data is shown in Figure 10.20. The maximum principal normal stress ($\sigma_{\max}$) = $3.9462x10^4 psi$ and the minimum principal normal stress ($\sigma_{\min}$) = $-9.659x10^3 psi$. Hence, Alternating stress, $\sigma_a = 2.4560x10^4 psi$ and the Mean stress, $\sigma_m = 1.49015x10^4 psi$.

According to the Goodman's linear relationship, for a steel with tensile strength $80kpsi$, the fatigue stress using above data is $30.181kpsi$. The fatigue life for this stress is almost infinite.

10.11 Cumulative damage

The S-N curves discussed in previous section are developed for constant stress amplitude operation. But, in virtually every engineering application where fatigue is an important failure mode, the alternating stress amplitude may be expected to vary or change in some way during the service life. Hence the usage of S-N curves in such cases is inapplicable. Therefore theories based on cumulative damage are used while predicting fatigue failure.

The fatigue damage produced at any given cyclic stress amplitude will be related to the total number of cycles of operation at that stress amplitude and also related to the total number of cycles that would be required to produce failure of an undamaged specimen at that stress amplitude. It is further postulated that the damage incurred is permanent and operation at several different stress amplitudes in sequence will result in an accumulation of total damage equal to the sum of the damage increments accrued at each individual stress level. When the total accumulated damage reaches a critical value, fatigue failure occurs. Many different theories based on this concept of cumulative damage have been proposed. We discuss here two theories very commonly used for the purposes of assessing fatigue damage.

10.11.1 Linear damage theory

The linear damage theory is also referred as the Plamgren-Miner hypothesis or the linear damge rule. As discussed earlier the S-N curve(Figure 10.21) at a constant stress amplitude S_1 will produce complete damage, or failure, in N_1 cycles. Operation at stress amplitude S_1 for a number of cycles n_1 smaller than N_1 will produce a smaller fraction of damage, D_1. D_1 is usually termed as the damage fraction. Operation over a spectrum of different stress levels results in a damage fraction D_i for each of the different stress levels S_i in the spectrum. When this damage fractions sum to unity, failure is predicted, that is,

Failure is predicted to occur if:

$$D_1 + D_2 + ... + D_{i-1} + D_i \geq 1 \tag{10.12}$$

The Palmgren-Miner hypothesis asserts that the damage fraction at any stress level S_i is linearly proportional to the ratio of number of cycles of operation to the total number of cycles that would produce failure at that stress level, that is

$$D_i = \frac{n_i}{N_i} \tag{10.13}$$

Thus we can also say that failure is predicted to occur if:

$$\frac{n_1}{N_1} + \frac{n_2}{N_2} + ... + \frac{n_{i-1}}{N_{i-1}} + \frac{n_i}{N_i} \geq 1 \tag{10.14}$$

or failure is predicted to occur if:

$$\sum_{j=1}^{i} \frac{n_j}{N_j} \geq 1 \tag{10.15}$$

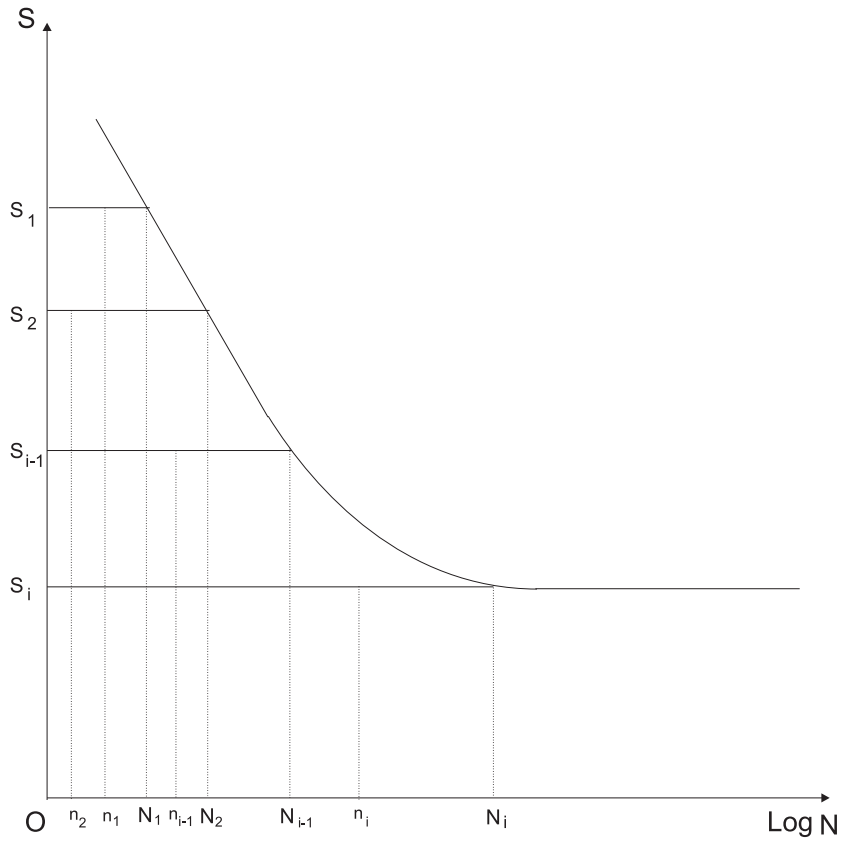

Figure 10.21: S-N plot illustrating the linear damage theory

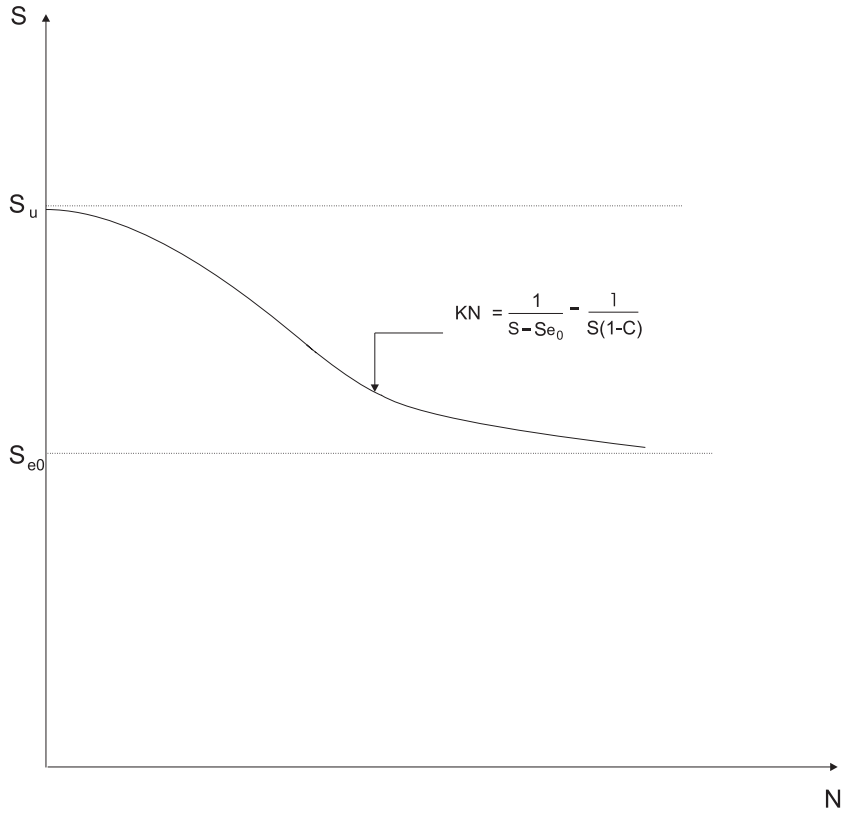

Figure 10.22: S-N curve approximation proposed by Gatt

The Palmgren-Miner hypothesis is widely used because of its simplicity and the experimental fact that the other much more complex cumulative damage theories do not always yield a significant improvement in failure prediction reliability. The most significant drawback of the theory though is that no influence of the order of application of various stress levels is recognized, and damage is assumed to accumulate at the same rate at a given stress level without regard to past history. Experimental data suggest that the order in which various stress levels are applied does have a significant influence and also that the damage rate at a given stress level is a function of the prior cyclic stress history.

10.11.2 Gatts Cumulative damage theory

Gatts postulated that the fatigue strength and the the fatigue limit change continuously with the application of stress cycles, and that the change is proportional to a function of the stress amplitude.

The S-N curve[3] according to the Gatt's theory is given as:

$$kN = \frac{1}{S - S_{e_0}} - \frac{1}{S(1-C)} \tag{10.16}$$

where,

[3]See Failure of materials in mechanical design by J.A. Collins.

$C, k =$ Material constant and proportionality constant
$S_{e_0} =$ fatigue limit when N = 0
$S_q =$ Instantaneous value of strength
$S_e =$ Fatigue limit, a function of cyclic stress history, not a constant
$= CS_q$
$N =$ Number of cycles of stress applied
$S =$ Amplitude of applied cyclic stress

Figure 10.22 shows the S-N curve based on the Gatt's cumulative damage theory.

Knowing the material properties and calculating the stress amplitude from the FE probe data it is possible to calculate the fatigue life for a hypoid gear pair based on the Gatts cumulative damage theory.

10.12 Fatigue life based on duty cycle for a gear set

We assume the gear set shown in example file `fatigue.ses` to be running at 90% of the total torque.

Load the file `fatigueload1.ses` located in the `FATIGUE` directory. We now run the gear set at about 110% of the total load(Torque=1222.22 *lbf.in*). For this load the maximum sress plot from the search stress menu is shown in Figure 10.23. The maximum stress point using the FE probe data is found to be (0.546,1.00,0.91). For this point the maximum and minimum principal normal stress plot is shown in Figure 10.25. The corresponding fatigue life hence obtained is $6.0 \times 10^4 cycles$.

Load the file `fatigueload2.ses` located in the `FATIGUE` directory. We now run the gear set at 100% load($Torque = 1111.11 lbf.in$). For the point (0.546,1.00,0.91) on element no.40 the maximum and minimum principal normal stress plot is shown in Figure 10.24. The corresponding fatigue life hence obtained is $2.3 \times 10^5 cycles$.

Load the file `fatigueload3.ses` located in the `FATIGUE` directory. We now run the gear set at $Torque = 500 lbf.in$. For the point (0.546,1.00,0.91) on element no.40 the maximum and minimum principal normal stress plot is shown in Figure 10.26. The corresponding fatigue life hence obtained is infinite.

Load the file `fatigueload4.ses` located in the `FATIGUE` directory. We now run the gear set at $Torque = 1000 lbf.in$. For the point (0.546,1.00,0.91) on element no.40 the maximum and minimum principal normal stress plot is shown in Figure 10.27. The corresponding fatigue life hence obtained is $5.2 \times 10^5 cycles$.

The load and the corresponding fatigue life is summarised in Table 10.9.

Table 10.9: Fatigue life for a duty cycle

Torque(lbf-in)	Fatigue life(cycles)	Running time (%)
500	∞	70%
1000	5.2e5	20%
1111.11	2.3e5	9%
1222.22	6.0e4	1%

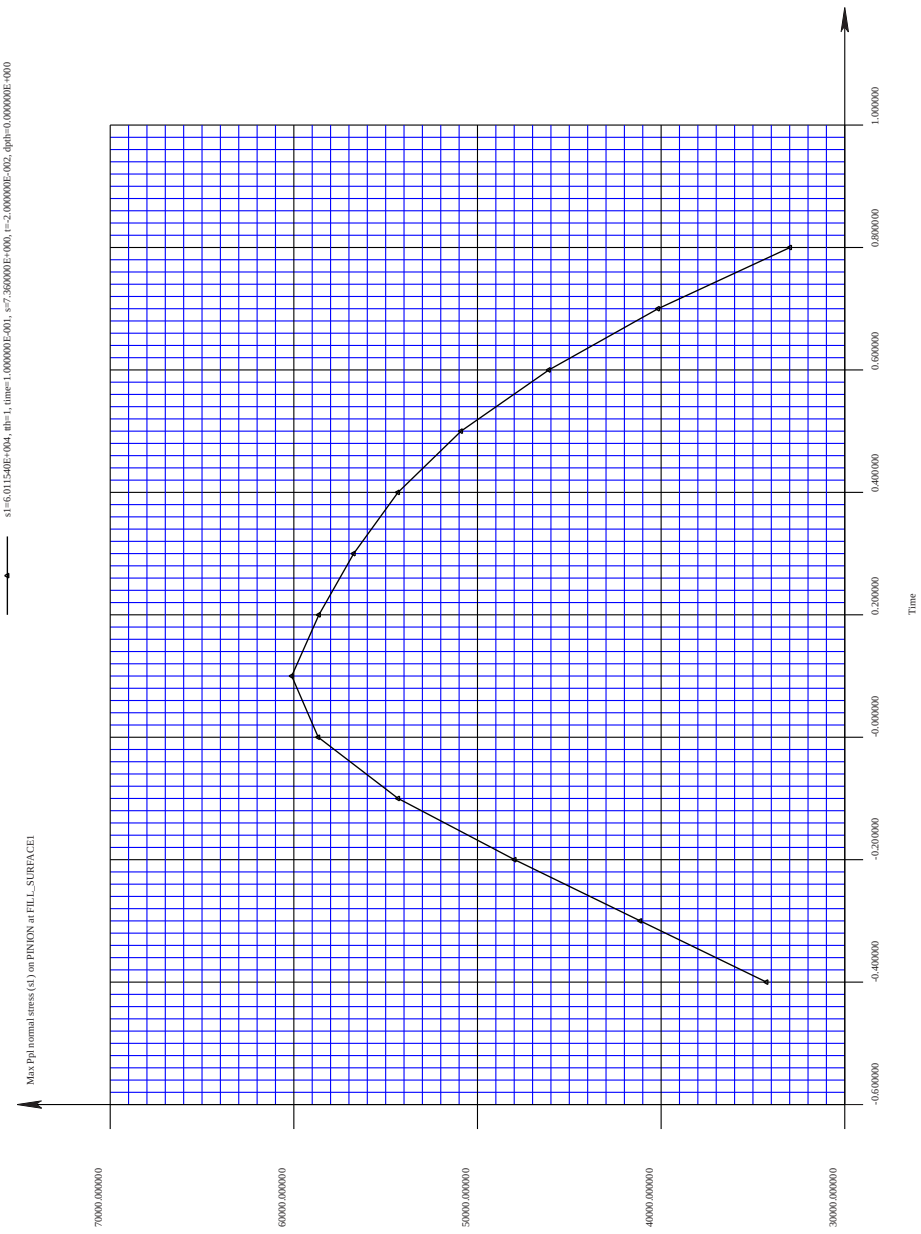

Figure 10.23: Maximum principal normal stress plot against time for pinion tooth no.1 for a output torque of 1222.22 lbf.in

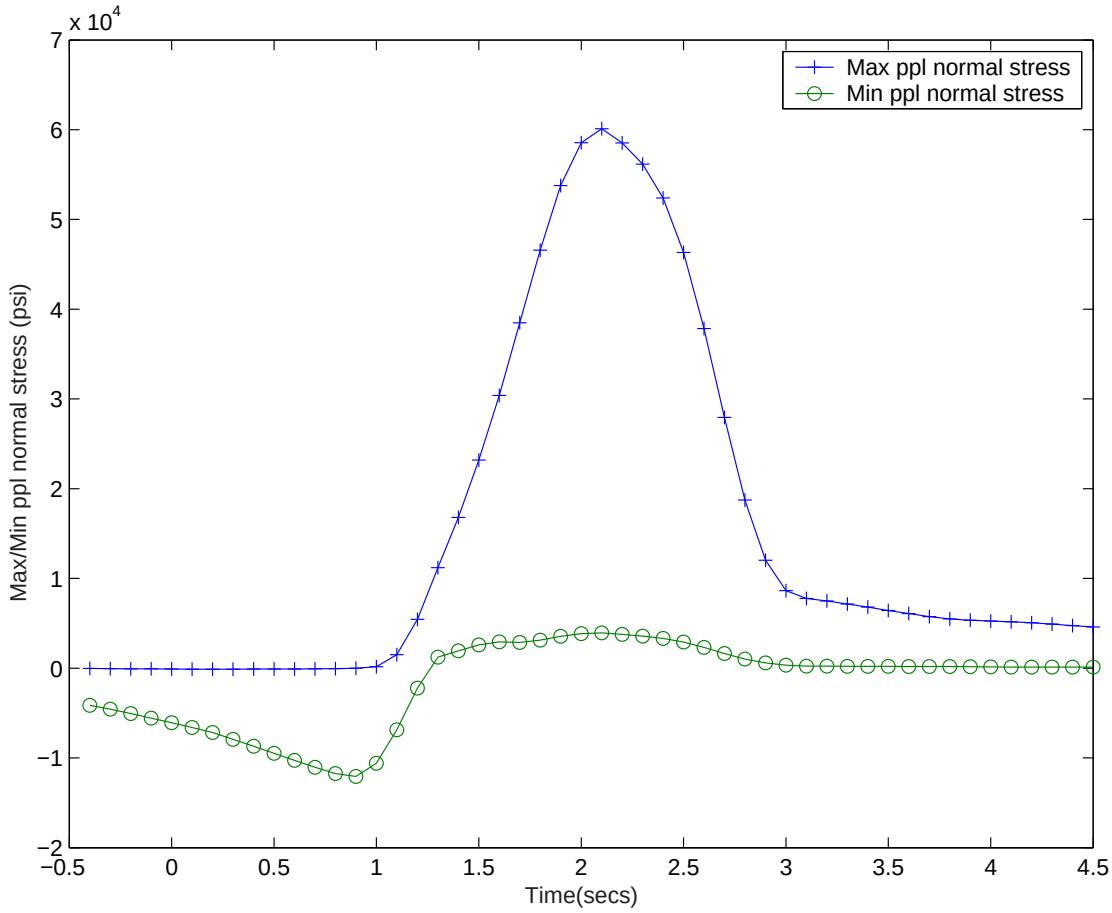

Figure 10.24: Maximum and minimum principal normal stress plot against time for pinion tooth for output torque of 1222.22 lbf.in

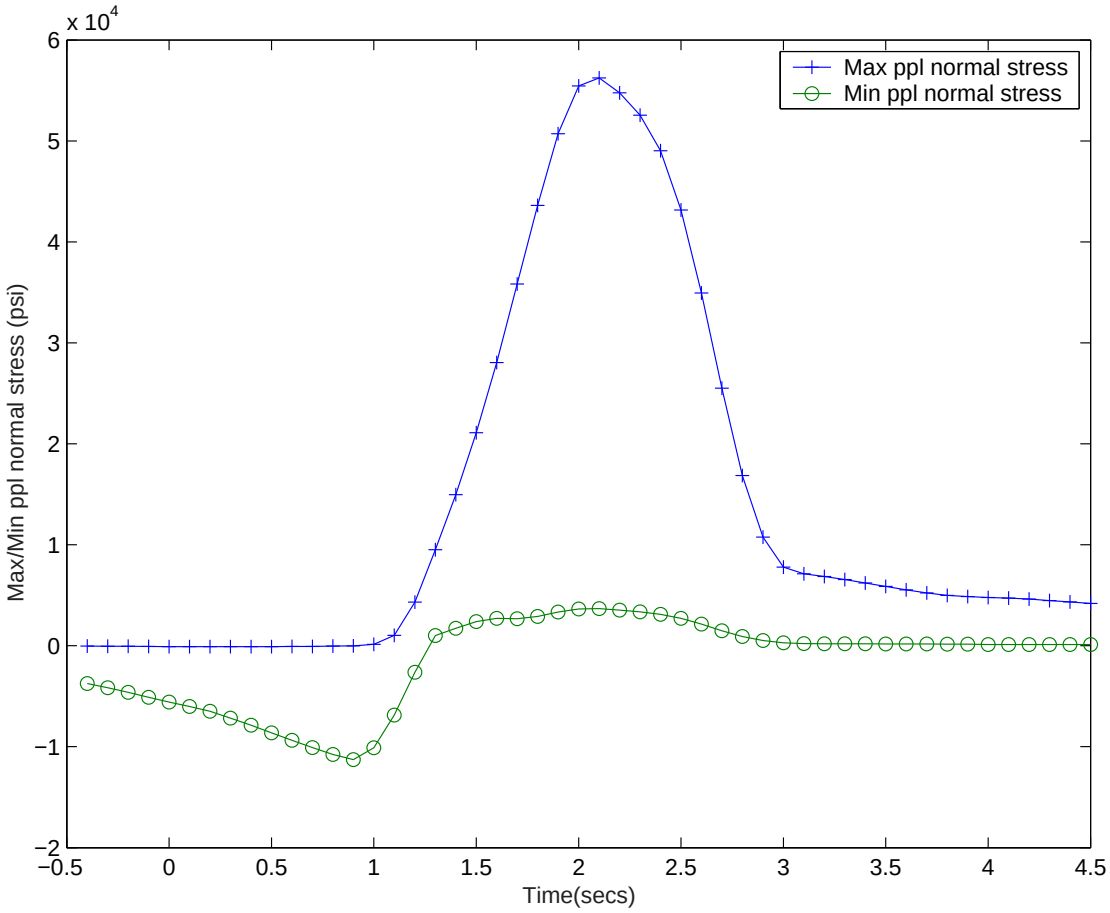

Figure 10.25: Maximum and minimum principal normal stress plot against time for pinion tooth for output torque of 1111.11 lbf.in

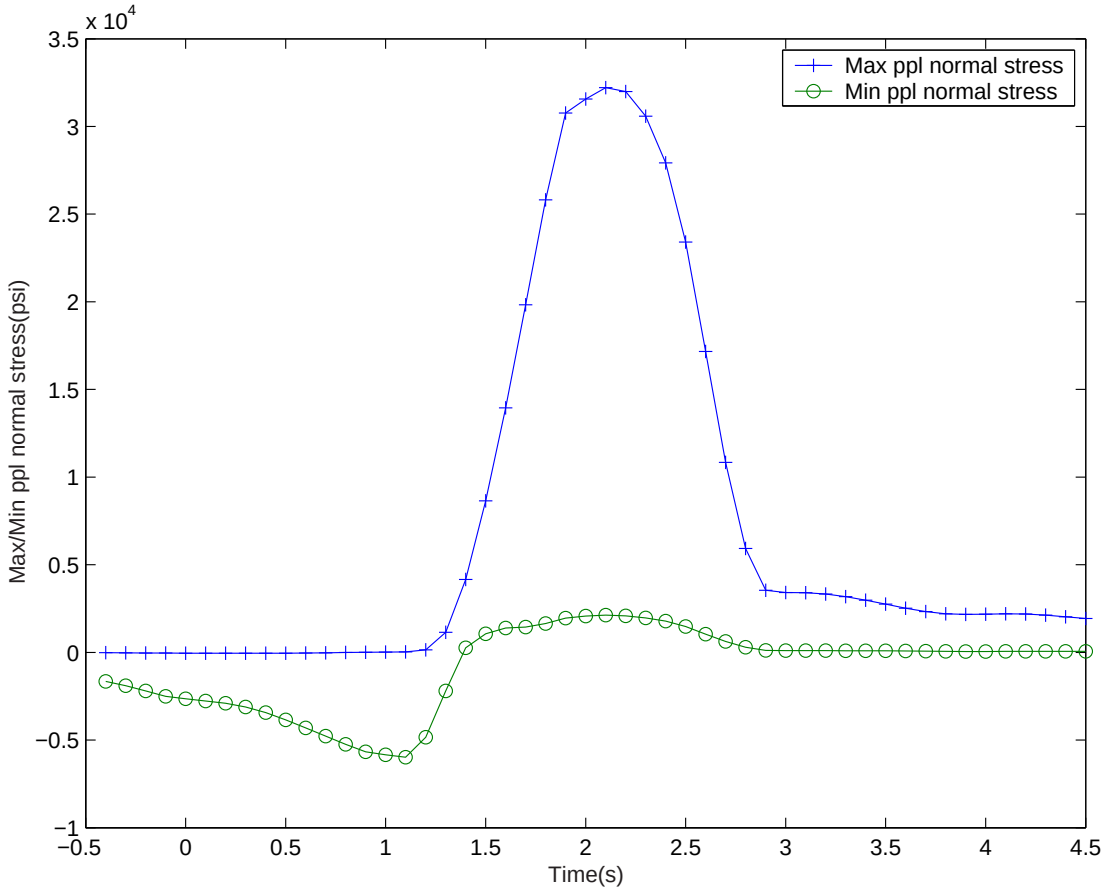

Figure 10.26: Maximum and minimum principal normal stress plot against time for pinion tooth for output torque of 500 lbf.in

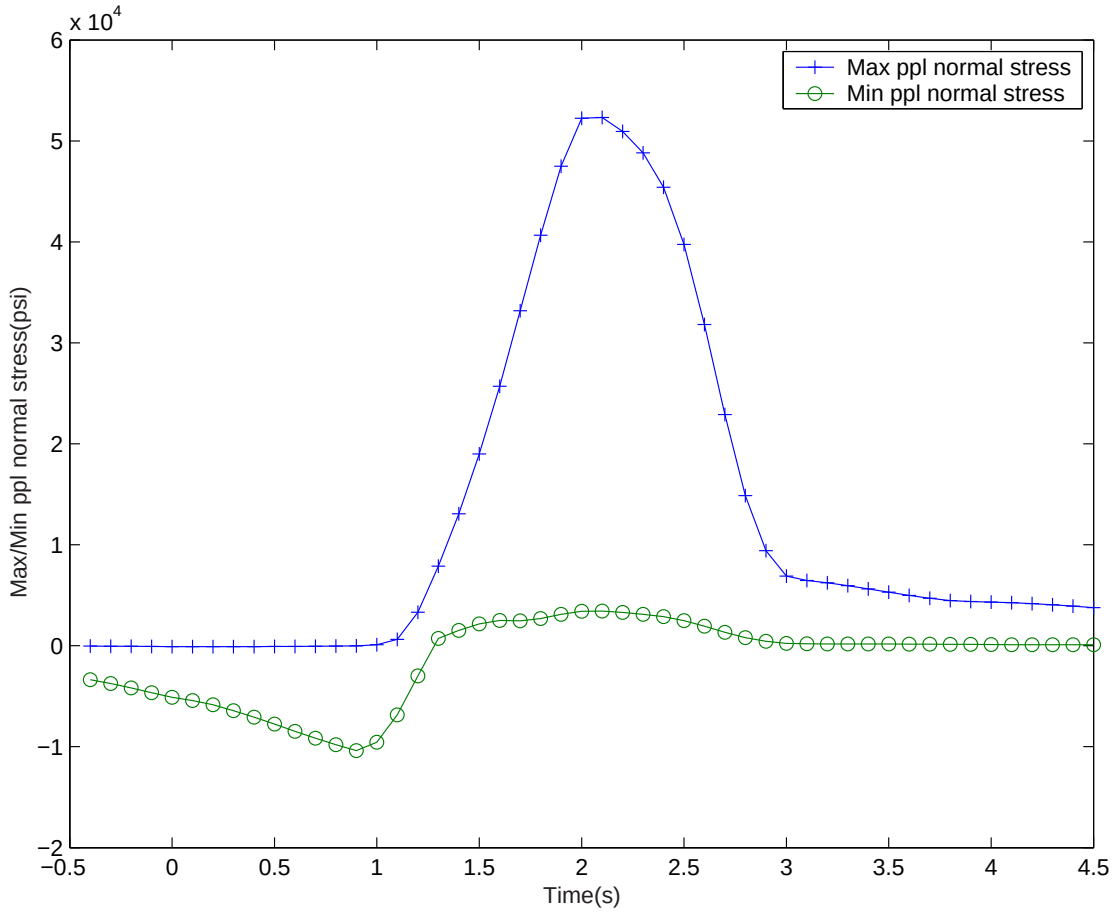

Figure 10.27: Maximum and minimum principal normal stress plot against time for pinion tooth for output torque of 1000 lbf.in

10.13 Calculating life based on cumulative damage theory

From the Linear damage theory failure occurs when:

$$\frac{n_1}{N_1} + \frac{n_2}{N_2} + ... + \frac{n_{i-1}}{N_{i-1}} + \frac{n_i}{N_i} = 1 \tag{10.17}$$

Substituting the values from Table 10.9 in the above we get:

$$\frac{0.7n}{\infty} + \frac{0.2n}{5.2 \times 10^5} + \frac{0.09n}{2.3 \times 10^5} + \frac{0.01n}{6.0 \times 10^4} = 1 \tag{10.18}$$

Thus, the life cycle for the gear set is $1.06091 \times 10^6 cycles$.

10.14 Conclusions

Helical3D program can be employed to calculate the fatigue life for gear bodies. Although for the example cases we gave considered a helical gear pair the same procedure can be applied to spur gear pair. As can be seen from the Table 10.9 as the load increases the fatigue life is found to decrease as expected. We feel *calyx* gives a reasonable approach towards calculation of fatigue life although we cannot verify the results obtained from *Calyx* with experimental or analytical calculations due to lack of information at this time.

Appendix A

Values of m and n for various values of θ

The following table(A.1) is taken from the paper by H.L.Whittemore and S.N.Petrenko, Natl. Bur. Std. Tech. Paper 201, 1921. An extension for $0 < \theta < 30^o$ is given by M.Kornhauser, J. Appl.Mech.,vol. 18, pp. 251-252, 1951.

Table A.1: Values of m and n for various values of θ

α(deg)	m	n
0	∞	0.00
0.5	61.40	0.108
1	36.89	0.1314
1.5	27.48	0.1522
2	22.26	0.1691
3	16.50	0.1964
4	13.31	0.2188
6	9.790	0.2552
8	7.860	0.2850
10	6.612	0.319
20	3.778	0.408
30	2.731	0.493
40	2.136	0.567
50	1.754	0.641
60	1.486	0.717
70	1.284	0.802
80	1.128	0.893
90	1.00	1.00

Bibliography

[1] *Planetary Gear Train Ring Gear and Support Structure Investigation*, Mark Valco, Ph.D. Dissertation, Cleveland State University, 1992.

[2] *Gear Tooth Stress Measurements of Two Helicopter Planetary Stages*, Krantz, T. L., NASA Technical Memorandum 105651, AVSCOM Technical Report 91-C-038, 1992.

[3] A combined surface integral and finite element solution for a three-dimensional contact problem, S. Vijayakar, *International Journal for Numerical Methods in Engineering*, vol.31, pp. 525-545, 1991.

[4] *Nonlinear and dynamic programming*, G. Hadley, Addison Wesley Publishing company, 1964.

[5] *Linear programming*, George Hadley, Addison Wesley, 1962.

[6] *Linear and Combinatorial Programming*, Katta G. Murty, John Wiley, 1976 ISBN: 0-471-57370-1.

[7] Linearization of multibody frictional contact problems, S. Vijayakar, H. Busby and D. Houser, *Computers and Structures*, vol. 29, no. 4, pp. 569-576, 1987.

[8] *Natural Frequency Spectra and Vibration Modes of Planetary Gears*, Jian Lin and Robert Parker, 1998 ASME Design Engineering Technical Conference, September 1998, Atlanta Georgia.

[9] *Gear Dynamics Experiments, Part I: Characterization of Forced Response*, Blankenship and Kahraman, ASME 7^{th} International Power Transmissions and Gearing Conference, San Diego, October 1996.

[10] *Gear Dynamics Experiments, Part II: Effect of Involute Contact Ratio*, Blankenship and Kahraman, ASME 7^{th} International Power Transmissions and Gearing Conference, San Diego, October 1996.

[11] *Gear Dynamics Experiments, Part III: Effect of Involute Tip Relief*, Blankenship and Kahraman, ASME 7^{th} International Power Transmissions and Gearing Conference, San Diego, October 1996.

[12] The use of boundary elements for the determination of the geometry factor, Vijayakar and Houser, 1986 *AGMA Fall Technical Meeting*, Paper no. 86-FTM-10.

[13] Finite element analysis of quasi-prismatic structures, S. Vijayakar, H. Busby and D. Houser, *International Journal for Numerical Methods in Engineering*, vol. 24, pp. 1461-1477, 1987.

[14] Edge effects in gear tooth contact, S. Vijayakar, *ASME 7^{th} International Power Transmissions and Gearing Conference*, San Diego, October 1996.

[15] Vibration Measurements on Planetary Gears of Aircraft Turbine Engines, M. Botman, *AIAA Journal*, vol. 17, no. 5, 1980.

[16] Dynamic Tooth Loads in Epicyclic Gears, F. Cunliffe, J. D. Smith, and D.B. Welbourn, *J. Eng. Ind. Trans. ASME*, May 1974.

[17] Effect of Internal Gear Flexibility on the Quassi-Static Behavior of a Planetary Gear Set, A. Kahraman, S. Vijayakar, *Transactions of the ASME*, September 2001.

[18] Study on bending fatigue strength of Helical gears, Oda, Koide, *Bull.JSME, Vol 26*, 1983.

[19] Bending strength estimation of thin-rimmed spur gears, Oda, Miyachika, *Transactions of the ASME*, October 1996.

[20] Contact Mechanics, Johnson, K. L., *Cambridge University Press*, 1985

[21] Theoryof Elasticity, Timoshenko and Goodier, *Mcgraw-Hill publication*, Third Edition, 1970

[22] Analysis of spur and helical gears using a combination of finite element and surface integral techniques, Avinashchandra Singh, *The Ohio State University*, M.S. Thesis, 1992